Dynamic and Spectral Features of Semiconductor Lasers

Thesis by

Kerry J. Vahala

In Partial Fulfillment of the Requirements

for the Degree of

Doctor of Philosophy

California Institute of Technology

Pasadena, California

1985

(Submitted May 16, 1985)

To my Parents

Acknowledgments

I would like to express my sincere gratitude to my advisor, Professor Amnon Yariv, for his encouragement and support throughout my graduate studies at Caltech. His keen scientific intuition has been a constant inspiration, and it has been a privilege to be a member of his highly motivated and talented quantum electronics group.

I would like to thank Dr. Christoph Harder and Joel Paslaski, who collaborated in much of the work presented here. Special thanks also go to Dr. Schlomo Margalit and Dr. L.C. Chiu for many fruitful and enlightening discussions, and to Dr. Kam-Yin Lau and Dr. Nadav Bar-Chaim for supplying many of the devices used in this thesis. I am indebted to Desmond Armstrong for expert technical assistance in construction of experimental apparatus and to Jana Mercado for help in day-to-day matters.

My appreciation also goes to my other colleagues at Caltech; in particular, I would like to thank Professor Yasuhiko Arakawa, Robert Lang and John S. Smith for many fruitful collaborations in areas not discussed in this thesis. I gratefully acknowledge the financial support I have received from the IBM Corporation, the California Institute of Technology, the National Science Foundation and the Office of Naval Research.

I am extremely grateful to Professor William Bridges and Dr. Bill Bottoms for their advice and friendship during my years as an undergraduate and graduate student.

Finally, my deepest gratitude goes to my parents for their constant support and encouragement.

Abstract

This thesis is divided into two main subject areas: the fluctuation properties of state of the art semiconductor lasers and the improvement of modulation and fluctuation properties in these devices through a technique called detuned loading.

The discussion of fluctuations in lasers is a topic as old as the device itself, and much of the pioneering work in this field was done in the sixties. Surprisingly, however, several new chapters in this field are being written, because of certain pecularities only recently observed in semiconductor lasers. Chapters 2 and 3 of this thesis will consider these pecularities, which, as it turns out, are quite important in many potential system applications of these devices.

One of the driving forces behind the development of semiconductor lasers has been their application as sources and local oscillators in optical communication systems. In general, such applications require lasers which have low phase and intensity noise, and which can be modulated at high data rates. As is often the case, these requirements are to a certain extent mutually exclusive. Chapter 4 introduces a technique which is an exception to this rule. It relies upon the semiconductor laser physics which produces the fluctuation abnormalities discussed in Chapters 2 and 3. The technique can be used to improve modulation speed while simultaneously reducing noise as compared to the conventional device.

Table of Contents

Chapter 1

Introduction

1.1 Historical perspective

Semiconductor lasers (SL's) are a class of lasers which achieve stimulated emission of photons from a nonequilibrium population of electrons and holes. The population can be created by indirect pumping such as optical excitation of the semiconductor or by directly injecting electrons and holes across a PN junction. The latter method is of greater technological importance and the devices so formed are called injection lasers.

Over the course of two decades semiconductor lasers have evolved into efficient, cheap and reliable sources of coherent near IR radiation. Lasing action in semiconductors was first demonstrated in GaAs homostructure diodes late in 1962 by several groups [1,2,3,4]. In these early years lasers in general were subjects of intense research. The SL's of that era operated only at low temperatures and were thus primarily only of scientific importance. They would probably have been recorded in the annals of technology as a scientific curiosity had it not been for the advent in the early 70's of devices which could lase continuously at room temperature [5,6,7]. These SL's were grown using the lattice matched systems AlGaAs and GaAs. This enables abrupt compositional changes to be engineered into a device to provide more efficient confinement of the electron-hole plasma and better waveguiding of the lasing mode. A state of the art double heterostructure SL which illustrates these ideas is depicted in Fig. 1.1.

By the time the first room temperature SL's were developed there was widespread realization that silica fibers could someday be manufactured with

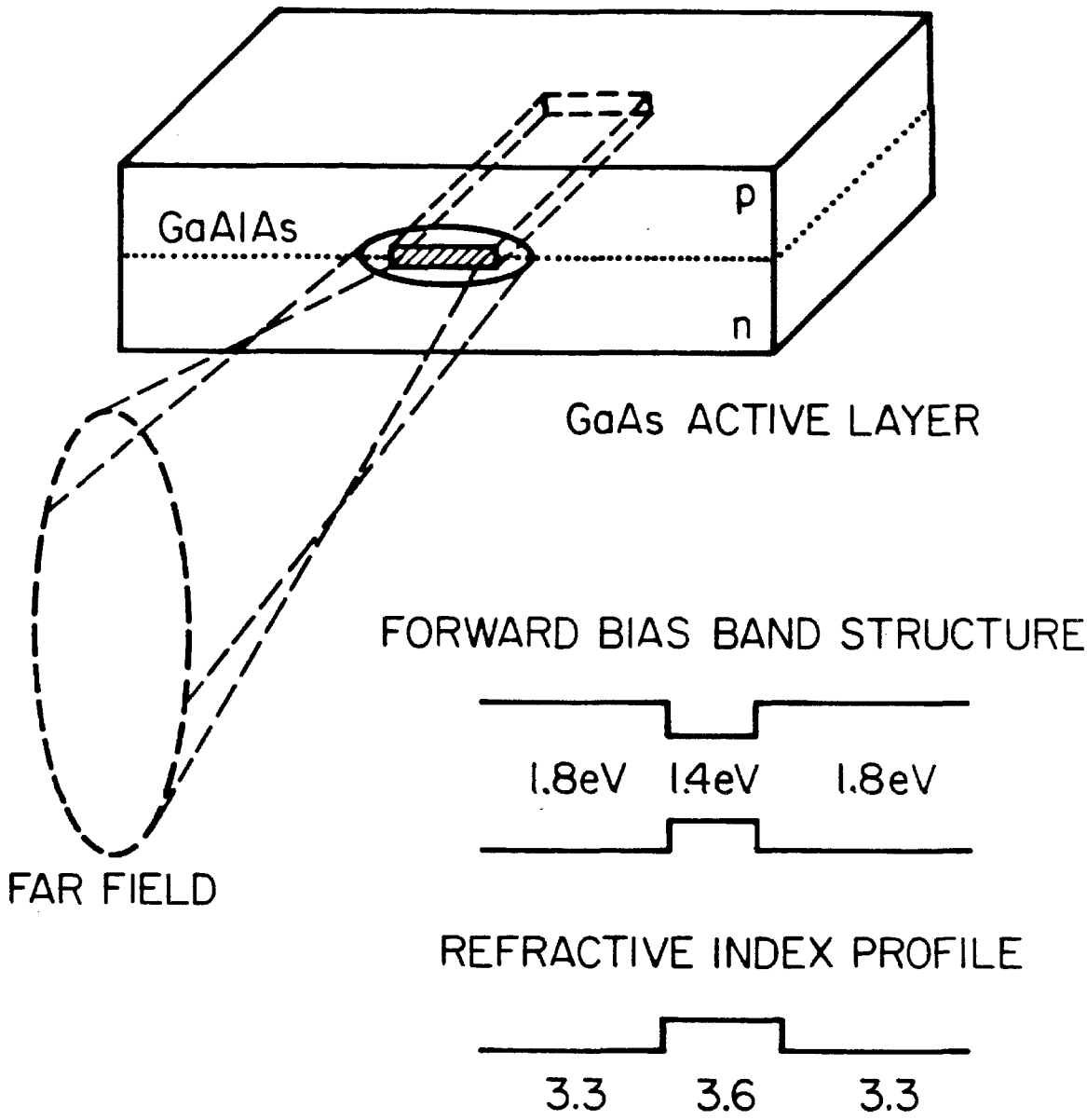

Figure 1.1 Heterostructure injection laser consisting of a low-bandgap high-refractive index GaAs active layer imbedded in high-bandgap low-refractive index AlGaAs. The active layer typically has dimensions 1.0μm.X0.2μm.X300μm. leading to the far-field pattern indicated.

very low loss and material dispersion in the spectral region where SL's operate. With a narrowband SL source such an optical system could convey information over perhaps 100's of kilometers without distortion or serious loss of signal strength. Around the same time it was also proposed by Yariv that the dual ∝erties of a direct gap and high electronic mobility in material systems such as GaAs(AlGaAs) and InGaAsP(InP) would someday lead to a new breed of integrated optical components [8] in which, for example, SL's and high-speed electronics would be monolithically integrated to interface a computer to an optical fiber communications network. These and other possible applications transformed the image of the SL from that of a laboratory curiosity into a potentially important commercial device, marking the beginning of a second phase in its history and sparking an enormous development effort which continues today.

Since the start of this second phase of work both low loss Silica fibers (see Fig. 1.2) [9] and integrated optics have become realities [10]; and the properties of state of the art SL's have become very impressive. Extrapolated room temperature lifetimes in excess of 10^7 hours and degradation rates of 10^{-5} hr.$^{-1}$ at 100°C have been obtained [11]. Devices which operate in the fundamental spatial mode at a single frequency and have cw output powers in excess of 40 mW. have been demonstrated [12]. Differential power efficiencies (i.e., the conversion of electrical input power to light output power) exceeding 80% and threshold currents as low as 2.5 mA. [13] have been measured. Two material systems have emerged as the workhorses of the SL industry. Devices grown in the InGaAsP(InP) system lase in the wavelength range 1.1 μm.-1.7μm. This falls in the region where modern optical fibers exhibit low loss and minimum material dispersion making these sources the preferred choice in long distance fiber communication systems. At the present time the record for repeaterless transmission is 222 km. which was set using a device in this system [14].

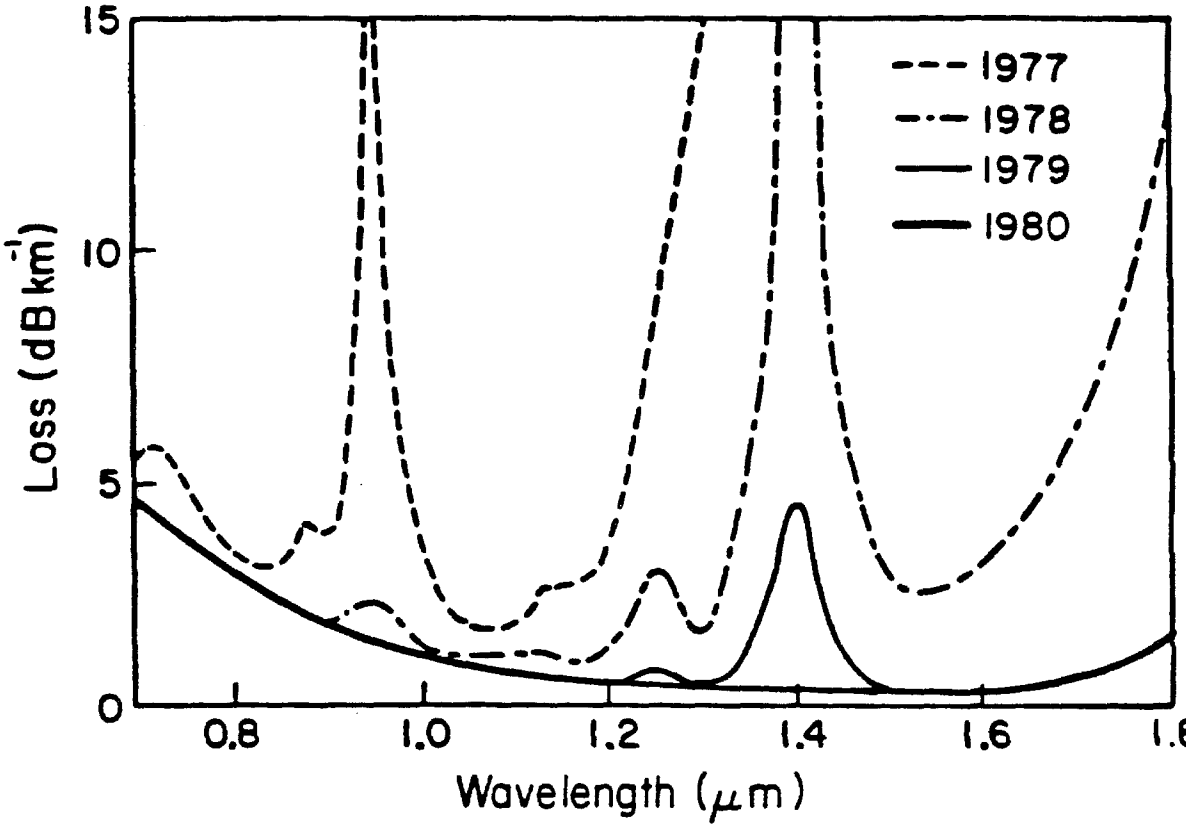

Figure 1.2 Loss spectrum of a graded index fiber.

Devices grown in the GaAs(AlGaAs) system lase in the wavelength range 0.7μm.-0.9μm. and have the advantage of a more mature material system with regard to integration as well as importance associated with short lasing wavelength. Since the attenuation and material dispersion of fibers are still quite low at these wavelengths these devices can easily function as sources in short optical links requiring high data rates. GaAs devices are also used in laser printers and high density storage systems, such as compact audio disc systems, which although not mentioned until now are at least equal to communications applications in their importance.

It is often the case as technology progresses that research and development cycle and feed off one another in a particular area. When this happens the two seem at times nearly indistinguishable. This is especially true in device work. When the SL moved from the laboratory animal phase into the development phase a large pool of resources became focused onto problems normally untouched by pure research (e.g., reliability). This effort has led to drastic improvements in all device characteristics as well as improvements in the material systems in which the devices are fabricated. As a result, state of the art semiconductor lasers bear little resemblence to their laboratory rat predecessors. They are now to a certain extent ideal, embodying the basic physics one would hope to ascribe to the device rather than exhibiting a jumbled variety of parasitic phenomena associated with imperfections in the material, problems with the growth procedure, bad contacts, etc. As such, SL's, in addition to their many uses in the "real" world, once again are objects of basic research. Now, however, rather than studying lasing action in a semiconductor, we can use the *in situ* lasing action as a probe to study the device and the material. This is the essence of much of the device physics work done at Caltech and is part of the motivation for the work presented in this thesis.

The other force motivating this work and all work in SL's today is simply that whereas SL's are ideal in the sense discussed above, their intrinsic properties are far from the ideal required in many system applications. This thesis considers the fluctuation and modulation properties of SL's. These are considerations essential in the design of any optical communication system. As sources, SL's are used either to generate the optical carrier or ,as local oscillators at the receiver end. Since there are a variety of modulation formats with corresponding detection schemes both the power and the phase noise spectra of the SL are of interest. If the information is to be impressed on the optical carrier by directly modulating the SL, then its modulation properties (e.g., ultimate speed, content of AM and FM components in light output) must also be considered. With only a few exceptions to be noted in Chapter 4, it is fair to broadly summarize the dynamic and spectral properties of conventional state of the art SL's by saying they can be made to be fast and noisy (modulation bandwidths exceeding 10 GHz [15], linewidths of 10 MHz.[16], power noise typically several orders larger than the shot noise limit [17]) or slow and quiet.

A logical goal is to understand the device physics which sets these limits so that device performance can be optimized for a particular application. By doing this one might also hope to find alternatives to the rule just stated: ways to modify either structure or material to make devices which are both fast and quiet. It is a surprising fact that only recently has the understanding of these properties been put on a solid foundation. To explain further and to provide an introduction to the basic topics covered in this thesis we now review lasing action in a semiconductor.

A basic familiarity with this topic is assumed throughout this thesis. For more comprehensive reviews of SL's the reader is referred to References

[18,19,20].

1.2 Lasing action in semiconductors

SL's and all other lasers are regenerative oscillators which emit at optical frequencies. All regenerative oscillators have two essential features: a gain mechanism and some kind of feedback to establish a set of modes for the gain to act on. An electronic ring oscillator is an example in which these essentials are very clear (see Fig. 1.3). In a SL, feedback is provided by the reflecting cleaved facets (mirrors) of the crystal (see Fig. 1.1). The optical modes of the resonator so formed derive gain via stimulated recombination in an inverted system of electrons and holes. As mentioned earlier this inversion is usually achieved by injecting electrons and holes across a PN junction.

In Fig. 1.4 we give the measured luminescence (not gain) spectrum at various pumping levels for a GaAs(AlGaAs) device like the one depicted in Fig. 1.1. The light-output current and current voltage characteristics for the device also appear in the figure and indicate a threshold current of 10 mA and a junction turn on voltage of approximately 1.4 Volts. Near threshold the luminescence spectrum extends over approximately 1000 Å. As threshold is approached a bump appears in the luminescence indicating stimulated emission is occurring (the necessary condition for stimulated emission in a semiconductor was first quantified by Bernard and Duraffourg [21]). At this pumping level optical gain for a small group of modes is nearly compensating the losses these modes experience at the mirrors or through other scattering mechanisms. In Fig. 1.5 we resolve these modes. Additional increases in the pumping level primarily go into stimulated recombination; the gain and the luminescence spectra becoming clamped at their threshold profiles. Well above threshold the gain spectrum profile will provide some longitudinal modal selectivity and predominantly single

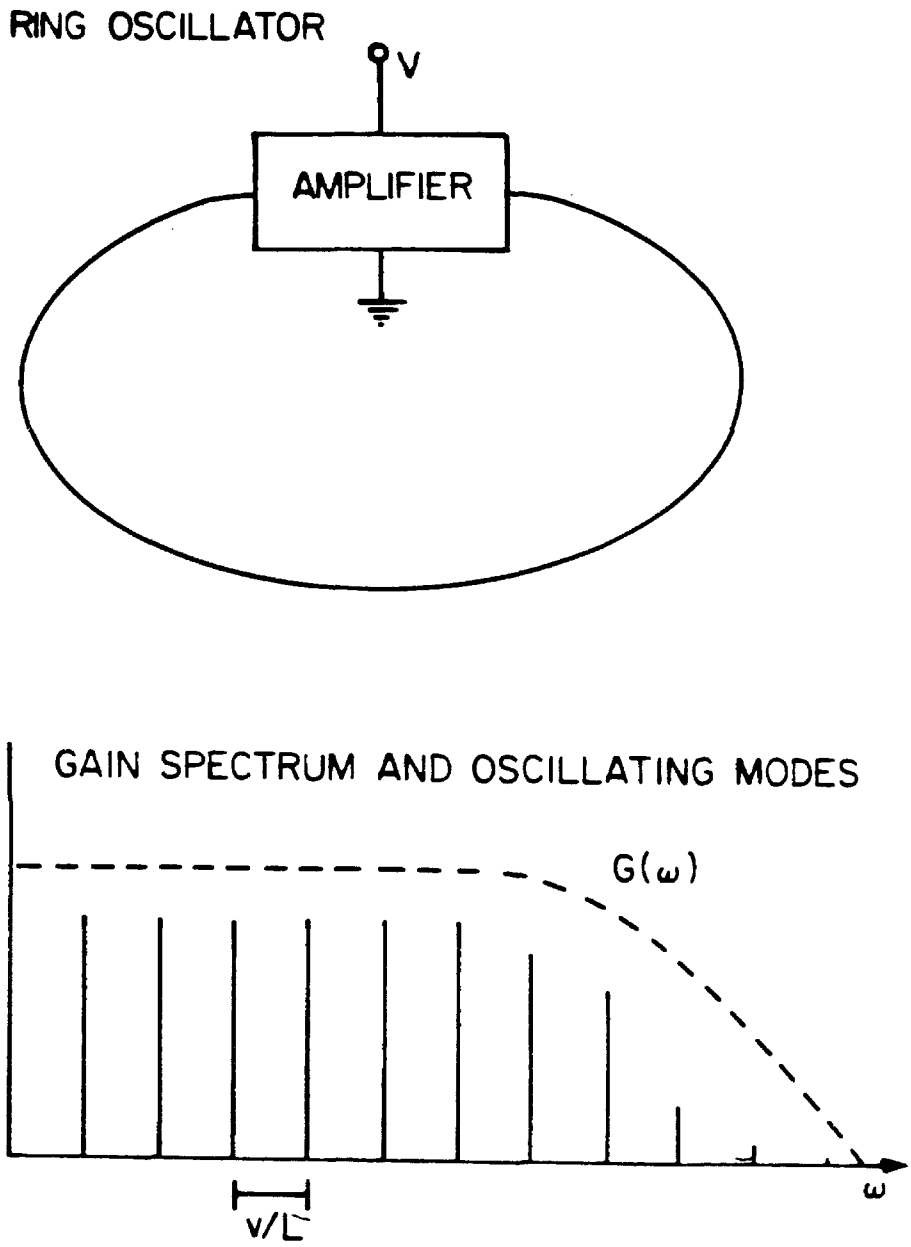

Figure 1.3 An electronic ring oscillator embodies the essential features of all regenerative oscillators. In this system modes of the ring have a free spectral range v/L where v is the voltage propagation speed in the ring of circumference L. These modes see a gain $G(\omega)$ provided by the amplifier.

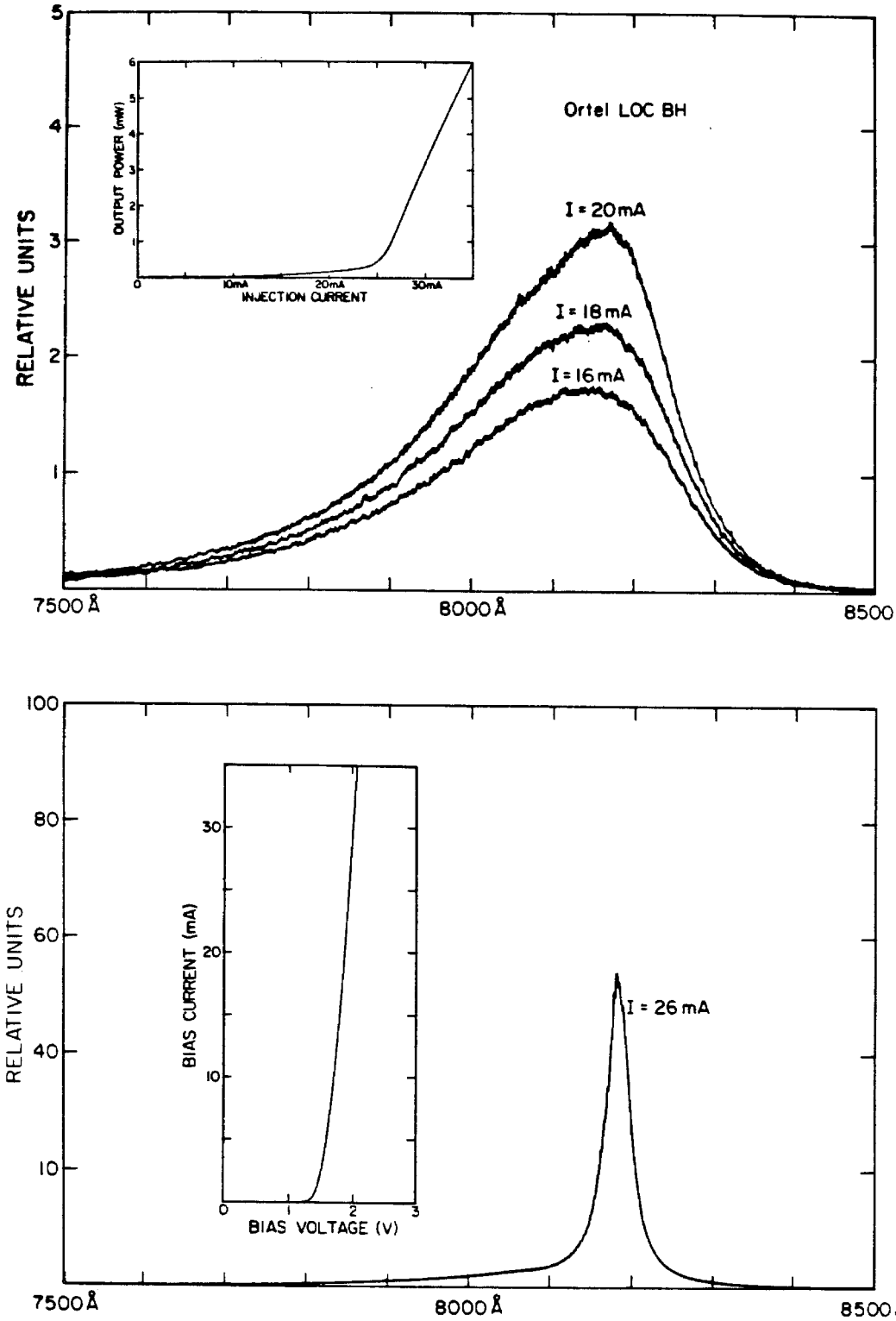

Figure 1.4 Luminescence from a semiconductor laser at various pumping levels below and near threshold. Near threshold a bump appears in the luminescence indicating that stimulated emission is beginning to occur. The upper inset gives the light output versus current curve for this device. Note that the threshold current is approximately 25 mA. The lower inset gives the current-voltage characteristic for the device which is typical of a junction diode.

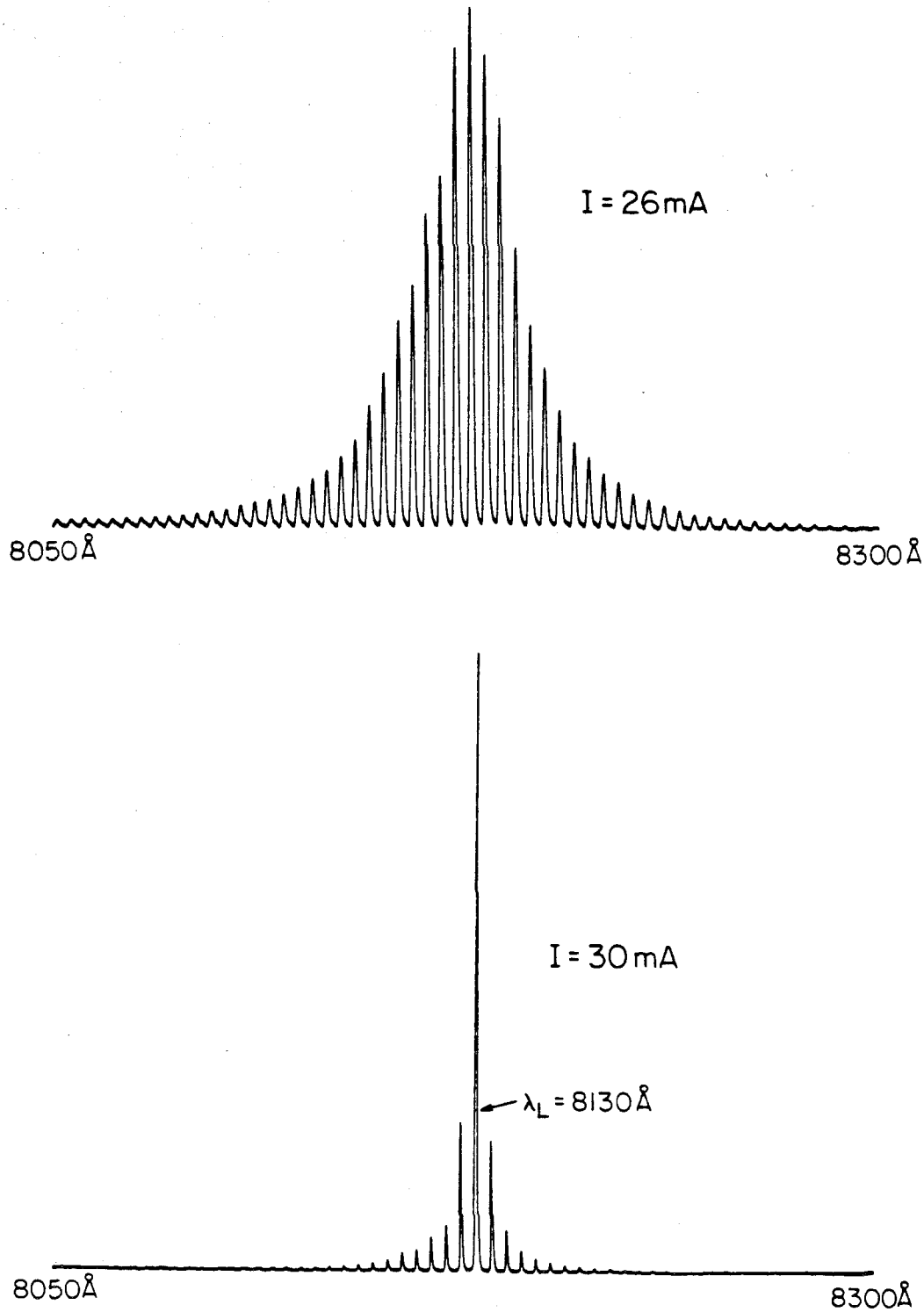

Figure 1.5 Stimulated emission resolved at pumping levels near and above threshold for the same device as Figure 1.4. The lasing wavelength is λ_L = 8130Å

mode operation can result.

This process as seen by the longitudinal mode m (which by choice eventually lases) is depicted in Fig. 1.6. Well below threshold the mode is fed by spontaneous photons or simply luminescence from the electron-hole plasma. These photons enter the mode randomly and are bled away by cavity losses. The spontaneous rate into the mode increases with increased pumping. Eventually, the mode m contains enough photons so that some stimulated events begin to occur. The stimulated photons are, in an intuitive sense, "phase coherent" with the mode. This is to say that they do not produce fluctuations of the field upon entry. Above threshold the spontaneous rate is clamped, but the stimulated rate continues to escalate as the number of photons in the mode and hence the output power associated with the mode m increase. Well above threshold the mode m is supplied primarily with stimulated photons. Barring fluctuation sources extrinsic to this process, such as cavity vibrations and temperature fluctuations, the principal source of noise is spontaneous emission. This is referred to as quantum noise.

Semiconductor lasers typically have enormous threshold spontaneous rates in comparison to other laser systems and are hence much noisier than other lasers. This results from operation with extremely poor passive cavity Q's (the photon lifetimes are typically a few picoseconds giving Q's of about 1000 as compared to Q's of 10 million for say a HeNe laser) thereby causing threshold gains (and spontaneous rates) to be high. This is a disadvantage from an applications point of view, but an advantage in the laboratory where it enables measurement of quantum noise effects without any special precautions to screen out extrinsic sources of fluctuations. That semiconductor lasers can operate at all with low Q passive resonators is a result of the enormous optical gains possible with an

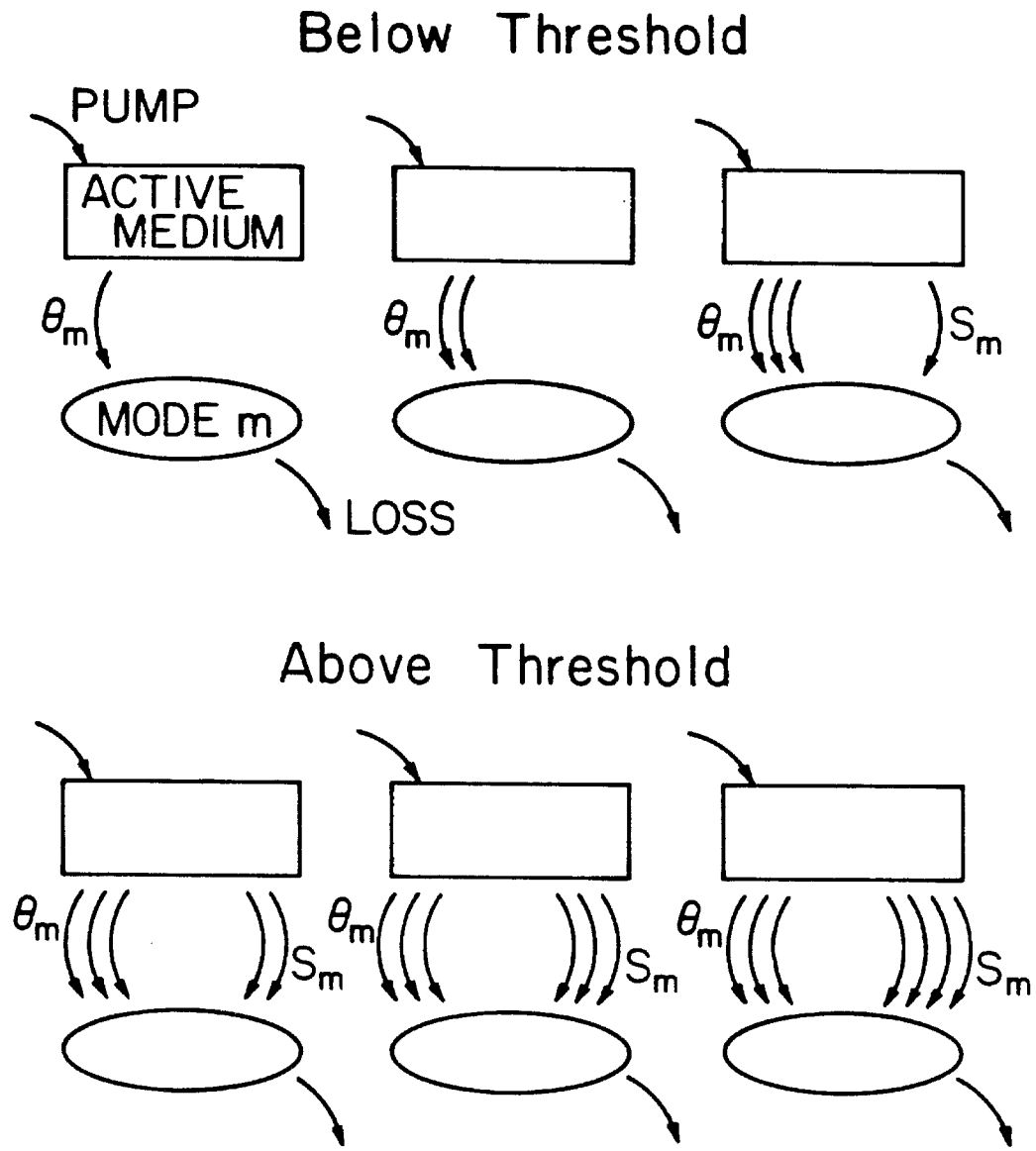

Figure 1.6 Schematic of the onset of lasing action. Below threshold the mode m and all modes are supplied by spontaneous photons at a rate θ_m which increases with increased pumping. When a sufficient number of photons are present in a particular mode m, the one with lowest loss, stimulated events begin to occur at a rate S_m which is proportional to the number of photons in mode m. As threshold is reached the spontaneous rate is clamped and additional increases in modal power come from the increasing stimulated emission rate.

electron-hole inversion. The results of a gain calculation based on a parabolic band model for GaAs are presented in Fig. 1.7.

The semiconductor laser is interesting in one other respect. This is a fact only recently appreciated and central to this thesis. It is, that as a regenerative oscillator it naturally operates in a detuned fashion. Normally, tuned and detuned operation imply operation at the gain line center or away from it as illustrated in Fig. 1.8. In detuned operation the lasing mode sees a contribution to refractive index from the inversion. This has the effect of coupling the amplitude and phase of the optical mode since changes in the optical intensity will disturb the inversion, which will change the refractive index, and in turn the phase of the optical mode.

That a semiconductor laser operates as a detuned oscillator can be seen by considering its gain spectra depicted in Fig. 1.9. This highly asymmetric spectrum is to first order the product of two terms: the effective density of states function which determines it shape near the band edge (i.e., low frequencies) and the quasi-Fermi distribution functions which determine the shape at higher frequencies. Lasing action occurs at the gain peak which we might guess is a detuned point owing to the asymmetry of the spectrum. In fact, all points on this curve are detuned in the sense discussed above: in a semiconductor, changes in the inversion, caused say from a disturbance in the field intensity, will shift the frequency of both the gain spectrum peak and the zero resonant dispersion point (the result of band filling changes). Thus, wherever the optical mode sits in the spectrum it perceives a change in refractive index and hence some amplitude-phase coupling.

Detuning manifests itself in both the noise and the modulation properties of semiconductor lasers. We mention two important ways which will be discussed

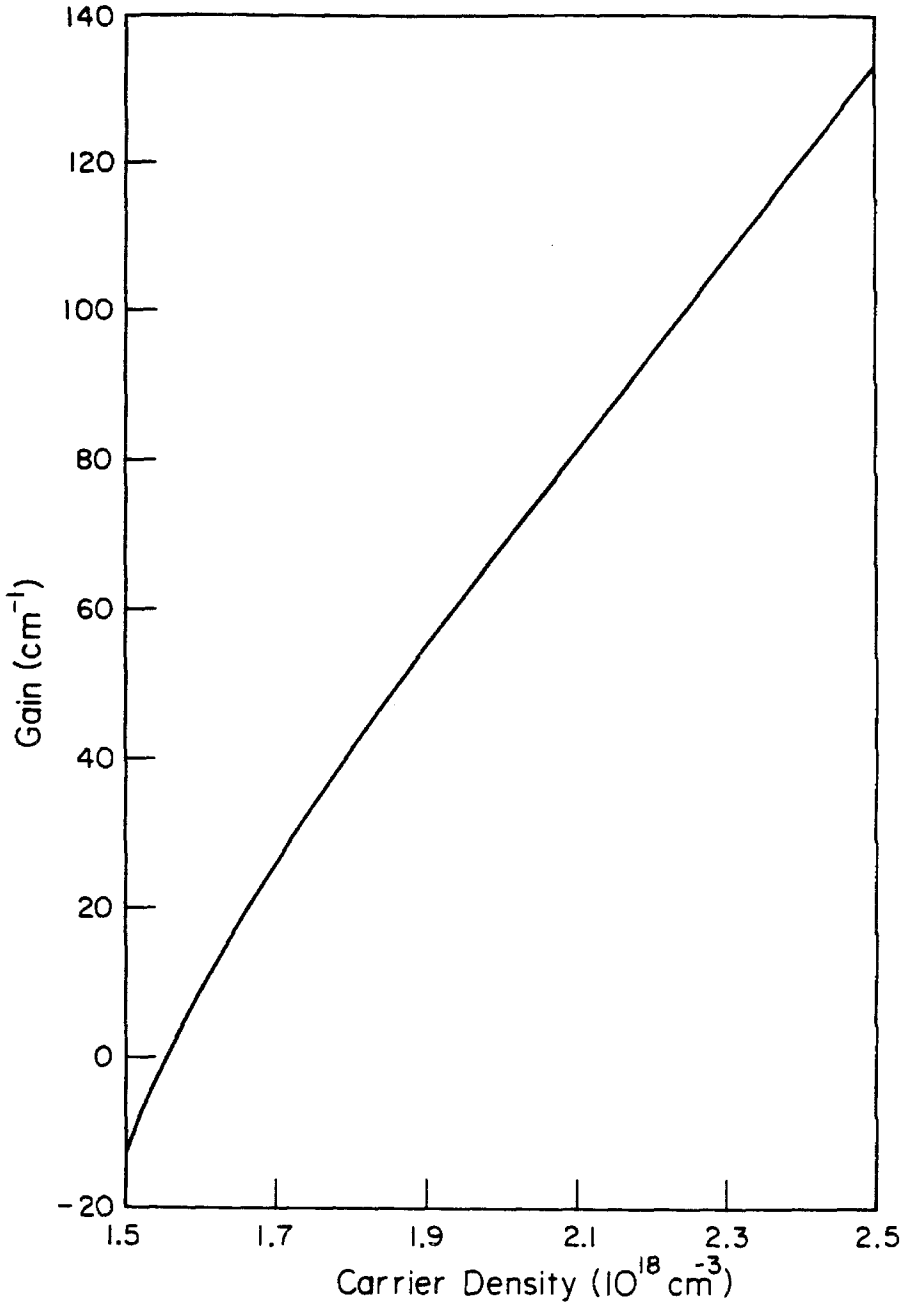

Figure 1.7 Gain as a function of carrier density for bulk GaAs.

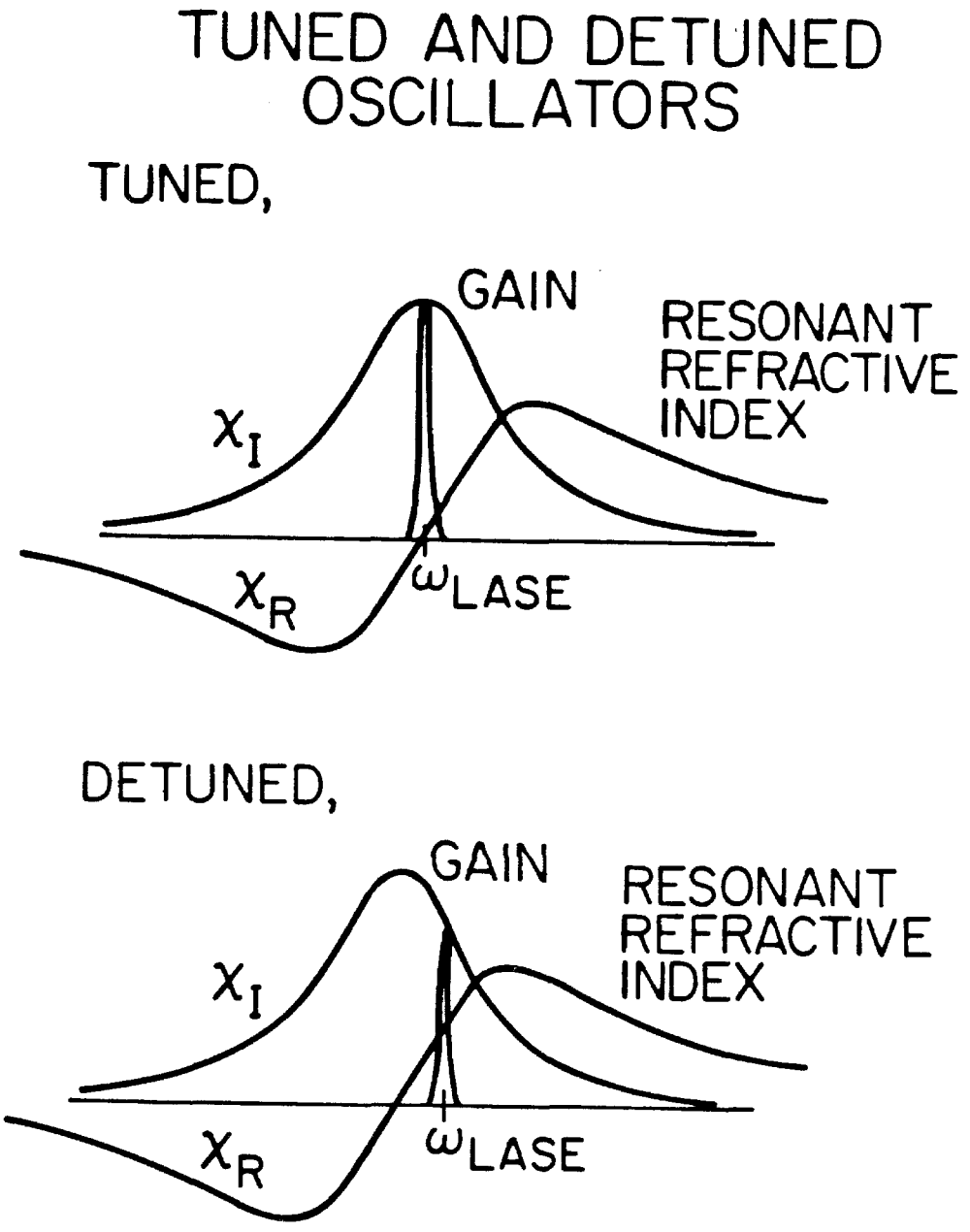

Figure 1.8 The definition of tuned and detuned operation in a regenerative oscillator. The curves shown are the gain and resonant refractive index spectra, or equivalently, the imaginary and real parts of the complex susceptibility function.

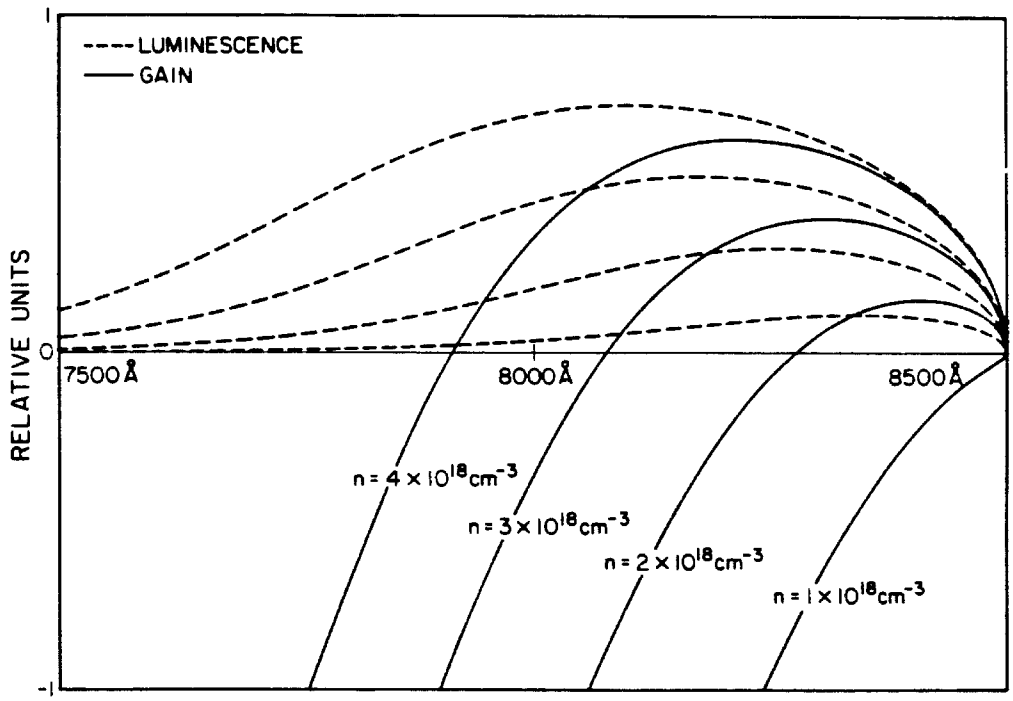

Figure 1.9 Calculated luminescence and gain spectra at various excitation levels in GaAs. The zero point at the extreme right corresponds to the band edge and the shapes of the spectra there are determined by the effective density of states function. For shorter wavelengths at the extreme left, the shape is set by the quasi-Fermi occupancy of states in the conduction and valence bands. These spectra should be compared with the measured spectra in Figure 1.4.

in greater detail later. Under current modulation detuning causes parasitic FM components in addition to the AM components (i.e., both gain and refractive index are being modulated). In noise spectra its presence is observed as an enhancement of the fundamental linewidth in single mode operation (a phase noise enhancement) by typically a factor of 30 times. In this case the detune induced amplitude-phase coupling allows spontaneous noise components which normally couple only into intensity noise to channel their way into the phase noise.

In Chapter 3 we will consider in detail the effect of gain spectrum detuning on the fluctuation properties of semiconductor lasers. The analysis there derives a variety of noise spectra for single and multimode semiconductor lasers. First, however, the rigorous quantum mechanical foundation to that analysis will be presented in Chapter 2. In this chapter a formalism based on electronic wavepacket operators is developed and used to derive local operator equations of motion for a multimode semiconductor laser. These equations can be used to study a number of other types of fluctuations which we do not consider in this thesis Finally, in Chapter 4, the problem of optimizing a semiconductor laser for high-speed low-noise performance is considered. We present one possible solution to this problem which actually turns the up-till-now troublesome detuned gain spectrum into an advantage. There, a technique we call detuned loading is described. It is first shown theoretically that detuned loading should simultaneously cause an increase in modulation speed, suppression of parasitic FM, and reduction of both phase and intensity noise. We then present data taken with a particular detuned loading implementation which verifies some of these predictions.

Work presented in this thesis or related to it has been the subject of the published articles [22-33].

References

[1] R. N. Hall, G. E. Fenner, J. D. Kingsley, T. J. Soltys, and R. O. Carlson, Phys. Rev. Lett., vol. 9, p. 366 (1962).

[2] M. I. Nathan, W. P. Dumke, G. Burns, F. H. Dill, Jr., and G. Lasher, Appl. Phys. Lett., vol. 1, p. 62 (1962).

[3] M. Holonyak and S. F. Bevaqua, Appl. Phys. Lett., vol. 1, p. 82 (1962).

[4] T. M. Quist, R. H. Rediker, R. J. Keyes, W. E. Krag, B. Lax, A. L McWhorter, and H. J. Zeigler, Appl. Phys. Lett., vol. 1, p. 91, (1962).

[5] I. Hayashi and M. B. Panish, Device Research Conference, Seattle, Washington, June 1970.

[6] I. Hayashi, M. B. Panish, P.W. Foy, and S. Sumski, Appl. Phys. Lett., vol. 17, p. 109 (1970).

[7] Zh. I. Alferov, V. M. Andreev, D. Z. Garbuzov, Yu. V. Zhilyaev, E. P. Morozov, E. L. Portnoi, and V. G. Trofim, Sov. Phys. Semicond., vol. 4, p. 1573 (1971) [Translated from Fiz. Tekh. Poluprovodn., vol. 4, p. 1826 (1970)].

[8] A. Yariv, Proc. Esfahan, Symposium on fundamental and applied laser physics, Wiley Interscience, New York p.897, 1973.

[9] K. Inada, IEEE Trans. Microwave Theory Tech., vol. 30, p. 1412, 1982.

[10] N. Bar-chaim, Ch. Harder, J. Katz, S. Margalit, and A. Yariv, Appl. Phys. Lett., vol. 40, p. 556 (1982).

[11] D. Botez, Appl. Phys. Lett., vol. 36, p. 190 (1980).

[12] H. D. Wolf, K. Mettler, and K. H. Zschauer, Jap. J. of Appl. Phys., vol. 20, p. L693 (1981).

[13] W. T. Tsang and R. A. Logan, Electron. Lett., vol. 18, p. 845 (1982).

[14] L. Bickers, L. C. Blank, and S. D. Walker, Electron. Lett., vol. 21, p. 267, (1985).

[15] K. Y. Lau, N. Bar-Chaim, I. Ury, Ch. Harder, and A. Yariv, Appl. Phys. Letts.,

vol. 43, p. 1 (1983).

[16] M. W. Fleming and A. Mooradian, Appl. Phys. Lett., vol. 38, p. 511 (1981).

[17] T. K. Yee, Paper #TUH3 presented at CLEO 1983, Baltimore.

[18] H. C. Casey and M. B. Panish, "Heterostructure lasers," Academic Press, New York, 1978.

[19] H. Kressel and J. K. Butler, "Semiconductor lasers and heterojunction LEDs," Academic Press, New York, 1977.

[20] G. H. B. Thompson, "Physics of semiconductor laser devices," John Wiley and Sons, Chichester, England, 1980.

[21] M. G. A. Bernard and G. Duraffourg, Phys. Stat. Solidi, vol. 1, p. 699 (1961).

[22] K. Vahala, L. C. Chiu, S. Margalit, and A. Yariv, Appl. Phy. Lett., vol. 42, p. 631 (1983).

[23] K. Vahala and A. Yariv, IEEE J. Quantum Electron., vol. QE-19, p. 1096 (1983).

[24] K. Vahala and A. Yariv, IEEE J. Quantum Electron., vol. QE-19, p. 1102 (1983).

[25] K. Vahala and A. Yariv, Phys. Rev. A , vol. 31, no. 6 (1985).

[26] K. Vahala, Ch. Harder, and A. Yariv, Appl. Phys. Lett., vol. 42, p. 211 (1982).

[27] Ch. Harder, K. Vahala, and A. Yariv, Appl. Phys. Lett., vol. 42, p. 328 (1983).

[28] K. Vahala and A. Yariv, Appl. Phys. Lett., vol. 45, p. 501 (1984).

[29] K. Vahala, J. Paslaski and A. Yariv, Appl. Phys. Lett., vol. 46, no. 11 (1985).

[30] K. Vahala and A. Yariv, Appl. Phys. Lett. vol. 43, p. 140 (1983).

[31] A. Yariv and K. Vahala, IEEE J. Quant. Electron., vol. QE-19, p. 889 (1983).

[32] Y. Arakawa, K. Vahala, and A. Yariv, Appl. Phys. Lett., vol. 45, p. 201 (1984).

[33] R. Lang, K. Vahala, and A. Yariv, IEEE J. Quant. Electron., vol. QE-21 (1985).

Chapter 2

Application of an electronic wave-packet formalism to local-operator equations of motion for semiconductor lasers

2.1. Introduction

In studying lasers, it is often necessary to consider interactions between the lasing modes and the active medium locally (i.e., local material equations of motion) rather than in a spatially averaged fashion. Examples of this can be found in a myriad of topics which include intermodal beating, spatial hole burning, and diffusion damping of relaxation oscillations. In most laser systems the development of local equations of motion to study these effects is greatly facilitated by the atomic nature of the active medium. In such cases the individual components of the system, by their spatial smallness, conveniently sample the electron-radiation interaction locally and lead naturally to local rate equations. Exhaustive treatments by Lamb [1] and by Haken [2] can be cited which elegantly illustrate this approach. Unfortunately, there do exist laser systems which do not fall within the scope of these local treatments; these are systems having delocalized eigenstates. A very important example is the semiconductor laser (SL) system in which the preferred state space for all quantum treatments to date has been the electronic Bloch state space (see, for example, Refs. [3-6]). This space leads to convenient selection rules for electron-radiation-induced transitions, but is an extremely awkward space to use for treating local phenomena.

Despite the difficulties involved in formulating a set of local rate equations for SL's from first principles, a large number of treatments do exist which have successfully accounted for many aspects of local phenomena in SL's. These seem to fall into two categories: those which directly apply rate equations derived for gas lasers to the SL case and thus assume forms *a priori* for electron-radiation interaction terms in local rate equations; and those in which a classical electric field interacts with an active layer crystal sliced into small local systems, each quantized with its own Bloch state space [7]. The latter approach, albeit more rigorous than the first, is somewhat artificial and must still treat interactions between local cubical systems in a heuristic fashion. Even with the success of the above methods, one is led to wonder what phenomena are overlooked through their simplicity; a glaring example is their inability to account for quantum fluctuation phenomena.

One goal of this chapter is then to derive from first principles a set of local quantum mechanical equations of motion for a SL. To do this we will work in a space of electronic wave-packet states. These wave-packets have well-defined position and crystal momentum, and are often used as a conceptual tool to justify the tenets of semiclassical solid state theory in which electrons and holes are treated in a classical fashion through the use of concepts such as effective mass, crystal momentum, etc. [8]. In this treatment we will define operators which create and destroy electronic wave-packets within semiclassical phase spaces associated with each energy band of the crystal. The operators so defined will serve as the dynamic variables characterizing the active medium. An exact treatment based on these operators offers no advantage over a treatment based on Bloch states. We will show, however, that for certain classes of quantum interaction potentials, the electron-radiation interaction being one, a perturbation expansion of both matrix elements and operator anticommutators is

possible. The approximation here requires that the system Hamiltonian and the dynamic variables vary slowly in comparison to the extent of an electronic wave-packet (This approximation is satisfied by a variety of interaction potentials and is not restricted to electronic wave-packets; recently, Glushko has employed the approximation in a treatment of exciton-phonon interactions based on an exciton wave-packet state [9]). We will derive operator equations of motion correct to first order in this approximation; higher-order corrections will also be discussed.

As a quantum analog of classical phase space dynamics the electronic wave-packet approach is in direct competition with certain well- established techniques in quantum kinetic theory [10-13]. Of these methods the wave-packet approach is most closely related to the method of second quantization in phase space introduced by Klimontovich [11]. In that method the dynamic variables are quantum fields in phase space whose quantum averages are Wigner distribution functions [10,12]. In the present method it will be seen that certain operator pairs can be interpreted as density operators whose quantum average resembles a first order distribution function (higher-order functions are also possible by taking groups of operator pairs, but these will not be discussed). We intend to contrast these methods elsewhere [14]. Very briefly, however, the method of second quantization in phase space has the advantage of leading naturally to representations which are diagonal in x and p. The wave-packet approach, as a result of the overcompleteness of the electronic wave-packet states, suffers from representations which are diagonal only to first order in the approximation discussed above. In many cases this is a serious disadvantage. When the approximation can be invoked, however, the wave-packet approach can become the preferable method. In the case considered here of electronic motion in a crystal with coupling to the radiation field, this is especially true.

Under these circumstances the Bloch-like character of the electronic wave-packet states makes them approximate eigenstates of the crystal, thus simplifying treatment of both the electron-lattice interaction and the electron-radiation interaction. The second goal of this chapter is to serve as a pedagogic example of the application of this wave-packet formalism to the specific case of the electron-radiation interaction.

2.2 Wave-packet operators and the system Hamiltonian

In this section we define the field operators of the material and the lasing optical modes, and then write the system Hamiltonian in terms of these operators. The field operators of this analysis distinguish it from previous quantum treatments of the SL, giving a local description of the active medium and thus facilitating the treatment of multimode effects as well as transport phenomena. To illustrate some of the difficulties normally encountered in modeling a multimode SL quantum mechanically (besides the obvious problems involving electronic transport) we will first review an approach frequently employed, this being a nonlocal description based on Bloch states. Following this discussion we introduce the field operators of this analysis and their associated anticommutation relations. These operators will be seen to create and destroy electronic wave-packets having well- defined position and crystal momentum, in the same sense as the electronic wave-packets which make up the semiclassical picture of the Bloch electron. Finally, we will derive anticommutation relations and a system Hamiltonian, both correct to first order in the approximation discussed above. During the course of the derivation the limitations of this approximation are discussed and it is also shown how higher-order corrections to the Hamiltonian can be calculated.

A common approach to a quantum description of the electronic system of a semiconductor is to assume a multielectron wavefunction given by a symmetrized product of single electron wavefunctions, as, for instance, can be accomplished using a Slater determinant. Most often the single electron states are taken as Bloch states $\varphi_m(\vec{j},\vec{x})$ (i.e., band index m and crystal momentum wavevector $\vec{j}$; spin is neglected throughout this treatment) which satisfy the single electron Schrodinger equation,

$$\left[T + V\right]\varphi_m(\vec{j},\vec{x}) = \varepsilon_m(\vec{j})\varphi_m(\vec{j},\vec{x}) \tag{2.1}$$

where T is the kinetic energy operator and V describes only the crystal potential (both operators in the $\vec{x}$ representation). Using the basis set of symmetrized Bloch functions, annihilation and creation operators for these electronic states are defined. These operators obey the Fermion anticommutation relations,

$$\left\{a_m(\vec{j},t),a_n^+(\vec{k},t)\right\} = \delta_{mn}D(\vec{j} - \vec{k}) \tag{2.2}$$

$$\left\{a_m(\vec{j},t),a_n(\vec{k},t)\right\} = 0 \tag{2.3}$$

$$\left\{a_m^+(\vec{j},t),a_n^+(\vec{k},t)\right\} = 0 \tag{2.4}$$

where { } represents the operation of anticommutation, δ_{mn} is the Kronecker delta, and $D(\vec{j} - \vec{k})$ is the Dirac delta function (i.e., we assume the crystal is large enough to justify treating the crystal momentum as a continuous quantity). The system Hamiltonian is then expressed in terms of these operators, a simple example being the unperturbed Bloch electron system,

$$H = \sum_{mn} \int d\vec{j} d\vec{k} < m\vec{j} | H | n\vec{k} > a_m^+(\vec{j},t) a_n(\vec{k},t) = \sum_m \int d\vec{j} \varepsilon_m(\vec{j}) a_m^+(\vec{j},t) a_m(\vec{j},t) \qquad (2.5)$$

which is the familiar sum of number operators over all states weighted by the energy of each state. Then, with Hamiltonian and anticommutation relations in hand, the Heisenberg equations of motion can be written for a particular set of self-consistent operators. The final step is to solve these equations of motion.

Several aspects of the above approach make it unsuitable for our purposes. First consider the electron-radiation interaction matrix element,

$$< m\vec{j} | H_I | n\vec{k} > = < m\vec{j} | -\frac{e}{m} \vec{A}(\vec{r},t) \cdot \vec{p} | n\vec{k} > \qquad (2.6)$$

in particular, the treatment of the vector potential $\vec{A}(\vec{r},t)$ spatial dependence in this matrix element. For an atomic system this spatial dependence can be approximated by the vector potential's value at the atom's position (as given say by its nucleus), because the atomic wave states involved in the transition are highly localized in comparison to the scale of the optical wavelength. As such, the resulting matrix element takes on a unique spatial dependence characterized by the optical mode. It is this spatial dependence which leads to spatial hole burning of a gas of inverted atoms or molecules, and which is also of importance in multimode lasers where the spatial dependence of the induced polarization determines, in part, mode coupling. At the opposite extreme are the electronic Bloch states. These states are delocalized, having the well-known translational property,

$$\varphi_m(\vec{j},\vec{x}+\vec{R}) = \varphi_m(\vec{j},\vec{x})e^{i\vec{j}\cdot\vec{R}} \tag{2.7}$$

where $\vec{R}$ is a lattice translation vector. Using this property the matrix element (2.6) can be rewritten as follows:

$$< m\vec{j}|-\frac{e}{m}\vec{A}(\vec{r})\cdot\vec{p}|n\vec{k}> \approx -\frac{e}{m}\sum_{\vec{R}} e^{i(\vec{k}-\vec{j})\cdot\vec{R}}\vec{A}(\vec{R})\cdot < m\vec{j}|\vec{p}|n\vec{k}>_{pc} \tag{2.8}$$

where the integration now takes place over a primitive cell and, as with the atomic system, the slowly (over a unit cell) varying vector potential has been removed from the integral. This leaves only the evaluation of the sum over Crystal translation vectors. Assuming $\vec{A}(\vec{r})$ represents a single longitudinal mode with wavevector $\vec{k}_m'$, it is clear that the sum is strongly peaked for $\vec{k}-\vec{j} = \pm\vec{k}_m'$, which is the selection rule describing a shift in crystal momentum caused by the photon emission or absorption. This shift is relatively small in comparison to the dimensions of the Brillouin zone and therefore it is standard practice to neglect it altogether, resulting in the "k selection rule" for direct optical transitions in a semiconductor. Unfortunately, this rule altogether eliminates the spatial dependence of the optical mode and therefore precludes the study of multimode interactions and effects such as spatial hole burning. If the $\vec{k}_m'$ dependence of the selection rule is retained, then the resulting equations become rather complicated, each mode coupling different pairs of states. It is also obvious that the inclusion of transport phenomena into the model is made very cumbersome by this approach. The aforementioned difficulties have at their root the delocalized nature of the chosen electronic state space.

An inherently local description of the electronic system, which successfully explains many aspects of electronic transport, is semiclassical solid-state theory. In this approach electrons and holes in a crystal are ascribed properties

characteristic of their free classical counterperts (e.g., effective mass, momentum, position, etc.). Such notions greatly simplify the study of transport, but being to a certain extent classical they are either incapable of accounting for certain quantum interactions (e.g., interband transitions) or must be modified heuristically to do so, as, for instance, is done in writing a local carrier density rate equation which includes electron-radiation stimulated recombination terms. From a quantum mechanical viewpoint the semiclassical electron is a wave-packet whose spatial extent is macroscopically small, but microscopically large enough to give the packet a well- defined crystal momentum. Such a wave-packet would encompass several hundred lattice sites along a given direction, thus having a breadth in k-space much narrower than a Brillouin zone (see Fig 2.1). We now explore the use of these quasiclassical wave-packets as a basis set instead of Bloch states. By themselves these new states will not improve matters over an analysis based on Bloch states; in fact, they will appear at first to be a complication. Combined with an approximation, discussed later in the Section, however, a significant simplification of the problem occurs. With the approximation, the wave-packet states allow us to extend the semiclassical picture of the electron to rigorously account for certain classes of perturbing potentials while maintaining quantum mechanical consistency.

The Bloch states and their respective annihilation and creation operators will be used as a tool to develop the quasi-classical wave-packet states and their respective annihilation and creation operators. To begin we define a quasi-classical wave-packet localized about $\vec{x}$ and $\vec{k}$ in the m^{th} band as,

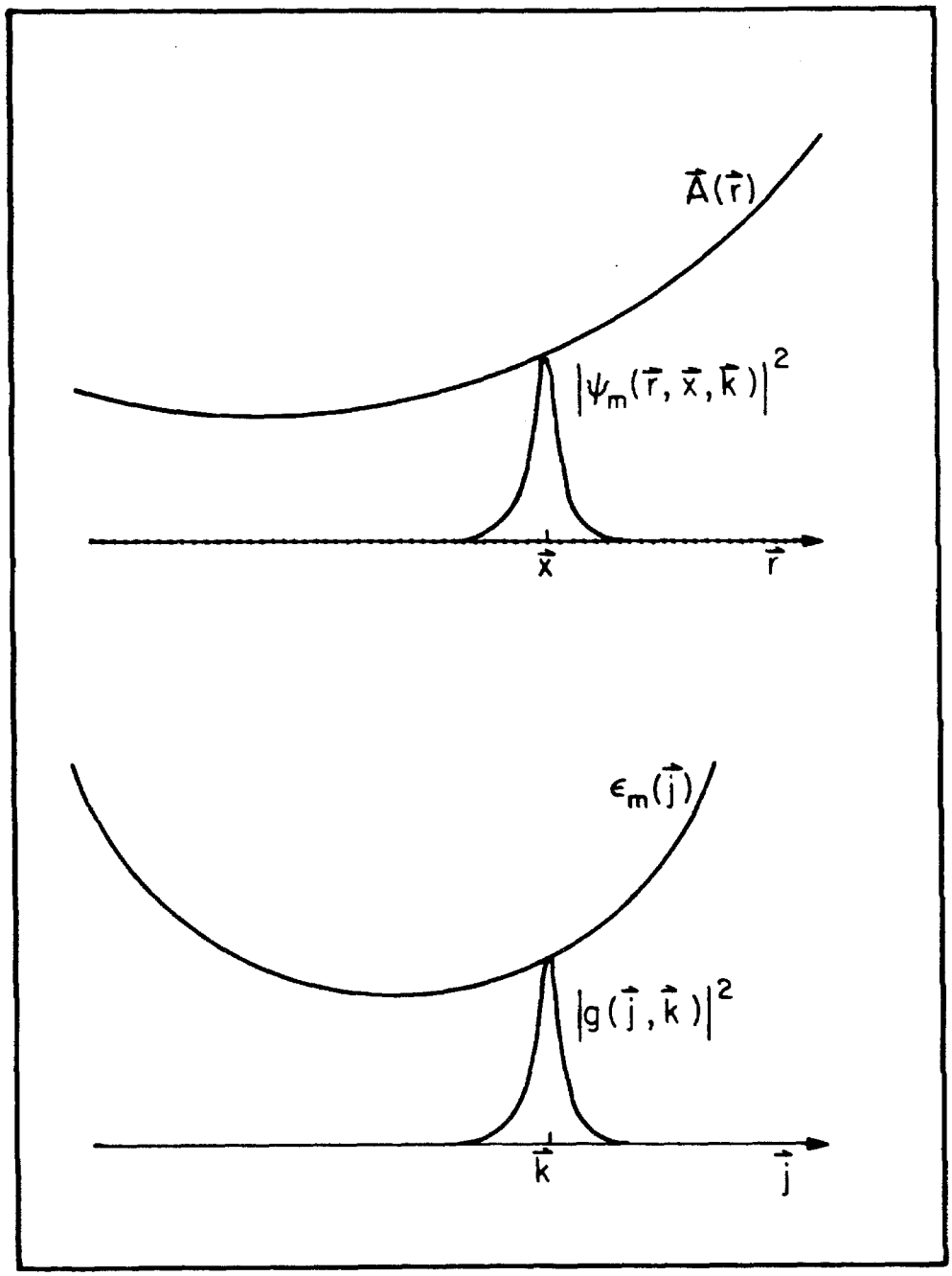

Figure 2.1 Projection of a single particle wave-packet state onto real $|\vec{r}>$ space (upper plot) and Bloch space $|m,\vec{j}>$ (lower plot). The wave-packet is macroscopically small so that it effectively samples the vector potential $\vec{A}(\vec{r})$ locally, but is microscopically large enough to retain "Bloch" character and have a well-defined crystal momentum and energy.

$$|\psi(m,\vec{x},\vec{k})> \equiv \int d\vec{j}\, g(\vec{j},\vec{k}) e^{-i\vec{j}\cdot\vec{x}} |m\vec{j}> \tag{2.9}$$

where the integration is over the Brillouin zone and where $g(\vec{j},\vec{k})$ is a crystal momentum weighting function localized on $\vec{k}$; the exact nature of this weighting function is unimportant for our purposes, so long as it leads to an electronic wave-packet in the sense discussed above. In Fig. 2.1 we show the general shape of $|g(\vec{j},\vec{k})|^2 = |< m,\vec{j}|\psi(m,\vec{x},\vec{k})>|^2$ and $|\psi_m(\vec{r},\vec{x},\vec{k})|^2 \equiv |<\vec{r}|\psi(m,\vec{x},\vec{k})>|^2$. Both are localized functions in comparison to variations of the Hamiltonian which include variations of the unperturbed Bloch energy function $\varepsilon_m(\vec{j})$ and variations of the perturbation energy brought about through the vector potential $\vec{A}(\vec{r})$. Expression (2.9) transforms our picture from one based on the variable $\vec{j}$ within a given band m to one based on the variables $(\vec{x},\vec{k})_m$ which represent the semiclassical "center of mass" position (in real and crystal wavevector space) of a wave-packet in band m. In this picture each band has associated with it a semiclassical phase space in which wave-packets appear highly localized. Inter-band transitions represent particle exchanges between the phase spaces. It is straightforward to verify that the wave-packet states satisfy the completeness relation,

$$\sum_m \int d\vec{x} d\vec{k}\, |\psi(m,\vec{x},\vec{k})> < \psi(m,\vec{x},\vec{k})| = \sum_m \int d\vec{j}\, |m\vec{j}> < m\vec{j}| = I \tag{2.10}$$

provided

$$(2\pi)^3 \int d\vec{k}\, |g(\vec{j},\vec{k})|^2 = 1 \tag{2.11}$$

where I is the identity operator. As is often true for quasi-classical states in general, the wave-packet states are not orthogonal; from (2.9) we calculate,

$$< \psi(m,\vec{x},\vec{k}) | \psi(n,\vec{x}',\vec{k}') > = \delta_{mn} \int d\vec{j}\, g^*(\vec{j},\vec{k}') g(\vec{j},\vec{k}) e^{i\vec{j}\cdot(\vec{x}-\vec{x}')} \quad . \tag{2.12}$$

Thus, wave-packets in different bands are orthogonal, but within a given band are not. It is obvious, however, that packets sufficiently well separated in a given phase space $(\vec{x},\vec{k})_m$ are approximately orthogonal. As a specific case consider a weighting function $g(\vec{j},\vec{k})$ with a Gaussian shape given by,

$$g(\vec{j},\vec{k}) = \frac{\sigma^{3/2}}{(2\pi)^{9/4}} e^{-\frac{\sigma^2}{4}|\vec{j}-\vec{k}|^2} \tag{2.13}$$

where σ has units of length in x-space and will be seen momentarily to give the approximate spatial breadth of a wave-packet. (2.13) has been normalized in accordance with (2.11) and when substituted into (2.12) yields,

$$< \psi(m,\vec{x},\vec{k}) | \psi(m,\vec{x}',\vec{k}') > = \frac{1}{(2\pi)^3} e^{\frac{i}{2}(\vec{k}+\vec{k}')\cdot(\vec{x}-\vec{x}')} e^{-\frac{\sigma^2}{8}|\vec{k}-\vec{k}'|^2} e^{-\frac{1}{2\sigma^2}|\vec{x}-\vec{x}'|^2} \tag{2.14}$$

where in calculating this expression we have extended the limits of integration in (2.12) to infinity. Eqn. (2.14) shows clearly that as wave-packets of this prescribed form become more separated within a given phase space, they also appear to be more orthogonal. We can also use (2.13) to calculate the approximate spatial dependence for such a Gaussian wave-packet. Using (2.9) we find the following,

$$\psi_m(\vec{r},\vec{x},\vec{k}) \equiv < \vec{r} | \psi(m,\vec{x},\vec{k}) > = \left(\frac{2}{\pi\sigma^2}\right)^{3/4} e^{-\frac{1}{\sigma^2}|\vec{r}-\vec{x}|^2 - i\vec{k}\cdot\vec{x}} \varphi_m(\vec{k},\vec{r}) \tag{2.15}$$

where we have assumed that the lattice periodic part of the Bloch state varies slowly with respect to $\vec{k}$. This expression shows that the Gaussian wave-packet exhibits a Bloch state spatial dependence weighted by a Gaussian envelope function. This obvious result is in direct analogy to the minimum uncertainty wave-

packet states which can be easily derived for a free particle [15]. The reader is also referred to a discussion of minimum uncertainty packets by Stoler [16].

We now return to a discussion of wave-packet states in general and define field operators associated with these states. These operators are given by,

$$\psi(m,\vec{x},\vec{k},t) \equiv \int d\vec{j}\; g^{*}(\vec{j},\vec{k})e^{i\vec{j}\cdot\vec{x}}a_m(\vec{j},t) \tag{2.16}$$

$$\psi^{+}(m,\vec{x},\vec{k},t) \equiv \int d\vec{j}\; g(\vec{j},\vec{k})e^{-i\vec{j}\cdot\vec{x}}a_m^{+}(\vec{j},t) \tag{2.17}$$

with associated anticommutation relations,

$$\left\{\psi(m,\vec{x},\vec{k},t),\psi^{+}(n,\vec{x}',\vec{k}',t)\right\} = \delta_{mn}\langle\, \psi(m,\vec{x},\vec{k})\,|\,\psi(m,\vec{x}',\vec{k}')\rangle \tag{2.18}$$

$$\left\{\psi(m,\vec{x},\vec{k},t),\psi(n,\vec{x}',\vec{k}',t)\right\} = 0 \tag{2.19}$$

$$\left\{\psi^{+}(m,\vec{x},\vec{k},t),\psi^{+}(n,\vec{x}',\vec{k}',t)\right\} = 0 \tag{2.20}$$

which are easily verified using (2.2), (2.3),and (2.4); and (2.12), (2.16), and (2.17). $\psi^{+}(m,\vec{x},\vec{k},t)$ and $\psi(m,\vec{x},\vec{k},t)$ can be interpretted as operators which create and destroy a wave-packet $|\psi(m,\vec{x},\vec{k})\rangle$, a simple test of which is to apply $\psi^{+}(m,\vec{x},\vec{k},t)$ to the vacuum state $|0\rangle$. In addition, by using (2.16) and (2.17), we can also show that,

$$\int d\vec{x}d\vec{k}\psi^{+}(m,\vec{x},\vec{k},t)\psi(m,\vec{x},\vec{k},t) = \int d\vec{j}a_{m}^{+}(\vec{j},t)a_{m}(\vec{j},t) \tag{2.21}$$

from which $\psi^{+}(m,\vec{x},\vec{k},t)\psi(m,\vec{x},\vec{k},t)$ is interpreted as an operator giving the number density of electrons at a point $(\vec{x},\vec{k})_m$ in the phase space associated with band m.

As is the case with $a_m^{+}(\vec{j},t)$ and $a_m(\vec{j},t)$, any operator can be expressed in terms of $\psi^{+}(m,\vec{x},\vec{k},t)$ and $\psi(m,\vec{x},\vec{k},t)$. Consider, for example, a one-body Hamiltonian. Using completeness relation (2.10) twice we find,

$$H = \sum_{mn}\int d\vec{x}d\vec{x}'d\vec{k}d\vec{k}'M_{mn}(\vec{x},\vec{x}',\vec{k},\vec{k}')\psi^{+}(m,\vec{x},\vec{k},t)\psi(n,\vec{x}',\vec{k}',t) \tag{2.22}$$

where a matrix element connecting points $(\vec{x},\vec{k})_m$ and $(\vec{x}',\vec{k}')_n$ in phase spaces m and n has been defined as,

$$M_{mn}(\vec{x},\vec{x}',\vec{k},\vec{k}') \equiv \langle \psi(m,\vec{x},\vec{k})\,|H|\,\psi(n,\vec{x}',\vec{k}')\rangle \quad . \tag{2.23}$$

To conclude the definitions associated with the wave-packet states we give the inverted forms of (2.9), (2.16) ,and (2.17). They are:

$$|m\vec{j}\rangle = \int d\vec{x}d\vec{k}\; g^{*}(\vec{j},\vec{k})e^{i\vec{j}\cdot\vec{x}}\,|\psi(m,\vec{x},\vec{k})\rangle \tag{2.24}$$

$$a_m^{+}(\vec{j},t) = \int d\vec{x}d\vec{k}\; g^{*}(\vec{j},\vec{k})e^{i\vec{j}\cdot\vec{x}}\psi^{+}(m,\vec{x},\vec{k},t) \tag{2.25}$$

$$a_m(\vec{j},t) = \int d\vec{x}d\vec{k}\; g(\vec{j},\vec{k})e^{-i\vec{j}\cdot\vec{x}}\psi(m,\vec{x},\vec{k},t) \quad . \tag{2.26}$$

In contrast to the electronic system, each lasing mode will be treated using the standard delocalized annihilation and creation operators which result from quantizing a noninteracting optical mode (for an alternate approach related to the wave-packet formalism of this treatment, see Ref. [17] which contains an

interesting application of optical wave-packet operators). Proceeding in the normal fashion we quantize the vector potential as,

$$\vec{A}(\vec{r},t) = \sum_l \left[\frac{\hbar}{2\varepsilon\omega_l}\right]^{\frac{1}{2}} \left[b_l(t) + b_l^+(t)\right]\vec{u}_l(\vec{r}) \tag{2.27}$$

where,

$$\int d\vec{r}\,\vec{u}_l(\vec{r})\cdot\vec{u}_m(\vec{r}) = \delta_{lm} \tag{2.28}$$

$$\left[b_l(t), b_m^+(t)\right] = \delta_{lm} \tag{2.29}$$

$$\left[b_l(t), b_m(t)\right] = 0 \tag{2.30}$$

$$\left[b_l^+(t), b_m^+(t)\right] = 0 \tag{2.31}$$

and where [ ] signifies commutation. This simplified approach neglects any spatial modification of the mode which results from its interaction with the gain medium. For facet reflectivities greater than 30%, however, these modifications are not severe [18].

The model envisioned throughout this analysis is typical of state of the art double heterostructure SL's. In it, an active layer, having optical and carrier confining qualities, has properties which are described in terms of the electronic wave-packet operators discussed above. The wave-packets interact with the optical modes via dipole transitions and also with bulk crystal wave-packets, phonons, crystal defects, and among themselves by various scattering mechanisms which produce the observed transport phenomena. The lasing modes, besides interacting with the electronic wave-packets in the crystal, also interact with the free radiation modes since the resonator has a finite Q. Even though nearly all

of these aspects of the model will eventually be accounted for in this treatment, the "system" in our model consists only of the active layer wave-packets and the lasing optical modes. All other interactions will be referred to as bath interactions; and damping and fluctuations which result from these interactions will be included by using the quantum mechanical fluctuation dissipation theorem which is discussed in Section 2.3. As such, the system Hamiltonian accounts only for the noninteracting electronic wave-packets, the lasing modes, and the mutual interaction between these subsystems. Using the one-body representation (2.22), this Hamiltonian is given by,

$$H = \sum_{mn} \int d\vec{x} d\vec{x}' d\vec{k} d\vec{k}' M^{e}_{mn}(\vec{x},\vec{x}',\vec{k},\vec{k}') \psi^{+}(m,\vec{x},\vec{k},t) \psi(n,\vec{x}',\vec{k}',t) + \tag{2.32}$$

$$\sum_{mn} \int d\vec{x} d\vec{x}' d\vec{k} d\vec{k}' M^{I}_{mn}(\vec{x},\vec{x}',\vec{k},\vec{k}') \psi^{+}(m,\vec{x},\vec{k},t) \psi(n,\vec{x}',\vec{k}',t) +$$

$$\sum_{l} \hbar\omega_l \left(b_l^{+}(t) b_l(t) + \frac{1}{2} \right)$$

where M^{e}_{mn} is the free electron part,

$$M^{e}_{mn}(\vec{x},\vec{x}',\vec{k},\vec{k}') \equiv \langle \psi(m,\vec{x},\vec{k}) | \left[T + V \right] | \psi(n,\vec{x}',\vec{k}') \rangle \tag{2.33}$$

and M^{I}_{mn} is the electron-radiation interaction part,

$$M^{I}_{mn}(\vec{x},\vec{x}',\vec{k},\vec{k}') \equiv \langle \psi(m,\vec{x},\vec{k}) | -\frac{e}{m} \vec{A}(\vec{x}) \cdot \vec{p} | \psi(n,\vec{x}',\vec{k}') \rangle \tag{2.34}$$

These matrix elements give transition amplitudes between points $(\vec{x},\vec{k})_m$ and $(\vec{x}',\vec{k}')_n$ in the semiclassical phase spaces. In their present form, however, they appear only to complicate matters over a treatment based on Bloch states. To benefit from this formalism two approximations must be made. Both take

advantage of the localization in $\vec{x}$ and $\vec{k}$ of the electronic wave-packet states. The first is an approximation of the electronic matrix elements. For M^e_{mn} we write,

$$M^e_{mn}(\vec{x},\vec{x}',\vec{k},\vec{k}') \approx \varepsilon_m(\vec{k}) < \psi(m,\vec{x},\vec{k}) | \psi(m,\vec{x}',\vec{k}') > \delta_{mn} \quad ; \tag{2.35}$$

that is, we assume the wave-packet states are approximately electronic eigenstates of the unperturbed crystal. Such an assumption is justified provided the wave-packet states span only a small volume in crystal momentum space. For M^I_{mn} we write,

$$M^I_{mn}(\vec{x},\vec{x}',\vec{k},\vec{k}',t) \approx -\frac{e}{m}\sum_l \left(\frac{\hbar}{2\varepsilon\omega_l}\right)^{\frac{1}{2}} \left(b_l + b_l^+\right) \vec{u}_l(\vec{x}) \cdot < \psi(m,\vec{x},\vec{k}) | \vec{p} | \psi(n,\vec{x}',\vec{k}') > \tag{2.36}$$

$$\approx \sum_l h_{mn}(\vec{k}) u_l(\vec{x}) \left(b_l + b_l^+\right) < \psi(m,\vec{x},\vec{k}) | \psi(m,\vec{x}',\vec{k}') > \tag{2.36a}$$

where the vector nature of $\vec{u}_l(\vec{x})$ has been absorbed into $h_{mn}(\vec{k})$. In (2.36), the slowly varying spatial dependence of the optical field in comparison to the electronic wave-packets has been used to remove the optical space variation $\vec{u}(\vec{r})$ outside the wave-packet bras and kets - the same approximation which comprises the dipole approximation in an atomic system. In (2.36a), the well-defined momentum of the wave-packets has been used again. Here we approximate a "k" conserving interband absorption or emission of a photon as a transition $(\vec{x},\vec{k})_m \rightarrow (\vec{x},\vec{k})_n$ between phase spaces m and n which conserves the semiclassical crystal momentum and in addition leaves the electron position unchanged. That is, the wave-packets are assumed to have enough "Bloch" character, by virtue of their microscoptic largeness in $\vec{x}$ space, so that a "k" conserving transition between Bloch states remains approximately a "k" conserving transition between wave-packet states (see Fig. 2.2). To first order the quantities

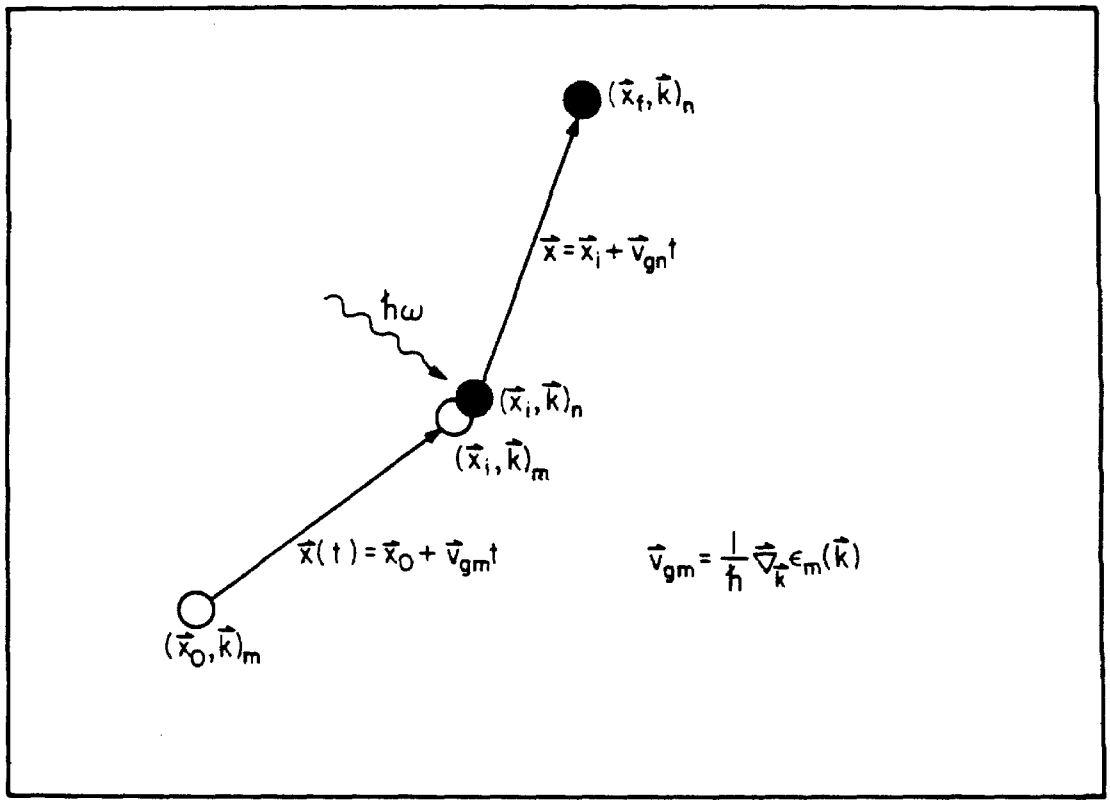

Figure 2.2 Intuitive picture of photon absorption by a wave-packet propagating in band m with group velocity $\vec{v}_{gm}(\vec{k})$ resulting in creation of a wave-packet in band n having group velocity $\vec{v}_{gn}(\vec{k})$ (and anihilation of the wave-packet in band m).

$\varepsilon_m(\vec{k})$ and $h_{mn}(\vec{k})$ are, in fact, the quantities found using the true Bloch eigenstates; the discrepency becoming smaller as the electronic wave-packets encompass larger volumes of the crystal. On the other hand, this volume cannot become so large that optical mode features or transport features become imperceptible. Thus, the spatial breadth σ of the electronic wave-packets must satisfy,

$$a << \sigma << \text{Min}(\lambda,\lambda_D) \tag{2.37}$$

where a is a typical lattice constant, λ is the optical wavelength in the crystal, and λ_D is the diffusion length. This, of course, is just the condition for wave-packet microscopic largeness and macroscopic smallness which was discussed earlier. Higher-order corrections to the matrix elements can be calculated by using (2.9) combined with Taylor expansion of the Hamiltonian about the center of mass coordinates. As an example, the first two terms in such an expansion of Eqn. (2.33) are shown below.

$$M^e_{mn}(\vec{x},\vec{x}',\vec{k},\vec{k}') = \delta_{mn}\varepsilon_m(\vec{k})\langle \psi(m,\vec{x},\vec{k}) | \psi(m,\vec{x}',\vec{k}')\rangle + \tag{2.38}$$

$$\delta_{mn}e^{i\vec{k}\cdot\vec{\xi}}\left(\vec{\nabla}_{\vec{k}}\varepsilon_m(\vec{k})\cdot\vec{\nabla}_{\vec{\xi}}\right)e^{-i\vec{k}\cdot\vec{\xi}}\langle \psi(m,\vec{x},\vec{k}) | \psi(m,\vec{x}',\vec{k}')\rangle$$

where $\vec{\xi} \equiv \vec{x} - \vec{x}'$.

Provided condition (2.37) holds, the wave-packet states appear highly localized in the various phase spaces in comparison to variations of the Hamiltonian. This also implies that the dynamic variables will vary slowly, allowing the following additional approximation to be made,

$$< \psi(m,\vec{x},\vec{k}) | \psi(n,\vec{x}',\vec{k}') > \rightarrow M\delta_{mn}D(\vec{x}-\vec{x}')D(\vec{k}-\vec{k}') \quad . \tag{2.39}$$

Basically, this is a multipole expansion of $< \psi(m,\vec{x},\vec{k}) | \psi(n,\vec{x}',\vec{k}') >$ in which only the first term is retained. The coefficient M is the monopole term in this expansion and will depend on the specific form chosen for the wave-packet states. For simplicity, we take M=1 in this analysis. In retaining only the first term in the multipole expansion, we are in a sense taking the analysis to the semiclassical picture of the Bloch electron. Unlike the semiclassical picture, however, we now have a means of including interband transitions and other quantum transitions satisfying condition (2.37) in a quantum mechanically rigorous fashion. In addition, the Pauli exclusion principle is maintained through the anticommutation relations,

$$\left\{\psi(m,\vec{x},\vec{k},t),\psi^{+}(n,\vec{x}',\vec{k}',t)\right\} = \delta_{mn}D(\vec{x}-\vec{x}')D(\vec{k}-\vec{k}') \tag{2.40}$$

$$\left\{\psi(m,\vec{x},\vec{k},t),\psi(n,\vec{x}',\vec{k}',t)\right\} = 0 \tag{2.41}$$

$$\left\{\psi^{+}(m,\vec{x},\vec{k},t),\psi^{+}(n,\vec{x}',\vec{k}',t)\right\} = 0 \tag{2.42}$$

where the first relation is an approximation of (2.18) using (2.39), but the latter two relations remain exact.

Using (2.35) and (2.36) in (2.32) and then simplifying the result using (2.39), gives for the system Hamiltonian,

$$H = \sum_m \int d\vec{x} d\vec{k} \varepsilon_m(\vec{k}) \psi^+(m,\vec{x},\vec{k},t) \psi(m,\vec{x},\vec{k},t) + \tag{2.43}$$

$$\sum_l \hbar\omega_l \left[b_l^+(t) b_l(t) + \frac{1}{2} \right] +$$

$$\sum_{lmn} \int d\vec{x} d\vec{k} h_{mn}(\vec{k}) u_l(\vec{x}) \left[b_l(t) + b_l^+(t) \right] \psi^+(m,\vec{x},\vec{k},t) \psi(n,\vec{x},\vec{k},t) \quad .$$

We specialize this Hamiltonian to a two-band model (see Fig 2.3),

$$H = \int d\vec{x} d\vec{k} \left[\varepsilon_c(\vec{k}) \psi_c^+ \psi_c + \varepsilon_v(\vec{k}) \psi_v^+ \psi_v \right] + \tag{2.44}$$

$$\sum_l \hbar\omega_l \left[b_l^+ b_l + \frac{1}{2} \right] +$$

$$\sum_l \int d\vec{x} d\vec{k} u_l(\vec{x}) \left[b_l + b_l^+ \right] \left[h(\vec{k}) \psi_c^+ \psi_v + h^*(\vec{k}) \psi_v^+ \psi_c \right]$$

where coordinate and temporal dependences have been suppressed in the dynamic variables.

2.3 Equations of motion

The system Hamiltonian (2.44) includes the unperturbed energy terms of the Bloch electrons and the lasing modes as well as their interaction energy. The time evolution predicted by this Hamiltonian represents a zeroth order description of the laser, which although able to account for stimulated emission and absorption is seriously deficient in describing areas such as pumping and cavity loss. The missing terms in the system Hamiltonian responsible for these effects and others come under the heading of bath interactions: additional energy terms stemming from scattering of the system with other systems having a large number of degrees of freedom. The complete time evolution equation for

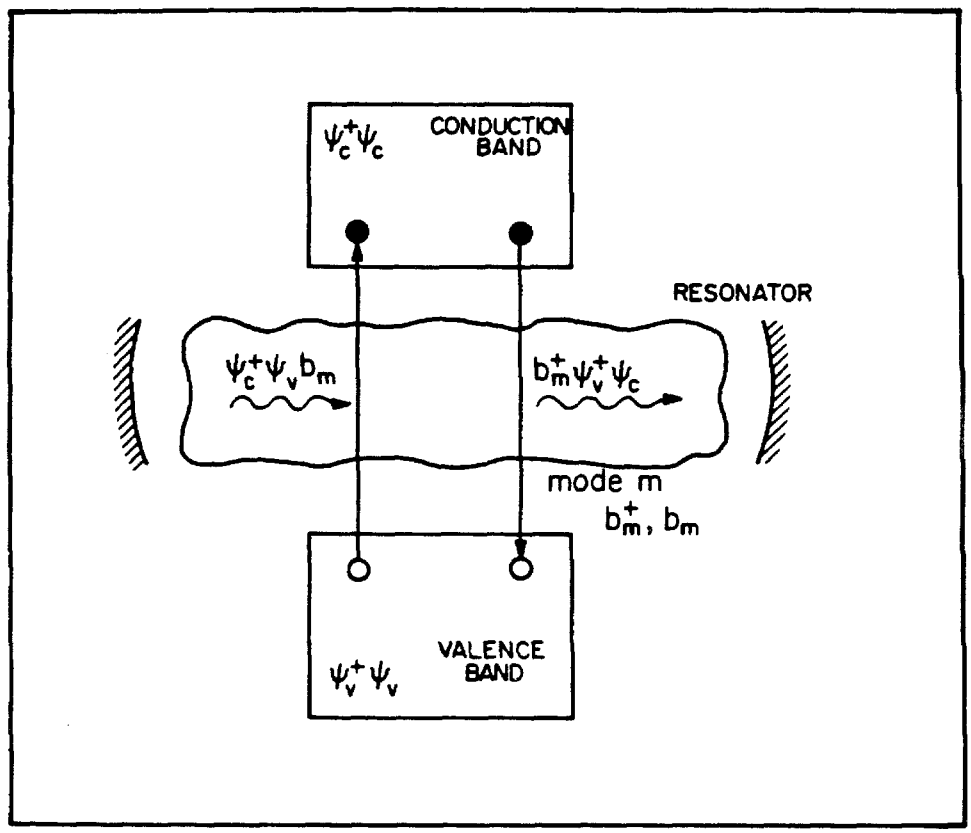

Figure 2.3 Schematic of model system for a semiconductor laser showing components and dynamic variables. Bath interactions are not included.

an operator A could thus be envisioned as,

$$\frac{dA}{dt} = \frac{\iota}{\hbar}\left[H_o + H_I + H_B, A\right] \tag{3.1}$$

where H_o and H_I are the unperturbed energy and interaction energy terms in the system Hamiltonian (2.44) and H_B comprises the various bath interactions. In this section we will develop a set of operator equations of motion governing lasing action and transport phenomena in SL's. We incorporate bath interactions into these equations in a standard way which is described below.

The concepts of system and bath are of profound importance in thermodynamics and statistical mechanics. The system lies at the focus of attention; its thermodynamic state variables or dynamic variables, as the case may be, are to be measured or calculated. The bath, on the other hand, has consequence only through changes it causes in the system by interacting with it. It is normally assumed to have a well-defined thermodynamic state, which, owing to its enormous size relative to the system, is unaffected by interaction with the system. These definitions put no restriction on the system so long as the bath or baths it interacts with can be chosen to be much larger than the system. In the present case, however, we assume the label "system" to imply, in addition to the above properties, an analytically managable set of dynamic variables; specifically, the operators $\psi_c^+\psi_c$, $\psi_v^+\psi_v$, $\psi_v^+\psi_c$, $\{b_l^+\}$, and $\{b_l\}$ which under the system Hamiltonian (2.44) constitute a self-consistent set. These operators interact with three independent baths: the conduction band, valence band, and free radiation baths. For the moment we consider the effect of these bath interactions in the absence of interactions between the components of the system (i.e., setting $H_I = 0$ in (3.1)). Without any interactions (i.e., setting $H_I = 0$ and $H_B = 0$), the system equations of motion are,

$$\dot{b}_l^+ = \imath\omega_l b_l^+ \tag{3.2}$$

$$\frac{d\psi_c^+\psi_v}{dt} = \imath\Omega(\vec{k})\psi_c^+\psi_v \tag{3.3}$$

$$\frac{d\psi_c^+\psi_c}{dt} = 0 \tag{3.4}$$

$$\frac{d\psi_v^+\psi_v}{dt} = 0 \tag{3.5}$$

where,

$$\Omega(\vec{k}) \equiv \frac{\varepsilon_c(\vec{k}) - \varepsilon_v(\vec{k})}{\hbar} \tag{3.6}$$

and where equations for b_l and $\psi_v^+\psi_c$ are merely the Hermitian adjoints of (3.2) and (3.3). Bath terms in the Hamiltonian affect these equations first by driving the equilibration or damping of the dynamic variables and second by superimposing fluctuations on their damped motion. Damping results from the enormous number of degrees of freedom in the various baths, making it highly unlikely that energy leaking out of the system will return from the baths. Fluctuations, on the other hand, are the result of bath energy which "couples into" or "pumps" the system. The basic problem is to incorporate these two aspects of the system-bath interaction into the equations of motion. One approach to this problem is to consider the system-bath interaction explicitly. It is clear, however, that in most cases such an approach is prohibitively complicated. Another approach, the one employed here, is to add damping phenomenologically to the system equations of motion and then to determine fluctuations with the quantum mechanical fluctuation dissipation theorem. We give only a basic outline of this theorem below, deferring a more rigorous explanation to comprehensive treatments of the subject by Lax [19] and Haken et. al. [20]. Our particular

formulation follows Lax's treatment.

The fluctuation dissipation theorem has both classical and quantum forms. In both cases it accounts for fluctuations caused by thermal energy coupling into a chosen system from a bath. In the quantum case, however, it is also essential to preserving the quantum mechanical nature of the damped system by maintaining the canonical commutation relations of the dynamic variables. The theorem presumes that damping can be incorporated in some way into the dynamic equations (normally phenomenologically). The mean (i.e., quantum average over all baths) motion of the dynamic variables $\{A_i\}$ is then given by,

$$\frac{d<A_i>}{dt} = <\Gamma_i\left(\{A_j\}\right)> \tag{3.7}$$

where $\{\Gamma_i\}$ are a set of transport functions which include damping. The unaveraged form of (3.7) contains a fluctuation operator to account for the thermal nature of the bath energy which couples into the system. Thus, the unaveraged form of (3.7) appears as follows,

$$\frac{dA_i}{dt} = \Gamma_i\left(\{A_j\}\right) + f_i(t) \tag{3.8}$$

where, on account of (3.7), the fluctuation operator $f_i(t)$ must vanish upon bath averaging,

$$<f_i(t)> = 0 \quad . \tag{3.9}$$

The stochastic operators $\{f_i(t)\}$ are normally assumed to be Gaussian, resulting from a central limit argument, and in addition Markovian,

$$< f_i(t + \tau)f_i(t)> = W_{ij}D(\tau) \tag{3.10}$$

where the normalization coefficient W_{ij} is often referred to as a generalized diffusion constant since it does, in fact, so function in Einstein's model of Brownian motion. (Note: in this analysis we will assume the fluctuation operators are delta correlated in phase space as well as in time). The final and most important part of the fluctuation dissipation theorem is that this diffusion constant can be determined from knowledge of the transport function in (3.7) by employing the generalized Einstein relation,

$$W_{ij} = \frac{d< A_iA_j>}{dt} - < \Gamma_i\left(\{A_k\}\right)A_j> - < A_i\Gamma_j\left(\{A_k\}\right)> \tag{3.11}$$

which can be derived quite readily from (3.6) and (3.10).

To recapitulate this approach consider the problem of incorporating damping and fluctuations into the optical field equation (see also [2]). Reasonable selections for damped unpumped optical field equatons are,

$$\dot{b}_l^+ = (\iota\omega_l - \frac{1}{2\tau_l})b_l^+ + g_l^+(t) \tag{3.12}$$

$$\dot{b}_l = (-\iota\omega_l - \frac{1}{2\tau_l})b_l + g_l(t) \tag{3.13}$$

where τ_l is the photon lifetime of lasing mode l in the unpumped cavity, and g_l^+ and g_l are the fluctuation operators. To normalize these operators, the transport terms in (3.12) and (3.13) are used in the generalized Einstein relation. In steady state the results are,

$$< g_l(t+\tau)g_m(t)> \ = 0 \tag{3.14}$$

$$< g_l^+(t+\tau)g_m^+(t)> \ = 0 \tag{3.15}$$

$$< g_l^+(t+\tau)g_m(t)> \ = \frac{1}{\tau_l}< b_l^+ b_m> D(\tau) = \frac{n_l}{\tau_l}D(\tau)\delta_{lm} \tag{3.16}$$

$$< g_l(t+\tau)g_m^+(t)> \ = \frac{1}{\tau_l}< b_l b_m^+> D(\tau) = \frac{n_l+1}{\tau_l}D(\tau)\delta_{lm} \tag{3.17}$$

where $n_l \equiv < b_l^+ b_l>$ is the number of thermal photons in the optical mode l as given by,

$$n_l = \frac{1}{e^{\hbar\omega_l/k_b T_R} - 1} \ . \tag{3.18}$$

T_R here is the temperature of the free radiation bath. It should be noted that lack of commutability between b_l^+ and b_l is reflected in the Einstein relations (3.16) and (3.17). This fact is central to preserving the quantum nature of b_l^+ and b_l in the damped system.

Both damping and fluctuations are introduced into Equations (3.3), (3.4), and (3.5) as follows:

$$\frac{d\psi_c^+\psi_v}{dt} = \left\{\iota\Omega(\vec{k}) - \gamma(\vec{x},\vec{k})\right\}\psi_c^+\psi_v + \Delta(\vec{x},\vec{k},t) \tag{3.19}$$

$$\frac{d\psi_c^+\psi_c}{dt} = -\frac{\psi_c^+\psi_c - f_c}{\tau_c(\vec{x},\vec{k})} + L_c(\vec{x},\vec{k},t) \tag{3.20}$$

$$\frac{d\psi_v^+\psi_v}{dt} = -\frac{\psi_v^+\psi_v - f_v}{\tau_v(\vec{x},\vec{k})} + L_v(\vec{x},\vec{k},t) \quad . \tag{3.21}$$

Each of these equations is driven by a Langevin fluctuation operator which is in general a function of time and location in the appropriate phase space. The second moments of these Langevin operators, found using (3.11), appear below:

$$< \Delta^+(\vec{x},\vec{k},t+\tau)\Delta^+(\vec{x}',\vec{k}',t)> \; = 0 \tag{3.22}$$

$$< \Delta^+(\vec{x},\vec{k},t+\tau)\Delta(\vec{x}',\vec{k}',t)> \; = 2\gamma f_v(1-(2\pi)^3 f_c)D(\vec{x}-\vec{x}',\vec{k}-\vec{k}',\tau) \tag{3.23}$$

$$< \Delta(\vec{x},\vec{k},t+\tau)\Delta^+(\vec{x}',\vec{k}',t)> \; = 2\gamma f_c(1-(2\pi)^3 f_v)D(\vec{x}-\vec{x}',\vec{k}-\vec{k}',\tau) \tag{3.24}$$

$$< L_c(\vec{x},\vec{k},t+\tau)L_c(\vec{x}',\vec{k}',t)> \; = \frac{2}{\tau_c} f_c(1-(2\pi)^3 f_c)D(\vec{x}-\vec{x}',\vec{k}-\vec{k}',\tau) \tag{3.25}$$

$$< L_v(\vec{x},\vec{k},t+\tau)L_v(\vec{x}',\vec{k}',t)> \; = \frac{2}{\tau_v} f_v(1-(2\pi)^3 f_v)D(\vec{x}-\vec{x}',\vec{k}-\vec{k}',\tau) \tag{3.26}$$

$$< L_c(\vec{x},\vec{k},t+\tau)L_v(\vec{x}',\vec{k}',t)> \; = 0 \quad . \tag{3.27}$$

Damping parameters also, in general, have a phase space dependence caused by energy dependent scattering rates and spatial inhomogeneities, such as a nonuniform carrier density. The damping parameter $\gamma(\vec{x},\vec{k})$ describes collisionally induced loss of polarization between states in a transition. Between Bloch states in the conduction and valence bands the time γ^{-1} is thought to be roughly 0.1 psec [7].

The damping form assumed in (3.20) and (3.21) is characteristic of the relaxation time approximation [8]. These terms give the relaxation rate of $\psi_c^+\psi_c$ and $\psi_v^+\psi_v$ to their local quasi-equilibrium forms given by f_c and f_v where, for example,

$$< f_c > \equiv \frac{1}{(2\pi)^3} \frac{1}{e^{(\varepsilon_c(\vec{k}) - \eta_c(\vec{x},t))/k_b T(\vec{x},t)} + 1} \tag{3.28}$$

is the quasi-Fermi distribution function for the conduction band with associated temporally and spatially varying temperature and electrochemical potential (to allow for the possibility of internal electric potentials). The factor involving $(2\pi)^3$ is a normalization which enters into this expression since f_c and f_v as well as $\psi_c^+\psi_c$ and $\psi_v^+\psi_v$ represent occupancy densities in $(\vec{x},\vec{k})$ phase spaces. In SL's local quasi-equilibrium is established extremely rapidly by intraband scattering. The phenomenalogical relaxation times for this thermalization within each band are the $\tau_c(\vec{x},\vec{k})$ and $\tau_v(\vec{x},\vec{k})$ appearing in (3.20) and (3.21). These times are generally thought to lie in the range 0.1 to 1.0 psec [21]. To be strictly correct we should also include thermal generation and spontaneous recombination rate terms in (3.20) and (3.21). These terms are utterly negligible, however, in comparison to the intraband scattering terms and are not considered for the moment. In fact, the absence of noticeable spectral hole burning in SL's implies that intraband scattering rates also dominate stimulated rate terms resulting from the electron-radiation interaction [7,22]. This extremely rapid thermalization is the basis for the assumption, often made, that local quasi-equilibrium holds during lasing action. We shall assume that this is the case in the remainder of this analysis. Local quasi-equilibrium of the conduction band and valence band baths is always assumed to hold and with it well-defined local temperature and quasi-electrochemical potentials. Spatial equilibrium is not assumed, however, as its characteristic equilibration time is comparable to relaxation times governing photon-inversion dynamics. Currents which result from spatial nonequilibrium (pump currents included) are assumed to be expressible as gradients of the temperature distribution and quasi-electrochemical potentials.

The assumption of local quasi-equilibrium means that Eqns. (3.20) and (3.21) are approximately correct even when the electron-radiation interaction is turned on. The short term motion of $\psi_c^+\psi_c$ and $\psi_v^+\psi_v$ therefore consists only of thermal fluctuations about f_c and f_v. The long term motion, including the action of stimulated rate terms, is absorbed almost completely by the quasi-Fermi operators f_c and f_v. This kind of approximate picture is very similar to that found in the Born-Oppenheimer approximation. The idea is illustrated in Fig. 2.4. Part (a) depicts a relaxation oscillation of $< f_c >$ or $< f_v >$ after the inversion has been disturbed from its operating point; part (b) shows $< \psi_c^+\psi_c >$ or $< \psi_v^+\psi_v >$ during the same oscillation, the added fuzziness resulting from intraband thermal fluctuations. The slowly varying time evolution of the quasi- Fermi operators can be found through application of the following obvious identities to (3.20) and (3.21):

$$\int d\vec{k} f_c = \int d\vec{k} \psi_c^+\psi_c \tag{3.29}$$

$$\int d\vec{k} f_v = \int d\vec{k} \psi_v^+\psi_v \tag{3.30}$$

A further simplification can be made by assuming that intraband scattering preserves the carrier density (there will, however, be fluctuations about an average value stemming from shot contributions of the balanced intraband scattering rates into and out of a particular location),

$$\int d\vec{k} \frac{\psi_c^+\psi_c - f_c}{\tau_c(\vec{x},\vec{k})} = 0 \tag{3.31}$$

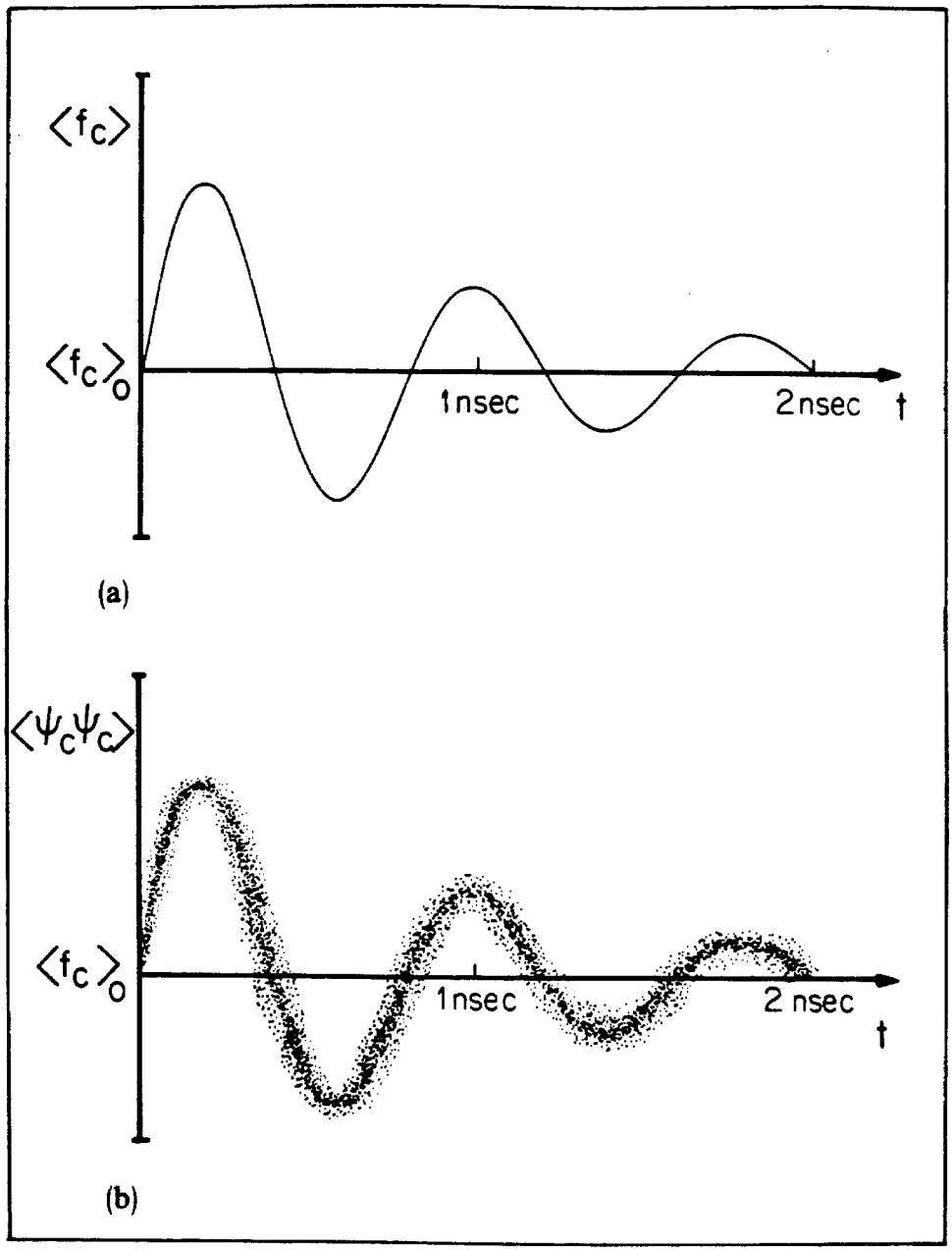

Figure 2.4 A relaxation oscillation of the Fermi number density f_c and the phase space number density $\psi_c^+\psi_c$ towards the operating point number density. Intraband scattering produces the added fuzziness in the lower plot.

$$\int d\vec{k} \frac{\psi_v^+ \psi_v - f_v}{\tau_v(\vec{x},\vec{k})} = 0 \tag{3.32}$$

Equations (3.12), (3.19), (3.20), and (3.21) describe the motion of the chosen dynamic variables under the Hamiltonian $H_o + H_B$. We now include the electron-radiation interaction term given in (2.44). Neglecting nonsynchronous terms, the resulting dynamic equations are,

$$\dot{b}_l^+ = \left(\iota\omega_l - \frac{1}{2\tau_l}\right) b_l^+ + \frac{\iota}{\sqrt{2\varepsilon\hbar\omega_l}} \int d\vec{x} d\vec{k} u_l(\vec{x}) q(\vec{k}) \psi_c^+ \psi_v + g_l^+(t) \tag{3.33}$$

$$\frac{d\psi_c^+ \psi_v}{dt} = \left(\iota\Omega(\vec{k}) - \gamma(\vec{x},\vec{k})\right) \psi_c^+ \psi_v \tag{3.34}$$

$$\frac{d\psi_c^+ \psi_v}{dt} = -\iota \sum_l \frac{u_l(\vec{x}) q^*(\vec{k})}{\sqrt{2\varepsilon\hbar\omega_l}} \left(\psi_c^+ \psi_c - \psi_v^+ \psi_v\right) b_l^+ + \Delta(\vec{x},\vec{k},t)$$

$$\frac{d\psi_c^+ \psi_c}{dt} = -\frac{\psi_c^+ \psi_c - f_c}{\tau_c(\vec{x},\vec{k})} + Y + L_c(\vec{x},\vec{k},t) \tag{3.35}$$

$$\frac{d\psi_v^+ \psi_v}{dt} = -\frac{\psi_v^+ \psi_v - f_v}{\tau_v(\vec{x},\vec{k})} - Y + L_v(\vec{x},\vec{k},t) \tag{3.36}$$

where,

$$q(\vec{k}) \equiv \frac{h(\vec{k})}{\hbar} \tag{3.37}$$

$$Y \equiv -R(\vec{x},\vec{k}) + G(\vec{x},\vec{k}) - \iota \sum_l \frac{u_l(\vec{x})}{\sqrt{2\varepsilon\hbar\omega_l}} \left(q(\vec{k}) \psi_c^+ \psi_v b_l - q^*(\vec{k}) b_l^+ \psi_v^+ \psi_c\right) . \tag{3.38}$$

$G(\vec{x},\vec{k})$ and $R(\vec{x},\vec{k})$ are generation and spontaneous recombination terms whose explicit dependence on system operators is not important for our purposes. From the above discussion, the operator Y can be omitted in (3.35) and (3.36) for consideration of the rapid variations of $\psi_c^+ \psi_c$ and $\psi_v^+ \psi_v$, whereas the slow

variations of the quasi-Fermi levels (or equivalently the carrier density) can be determined by application of (3.29) and (3.31) to (3.35),

$$\frac{dn}{dt} = \int d\vec{k} Y + \int d\vec{k} L_c(\vec{x},\vec{k},t) \tag{3.39}$$

where,

$$n(\vec{x},t) \equiv \int d\vec{k} f_c = \int d\vec{k} \psi_c^+ \psi_c \tag{3.40}$$

is the electron density operator. The corresponding equation for the valence band, found by applying (3.30) and (3.32) to (3.36), is omitted since it is determined from knowledge of f_c (or $n(\vec{x},t)$) with the quasi-neutrality condition. We now rewrite (3.39) using (3.38) and also reexpress the total time derivative in the form of a conservation equation.

$$\partial_t n + \vec{\nabla} \cdot \vec{J} = -R(\vec{x}) + G(\vec{x}) - \tag{3.41}$$

$$\iota \sum_l \frac{u_l(\vec{x})}{\sqrt{2\varepsilon\hbar\omega_l}} \int d\vec{k} \left[q(\vec{k}) \psi_c^+ \psi_v b_l - q^*(\vec{k}) b_l^+ \psi_v^+ \psi_c \right] + \int d\vec{k} L_c(\vec{x},\vec{k},t)$$

where,

$$R(\vec{x}) \equiv \int d\vec{k} R(\vec{x},\vec{k}) \tag{3.42}$$

$$G(\vec{x}) \equiv \int d\vec{k} G(\vec{x},\vec{k}) \tag{3.43}$$

and where $\vec{J}$ is the electron current density operator caused by drift and diffusion, for example.* Eqn. (3.41) is a carrier density operator rate equation which can be used to study both normal electronic transport in conjunction with electron-radiation induced interband transitions.

2.4 The rate equation approximation

Normally, it is possible to make one simplification of Eqns. (3.33)- (3.36), and (3.41) without much loss of generality. To do this Eqn. (3.34) is solved for the operator $\psi_c^+\psi_v$ by employing the rate equation approximation. Integrating the total time derivative in (3.34) yields,

$$\psi_c^+\psi_v = -\iota\sum_l \int_{-\infty}^{t} dt' \frac{u_l(\vec{x}')q^*(\vec{k}')}{\sqrt{2\varepsilon\hbar\omega_l}}\left(\psi_c^+\psi_c - \psi_v^+\psi_v\right)b_l^+ e^{(\iota\Omega(\vec{k}') - \gamma)(t-t')} + \tag{4.1}$$

$$\int_{-\infty}^{t} dt'\Delta(\vec{x}',\vec{k}',t')e^{(\iota\Omega(\vec{k}') - \gamma)(t-t')}$$

where $\vec{x}'$ and $\vec{k}'$ are functions of t'. As mentioned in Section 2.3 the damping parameter γ is of the order of 0.1 psec. in SL's and as such the above integrals sample a very narrow interval of time. The rate equation approximation exploits the rapid decay provided by γ to remove slowly varying quantities from these integrations. From discussions in Section III variations in $\psi_c^+\psi_c$ and $\psi_v^+\psi_v$ can be separated into slowly and rapidly varying parts as follows:

$$\psi_c^+\psi_c = f_c + v_c \tag{4.2}$$

$$\psi_v^+\psi_v = f_v + v_v \tag{4.3}$$

where f_c and f_v are the slowly varying quasi Fermi operators (varying on a nanosecond timescale) and v_c and v_v are the rapidly varying fluctuations caused by intraband thermalization. The time evolution of the Fermi operators is given by (3.41) and the time evolution of v_c and v_v follows immediately from (3.35) and (3.36).

$$\dot{v}_c = -\frac{v_c}{\tau_c} + L_c(\vec{x},\vec{k},t) \tag{4.4}$$

$$\dot{v}_v = -\frac{v_v}{\tau_v} + L_v(\vec{x},\vec{k},t) \tag{4.5}$$

where we have treated f_c and f_v adiabatically and have also neglected the operator Y in comparison to the intraband scattering terms. In addition to intraband scattering, multimode interactions can also cause rapid variations of the population (i.e., modal beating [1]). Provided that the intermodal beat frequency is smaller than the collisional dephasing rate (i.e., $|\omega_l - \omega_m| < \gamma$), however, the rate equation approximation will remain valid. Nearly all lasing modes will satisfy this condition, because of the large γ in SL's. Using the decomposition given in (4.2) and (4.3) and also separating the rapid optical variations in the operator b_l^+, we can apply the rate equation approximation to (4.1) to yield,

$$\psi_c^+\psi_v = -\iota\sum_l \frac{u_l(\vec{x})q^*(\vec{k})}{\sqrt{2\varepsilon\hbar\omega_l}} \frac{(f_c - f_v)b_l^+}{\iota(\bar{\omega}_l - \Omega(\vec{k})) + \gamma} + \tag{4.6}$$

$$-\iota\sum_l \frac{u_l(\vec{x})q^*(\vec{k})b_l^+}{\sqrt{2\varepsilon\hbar\omega_l}} \int_{-\infty}^{t} dt'(v_c - v_v)e^{\left[\iota(\Omega(\vec{k}) - \bar{\omega}_l) - \gamma\right](t - t')} +$$

$$\int_{-\infty}^{t} dt'\Delta(\vec{x},\vec{k},t')e^{\left[\iota\Omega(\vec{k}) - \gamma\right](t - t')}$$

where $\bar{\omega}_l$ is the lasing frequency of the l^{th} mode (not necessarily equal to ω_l). We have also replaced $(\vec{x}',\vec{k}')$ by $(\vec{x},\vec{k})$ throughout this expression since any point in one of the phase spaces will not evolve significantly during the time interval γ^{-1}.

The operators $\psi_c^+\psi_v$ and $\psi_v^+\psi_c$ represent contributions to the active medium polarization caused by the electron-radiation interaction between points in the respective conduction band and valence band phase spaces. Each term in (4.6) then represents a different contribution to polarization. The first term is the

induced polarization, giving rise to a complex susceptibility which depends on the excitation of the active layer; the second term is an intraband scattering contribution to polarization (the so called "Occupation Fluctuation" contribution to polarization [21]); and the third term is the main contributor to quantum fluctuations in lasers. This term in conjunction with a contribution from optical field vacuum fluctuations causes spontaneous emission fluctuations of the lasing modes.

The optical field and carrier density equations (3.33) and (3.41) are now rewritten using (4.6). We have

$$\dot{b}_l^+ = \left(\iota\omega_l - \frac{1}{2\tau_l}\right)b_l^+ + \iota\int d\vec{x}u_l(\vec{x})\sum_m \frac{\omega_m}{2\mu^2}\chi(n,\bar{\omega}_m)b_m^+u_m(\vec{x}) + \tag{4.7}$$

$$\sum_m \int d\vec{x}d\vec{k}\,\frac{|q(\vec{k})|^2u_l(\vec{x})u_m(\vec{x})}{2\varepsilon\hbar\omega_l}b_m^+\int_{-\infty}^{t}dt'(v_c - v_v)e^{\left[\iota(\Omega(\vec{k}) - \bar{\omega}_m) - \gamma\right](t-t')} +$$

$$\frac{\iota}{\sqrt{2\varepsilon\hbar\omega_l}}\int d\vec{x}d\vec{k}dt'u_l(\vec{x})q(\vec{k})\Delta(\vec{x},\vec{k},t')e^{\left[\iota\Omega(\vec{k}) - \gamma\right](t-t')} + g_l^+(t)$$

$$\partial_t n + \vec{\nabla}\cdot\vec{J} = -R(n,\vec{x}) + G(n,\vec{x}) + \sum_{l,m}\frac{\omega_m}{2\mu^2\iota}u_l(\vec{x})u_m(\vec{x})\left[\chi(n,\bar{\omega}_m)b_m^+b_l - H.A.\right] - \tag{4.8}$$

$$\sum_{l,m}\frac{u_l(\vec{x})u_m(\vec{x})}{2\varepsilon\hbar\sqrt{\omega_m\omega_l}}\int d\vec{k}\int_{-\infty}^{t}dt'|q(\vec{k})|^2(v_c - v_v)\left[b_m^+b_le^{\left[\iota(\Omega(\vec{k}) - \bar{\omega}_m) - \gamma\right](t-t')} + H.A.\right] -$$

$$\iota\sum_l\frac{u_l(\vec{x})}{\sqrt{2\varepsilon\hbar\omega_l}}\int d\vec{k}\int_{-\infty}^{t}dt'\left[q(\vec{k})\Delta(\vec{x},\vec{k},t')b_le^{(\iota\Omega(\vec{k}) - \gamma)(t-t')} - H.A.\right] + \int d\vec{k}L_c(\vec{x},\vec{k},t)$$

where in writing these equations we have defined a local complex susceptibility operator as follows:

$$\chi(n,\omega_1) = \frac{-\iota}{\varepsilon_0 \hbar \omega_1^2} \int d\vec{k} \frac{|q(\vec{k})|^2 (f_c - f_v)}{\iota(\omega_1 - \Omega(\vec{k})) + \gamma} \quad . \tag{4.9}$$

We take the complex susceptibility to be an explicit function of the carrier density n, rather than an equivalent representation in terms of either one of the electrochemical potentials.

Eqns. (4.4), (4.5), (4.7), and (4.8) represent the main result of our analysis. Although the rate equation approximation has been invoked in the case of (4.7) and (4.8), the equations should remain exceedingly accurate owing to the smallness of γ^{-1} in comparison to characteristic times of interest. Thus, these equations can be used to study a variety of phenomena ranging from multimode interactions to the effect of carrier diffusion on optical fluctuations. Under circumstances where the rate equation approximation does not hold the more general forms of these equations appearing in Section 2.3 can be used.

2.5 Conclusion

In this chapter we have developed an operator formalism based on electronic wave-packets which facilitates the treatment of local phenomena in semiconductors. In addition an example of its use has been presented by developing local operator equations of motion for a semiconductor laser. In doing this we have rigorously incorporated the electrooptic interaction into the semiclassical picture of the Bloch electron, and have given conditions under which other quantum interactions may also be treated using this formalism. Although the analysis we have presented treats only the electronic system in a local fashion, it is clear that one can do likewise for the optical field by developing a space of optical wave-packets [17]. Such a formalism might prove to be useful for interpreting femtosecond pulse propagation experiments.

* We assume it is possible to define diffusion and drift coefficients. A more fundamental approach would begin with the operator version of the Boltzmann transport equation given by Eqn. (3.35),

$$\frac{d\psi_c^+\psi_c}{dt} = \partial_t\psi_c^+\psi_c + \vec{v}_g\cdot\vec{\nabla}_{\vec{x}}\psi_c^+\psi_c + \dot{\vec{k}}\cdot\vec{\nabla}_{\vec{k}}\psi_c^+\psi_c = -\frac{\psi_c^+\psi_c - f_c}{\tau_c} + Y + L_c$$

where $\vec{v}_g = \dot{\vec{x}}$ is the group velocity of a wave-packet. Using this equation one could derive explicit formulas for the transport coefficients. For a related discussion see Ref. [8]; also see Refs. [11-13] in regard to operator transport equations.

References

[1] W. E. Lamb, Jr., Phys. Rev. vol. 134, 1429 (1964).

[2] H. Haken, "Laser Theory" (Springer-Verlag, New York, 1983).

[3] H. Haug, Phys. Rev. vol. 184, 338 (1969).

[4] H. Haug, Z. Physik vol. 200, 57 (1967).

[5] H. Haug, H. Haken, Z. Physik vol. 204, 262 (1967).

[6] H. Haug, Z. Physik vol. 206, 163, (1967).

[7] M. Yamada, Y. Suematsu, J. Appl. Phys. vol. 52, 2653 (1981).

[8] See, for example, N. W. Ashcroft, N. D. Mermin, "Solid State Physics" (Holt-Rhinehart-Winston, Philadelphia, 1976).

[9] E. Ya. Glushko, Phys. Stat. Sol. (b) vol. 114, 685 (1982).

[10] E. Wigner, Phys. Rev. vol. 40, 749 (1932).

[11] Iu. L. Klimontovich, JETP (USSR) vol. 33, 982 (1957).

[12] W. E. Brittin and W. R. Chappell, Rev. Mod. Phys. vol. 34, 620 (1962).

[13] H. Frohlich, Physica vol. 37, 215 (1967).

[14] K. Vahala and A. Yariv, unpublished.

[15] C. Cohen-Tannoudji, B. Diu, F. Laloe, "Quantum Mechanics," vol. 1 (Wiley, New York, 1977) pp. 61-66.

[16] D. Stoler, Phys. Rev. D vol 1, 3217 (1970).

[17] M. C. Teich, B. E. A. Saleh, J. Perina, J. Opt. Soc. Am. B vol. 1, 366 (1984).

[18] J. B. Moreno, J. Appl. Phys vol. 48, 4152 (1977).

[19] M. Lax, Phys. Rev. vol. 145, 110 (1966).

[20] H. Haken, W. Weidlich, Z. Physik vol. 189, 1 (1966).

[21] K. Vahala, A. Yariv, Appl. Phys. Lett. vol. 43, 140 (1983).

[22] R. Lang, J. Quant. Electron., QE-10, 825 (1974).

Chapter 3

Power, frequency, and field spectra for single and multimode semiconductor lasers

3.1 Introduction

In the last few years it has been conclusively demonstrated that amplitude and phase fluctuations of the lasing field in semiconductor lasers (SL's) are strongly coupled on account of the highly detuned gain spectrum produced by an electron-hole inversion [1,2]. Although some of the effects of detuning on laser noise spectra were considered in the sixties by several authors [3,4,5], its significance and strength in semiconductor lasers had long been overlooked and latest efforts in this area have explored additional effects which were previously neglected [6,7,8]. In this chapter we study the consequences of detuning in single and multi-longitudinal mode semiconductor lasers.

Only noise spectra associated with the phase are modified by the detuned gain spectrum, but for the purposes of comparison and for completeness we also calculate certain amplitude noise spectra for both single and multimode operation. Although multimode amplitude noise has been treated elsewhere [9] we give a different presentation of results in terms of a new dimensionless parameter that gauges the dynamic interaction strength between a mode and the inversion. This parameter is introduced in Section 3.5 and is of central importance in the calculation of all multimode noise spectra.

The starting point of this analysis is a set of semiclassical equations for a multimode SL. The form of these equations is consistent with the set of operator

equations which were derived in Chapter 2. We will take advantage of this correspondence throughout the analysis to add both rigor and depth beyond that normally possible in a semiclassical treatment. We do this by supplementing the main text with a set of appendices. At key points in the treatment fully quantum mechanical arguments given in an Appendix can be used in place of the less rigorous semiclassical arguments. Fluctuations are introduced into the semiclassical equations through the use of Langevin forces. Although fluctuations in SL's originate from many sources, our only concern in this chapter will be the most important such source, spontaneous emission. Thus mechanisms such as population fluctuations, diffusion, and temperature fluctuations are neglected. The equations of motion will be solved by applying a standard linearization procedure which has been used by several other authors. We narrow the scope of the treatment by focusing on the calculation of certain important optical spectra. These spectra are introduced below, followed by discussion of related experimental work. In Section 3.4 the equations of motion are introduced and linearized, and in Section 3.5 the optical spectra are calculated. We conclude in Section 3.6 by summarizing several results of the analysis.

3.2 Optical spectra

SL applications which must include laser light output fluctuation characteristics into their design and performance considerations can most often do so by modeling the lasing field as a classical field expanded into eigenmodes of the passive resonator,

$$\vec{E}(\vec{r},t) = \frac{1}{2}\sum_m \left[b_m(t) + b_m^*(t)\right]\vec{u}_m(\vec{r}) \tag{2.1}$$

where the complex field amplitudes can be expressed as,

$$b_m(t) = A_m\left[1 + \rho_m(t)\right]e^{i\left[\bar{\omega}_m t + \varphi_m(t)\right]} \tag{2.2}$$

In (2.2) $\bar{\omega}_m$ is the line center frequency of the lasing mode, $\rho_m(t)$ is the normalized field amplitude fluctuation, and $\varphi_m(t)$ is a field phase fluctuation. By setting these fluctuation terms equal to zero and taking single mode operation in (2.1), a perfectly coherent classical field results (quantum mechanically, a quasi-classical state [11]). Square law detection of such a signal, using a unit quantum efficiency detector, would suffer only from shot noise caused by the Poisson statistics of the arriving photons; far above threshold the output of a single mode laser would mimic this ideal behavior. The degree to which the laser output deviates from this ideal, because of various noise mechanisms, is thus accounted for classically by the fluctuation quantities ρ_m and φ_m. The amplitude fluctuation component ρ_m, for instance, causes square law detection noise in addition to the shot noise component discussed above, and the phase fluctuation component φ_m is primarily responsible for smearing of the lasing frequency or frequencies, giving each lasing mode a finite linewidth. The framework of this analysis is based on these variables and its goal will be the calculation of noise spectra associated with $\{\rho_m\}$ and $\{\varphi_m\}$.

With this goal in mind, we now give the definitions of six laser noise spectra. These spectra do not fully characterize fluctuations of the electric field; such complete characterization requiring calculation of a probability distribution function or system density matrix [5,12,13,14]. They are, however, of importance for consideration of optical information transmission and detection, and

are readily obtained in measurement. The definitions given are similar to those found elsewhere [7,15] with the exception of the spectra $W_{\rho\phi}^{mn}(\Omega)$ and the "off diagonal" spectra $W_{\Delta\omega}^{mn}(\Omega)$ which are new and as discussed later only significant in lasers or oscillators with strong gain spectrum "detuning". In all that follows we will invoke the so-called quasi-linear approximation in which only terms of lowest order in ρ_m are retained in calculations [16]. The justification for doing this is that gain saturation effectively damps the amplitude fluctuations of well-excited modes so that higher-order terms in ρ_m can be neglected. The quieting effect of this damping mechanism (which is characteristic of all regenerative oscillators) was first observed in laser oscillators by Armstrong and Smith [17]. We will quantify later in the analysis what is meant by "well-excited" mode.

A spectrum which arises in square law detection of an optical signal is the power fluctuations spectrum of an optical carrier. It describes a component of noise which appears in addition to the shot noise component in the detected signal, and for this reason it is sometimes referred to as excess noise. Using (2.1) and (2.2), the instantaneous output power fluctuation to highest order in the amplitude fluctuation is given by,

$$\Delta I(t) \equiv I(t) - I_T = \sum_m 2I_m \rho_m(t) \tag{2.3}$$

where I_T is the average total output power and $\{I_m\}$ are the average output powers associated with each lasing mode. Using the Wiener-Khintchine theorem [18], the power fluctuations spectrum is defined by,

$$W_{\Delta I}(\Omega) \equiv \int_{-\infty}^{+\infty} < \Delta I(t+\tau)\Delta I(t) > \; e^{-i\Omega\tau} d\tau = \sum_{m,n} 4 I_m I_n W_\rho^{mn}(\Omega) \tag{2.4}$$

where,

$$W_\rho^{mn}(\Omega) \equiv \int_{-\infty}^{+\infty} < \rho_m(t+\tau)\rho_n(t) > \; e^{-i\Omega\tau} d\tau \tag{2.5}$$

and where $< \; >$ denote appropriate classical averages (ensemble or otherwise). An important point, first noted by McCumber [9], is that correlations exist between the amplitude fluctuations of the lasing modes by virtue of their joint interaction with the active medium. These correlations enter into the total output power fluctuation spectrum through the "off diagonal" terms $W_\rho^{mn}(\Omega)$ in (2.4).

Analogous to the role of $W_{\Delta I}(\Omega)$ in AM transmission, the instantaneous frequency deviation spectrum $W_{\Delta\omega}^{mm}(\Omega)$ sets a noise floor in FM transmission using a particular mode m. Defined as,

$$W_{\Delta\omega}^{mm}(\Omega) \equiv \int_{-\infty}^{+\infty} d\tau < \dot{\varphi}_m(t+\tau)\dot{\varphi}_m(t) > \; e^{-i\Omega\tau} \tag{2.6}$$

this spectrum will also serve as a computational tool in the field spectrum calculation below. (2.6) can also be used to define off diagonal frequency fluctuation spectra (i.e., $W_{\Delta\omega}^{mn}(\Omega)$); these off diagonal spectra give the phase correlations which exist between different lasing modes. Normally, such correlations would be negligible, but in semiconductor lasers the strong amplitude phase coupling caused by the detuned nature of the gain spectrum leads to phase coupling between modes analogous to the amplitude coupling represented by the off diagonal spectra $W_\rho^{mn}(\Omega)$.

The detuned induced amplitude phase coupling itself is reflected in a spectrum we now introduce and refer to as the fluctuation coupling spectrum.

Defined as*,

$$W_{\rho\varphi}^{mm}(\Omega) = \iota\int_{-\infty}^{+\infty} d\tau e^{-\iota\Omega\tau}\langle \rho_m(t)\varphi_m(t+\tau) - \rho_m(t+\tau)\varphi_m(t)\rangle \qquad (2.7)$$

$$= \iota\left[\langle \rho_m(\Omega)\varphi_m(\Omega)\rangle - \langle \rho_m^*(\Omega)\varphi_m^*(\Omega)\rangle\right]$$

with $\rho_m(\Omega)$ and $\varphi_m(\Omega)$ the Fourier transforms of $\rho_m(t)$ and $\varphi_m(t)$, the diagonal members of this spectrum give a measure of the amplitude phase coupling intrinsic to a single lasing mode and the off diagonal members (which are defined analogously) give a measure of intermodal amplitude phase coupling. Although all components of this spectrum are nonzero, we will calculate only the diagonal spectra since they play a role in determining the structure of the field spectrum considered below. These spectra have the interesting property of being antisymmetric with respect to their arguments. It is a surprising fact that this spectrum has received only scant attention in the literature and yet is a very basic aspect of detuned oscillators.

When two optical fields are photomixed on a square law detector, as might be done in a heterodyne detection system, or when an optical spectrum analyzer (e.g., Fabry Perot) is used to sweep a laser's output field, it is the field spectrum which comes under scrutiny. To avoid computational difficulties the treatment of this spectrum is broken into two frequency regimes around the lasing frequency. The first and most important regime encompasses a frequency band surrounding the lasing linecenter frequency of a particular mode m. This band is defined by $|\omega - \bar{\omega}_m| \leq 1/\tau_R$ (where τ_R is the relaxation oscillation damping time); within it the inversion can effectively track field amplitude fluctuations and provide the gain saturation damping of amplitude fluctuations discussed earlier. The field autocorrelation of the m^{th} mode is thus approximately

described by,

$$< b_m(t+\tau)b_m^*(t)> = A_m^2 < e^{i\left[\varphi_m(t+\tau)-\varphi_m(t)\right]}> e^{i\Omega_m\tau} \quad ; \qquad (2.8)$$

that is, amplitude fluctuations $\rho_m(t)$ can be neglected. We digress briefly to note that a significant anomalous 1/f component has been observed at low frequencies (typically < 1 MHz.) in the power fluctuations spectra of SL's [19,20,21,22]. Such behavior indicates a breakdown of gain saturation damping at low frequencies and brings into question results obtained using expression (2.8). It would seem, however, that a meaningful comparison between theory and experiment can be made in at least two ways: first and simplest is to use a scanning Fabry Perot with a sweep rate adjusted so that on any given sweep the low frequency 1/f components are suppressed by the finite sampling time; a second method would be to suppress these components by a low frequency amplitude stabilization loop employing temperature feedback to the laser.

To simplify (2.8) further requires knowledge of the distribution function of $\varphi_m(t+\tau) - \varphi_m(t)$. Under most circumstances it is adequate to assume a Central Limit argument applies, making $\varphi_m(t+\tau) - \varphi_m(t)$ a Gaussian random variable. The Gaussian nature of the phase fluctuation has, in fact, been observed experimentally for single mode SL's [23]. It will be assumed for simplicity that $\varphi_m(t+\tau) - \varphi_m(t)$ is a Gaussian stationary variable throughout this analysis. Identifying the ensemble averaged quantity in (2.8) as the characteristic function with unity argument of a Gaussian distribution function, allows it to be rewritten as follows,

$$< b_m(t+\tau)b_m^*(t)> = A_m^2 e^{-\frac{1}{2}<\left[\varphi_m(t+\tau)-\varphi_m(t)\right]^2>} e^{i\bar{\omega}_m\tau} \quad (2.9)$$

It is convenient to further rewrite this expression in terms of the instantaneous frequency deviation spectrum,

$$< \left[\varphi_m(t+\tau)-\varphi_m(t)\right]^2> = 2\int_0^\tau dx \int_0^x dy < \dot{\varphi}_m(y)\dot{\varphi}_m(0)> \quad (2.10)$$

$$= \frac{1}{\pi}\int_0^\tau dx \int_0^x dy \int_{-\infty}^{+\infty} d\Omega\, W_{\Delta\omega}^{mm}(\Omega) e^{i\Omega y} = \frac{1}{\pi}\int_0^{+\infty} d\Omega\, W_{\Delta\omega}^{mm}(\Omega)\left[\frac{\mathrm{Sin}\left[\frac{\Omega\tau}{2}\right]}{\frac{\Omega}{2}}\right]^2$$

In deriving this expression we have utilized the stationary property of $\dot{\varphi}_m(t)$ and have also assumed that $W_{\Delta\omega}^{mm}(\Omega)$ is an even function. Using (2.10) in (2.9) and applying the Wiener-Khintchine theorem to the field autocorrelation (sum of positive and negative frequency field amplitude components) yields the field spectrum of the m^{th} lasing mode,

$$W_\varepsilon^m(\omega) = \frac{1}{4}\int_{-\infty}^{+\infty} d\tau < b_m(t+\tau)b_m^*(t) + b_m^*(t+\tau)b_m(t)> e^{-i\omega\tau} \quad (2.11)$$

$$= \frac{1}{2}A_m^2 \mathrm{Re}\int_{-\infty}^{+\infty} d\tau \exp\left[-i(\omega-\bar{\omega}_m)\tau - \frac{1}{2\pi}\int_0^{+\infty} d\Omega\, W_{\Delta\omega}^{mm}(\Omega)\left[\frac{\mathrm{Sin}\left[\frac{\Omega\tau}{2}\right]}{\frac{\Omega}{2}}\right]^2\right]$$

When $W_{\Delta\omega}^{mm}(\Omega)$ is flat over the low frequency regime (which is the case for the noise sources considered here) this expression simplifies to,

$$W_{\varepsilon}^{m}(\omega) = \frac{1}{4\pi} \frac{A_m^2 W_{\Delta\omega}^{mm}(0)}{(\omega - \bar{\omega}_m)^2 + \left[\frac{W_{\Delta\omega}^{mm}(0)}{2}\right]^2} \tag{2.12}$$

where $W_{\Delta\omega}^{mm}(0)$ represents the low frequency value of $W_{\Delta\omega}^{mm}(\Omega)$. (2.12) is the familiar expression for a lasing mode with a Lorentzian lineshape. The linewidth of mode m is thus given by the low frequency value of $W_{\Delta\omega}^{mm}(\Omega)$. In a multimode SL the separation between lasing modes is normally many orders larger than this linewidth so that the multimode field spectrum (valid only within the respective low frequency bands surrounding each lasing mode) is simply the sum of the single mode field spectra as given below,

$$W_{\varepsilon}(\omega) = \sum_{m} W_{\varepsilon}^{m}(\omega) \quad . \tag{2.13}$$

This spectrum is determined solely by the low frequency behavior of the diagonal frequency fluctuation spectra $W_{\Delta\omega}^{mm}(\Omega)$. As an aside, we note that cases do exist which require knowledge of off diagonal spectra, a good example being the linewidth resulting from photomixing two lasing modes on a fast photodetector. Using the same approach it can be shown that the beatnote spectrum is given by,

$$W_{beat}(\Omega) \alpha \frac{A_m A_n \Delta\omega_{mn}}{(\Omega - \bar{\omega}_m + \bar{\omega}_n)^2 + \left[\frac{\Delta\omega_{mn}}{2}\right]^2} \tag{2.14}$$

where the beatnote linewidth is,

$$\Delta\omega_{mn} = W_{\Delta\omega}^{mm}(0) + W_{\Delta\omega}^{nn}(0) - 2W_{\Delta\omega}^{mn}(0) \quad . \tag{2.15}$$

Phase correlation between the modes m and n thus alters the beatnote linewidth in a manner prescibed by the off diagonal spectrum $W_{\Delta\omega}^{mn}(\Omega)$.

Expression (2.11) and its simplified forms (2.12) and (2.13) for the field spectrum are valid only within the frequency bands $\{|\omega - \bar{\omega}_m| \leq 1/\tau_R\}$ because of the form assumed in (2.8). Within the complementary set of frequencies $\{|\omega - \bar{\omega}_m| > 1/\tau_R\}$ the neglect of amplitude fluctuations is no longer permissible. In this region the dynamics of the inversion-photon interaction are crucial and gain saturation damping is rendered inoperative. Fortunately, however, the fluctuation components in this range of frequencies are normally small enough to enable a small angle approximation of the field phase. Doing so, the field autocorrelation function for mode m is given by,

$$< b_m(t+\tau)b_m^*(t)> \approx A_m^2(1 - \frac{1}{2}< \left[\varphi_m(t+\tau) - \varphi_m(t)\right]^2> \tag{2.16}$$

$$+ < \rho_m(t+\tau)\rho_m(t)> + i\left[< \rho_m(t)\varphi_m(t+\tau) - \rho_m(t+\tau)\varphi_m(t)> \right])e^{i\bar{\omega}_m\tau}$$

where only terms up to second order in the fluctuations have been retained. The field spectrum which results from (2.16) is,

$$W_\varepsilon^m(\omega) = \frac{A_m^2}{2}(D(\omega - \bar{\omega}_m) + \frac{1}{2(\omega - \bar{\omega}_m)^2} W_{\Delta\omega}^{mm}(\omega - \bar{\omega}_m) \tag{2.17}$$

$$+ W_\rho^{mm}(\omega - \bar{\omega}_m) + W_{\rho\varphi}^{mm}(\omega - \bar{\omega}_m))$$

where (2.10) has been used and $D(\omega - \bar{\omega}_m)$ represents a delta function like singularity which results from the inadequacy of expansion (2.16) near the linecenter frequency $\bar{\omega}_m$. The appearance of $W_{\rho\varphi}^{mm}(\Omega)$ in this expression implies that the

field spectrum lineshape function in a detuned laser is slightly asymmetric about the lasing linecenter. This property has been observed by us in SL's [24].

Eqns. (2.13) and (2.17) give a composite representation of the field spectrum, and together with Eqns. (2.4), (2.5), (2.6), and (2.7) complete the noise spectra definitions needed for this analysis. It should be noted that, whereas six spectra have been defined, only three sets of spectra, $\{W_{\rho}^{mn}(\Omega)\}$, $\{W_{\Delta\omega}^{mn}(\Omega)\}$, and $\{W_{\rho\varphi}^{mm}(\Omega)\}$, need be calculated to determine all six. Experimental and theoretical results pertinent to some of these spectra are summarized below.

3.3 Spectral observations

As descibed earlier, the power fluctuations spectrum $W_{\Delta I}(\Omega)$ is most readily obtained through square law detection of the optical field followed by spectral analysis of the detection current (Fig. 3.1). Many investigators have used this method to study total output power fluctuations in SL's as well as the output power fluctuations in one or several longitudinal modes of a multimode SL [25,26,27,28,29,30,31]. These measurements have confirmed several predictions of early theoretical work: (1) For predominantly single mode operation, the output power fluctuations spectrum consists of a flat low frequency part which decreases in strength with increasing output power, followed by a "spiking" resonance at a frequency corresponding to the relaxation resonance frequency [9,32,33]; (2) For multimode lasers these same considerations apply to the total output power; however, when power fluctuations in a single lasing mode or a subgroup of all lasing modes are measured, an excess noise caused by the partitioning of energy between the gain medium and all lasing modes is observed [9].

In addition to the above behavior, the $W_{\Delta I}(\Omega)$ spectrum also exhibits the $1/f$ component discussed earlier. Recently, we have shown that spatially dependent

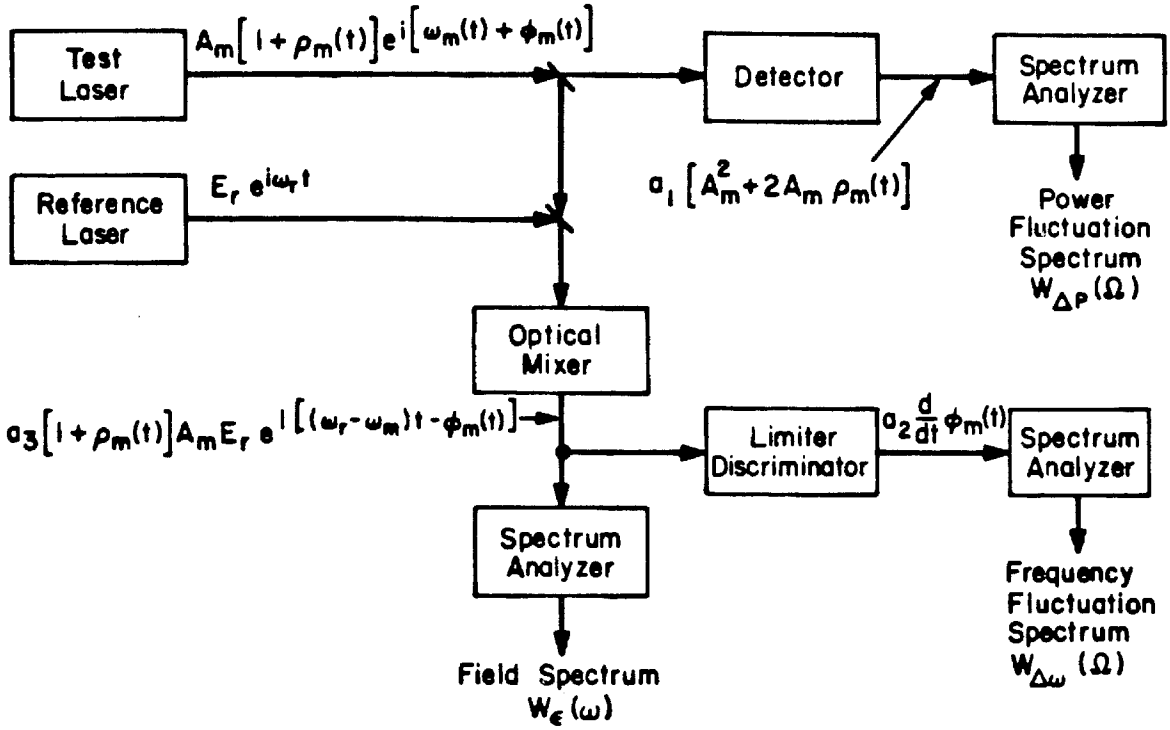

Figure 3.1 Schematic showing measurement techniques which can be used to obtain some of the spectra calculated in this analysis.

temperature fluctuations can produce 1/f components of the correct strength in the amplitude and phase noise spectra of semiconductor lasers [34].

Several groups have recently reported measurement of various portions of the $W_{\Delta\omega}^{mm}(\Omega)$ spectrum for GaAs SL's [23,35,36,37,38] This spectrum has structure very similar to $W_{\Delta I}(\Omega)$, both containing 1/f low frequency regions followed by a flat intermediate band and a "spiking" resonance. These results are not surprising in light of the strong detuning effect in SL's. All regions of this spectrum, with the exception of the 1/f portion, can be explained by the theory presented in this chapter. The measurement of $W_{\Delta\omega}^{mm}(\Omega)$ usually involves some kind of amplitude limiting procedure, followed by frequency discrimination and spectral analysis. Discrimination has been accomplished optically using a Michelson interferometer or by photomixing two sources and processing the photocurrent (Fig. 3.1).

The field spectrum $W_{\varepsilon}(\Omega)$ and its related single mode correlation function $< b_m(t+\tau)b_m^*(t)>$ have been measured in several ways. In the early sixties upper limits were set on SL field spectrum linewidth by measuring a fringe visibility function using an instrument bandwidth limited Fabry Perot spectrum analyzer [39]. In the late sixties Hinkley and Freed obtained the field spectrum of a PbSnTe SL by heterodyning it with a CO_2 laser at 10μM. [40] (Fig. 3.1). They observed the inverse power field spectrum linewidth broadening characteristic of a lasing line broadened by spontaneous emission. Homodyne measurements of the field spectrum which utilize an optical fiber delay line have also been reported [41] (Fig. 3.2). More recently a number of groups have reported measurement of the SL field spectrum using one or several of the above techniques [42,43]. The watershed of this current group of measurements was the observation of excess inverse power linewidth broadening in the GaAs system reported

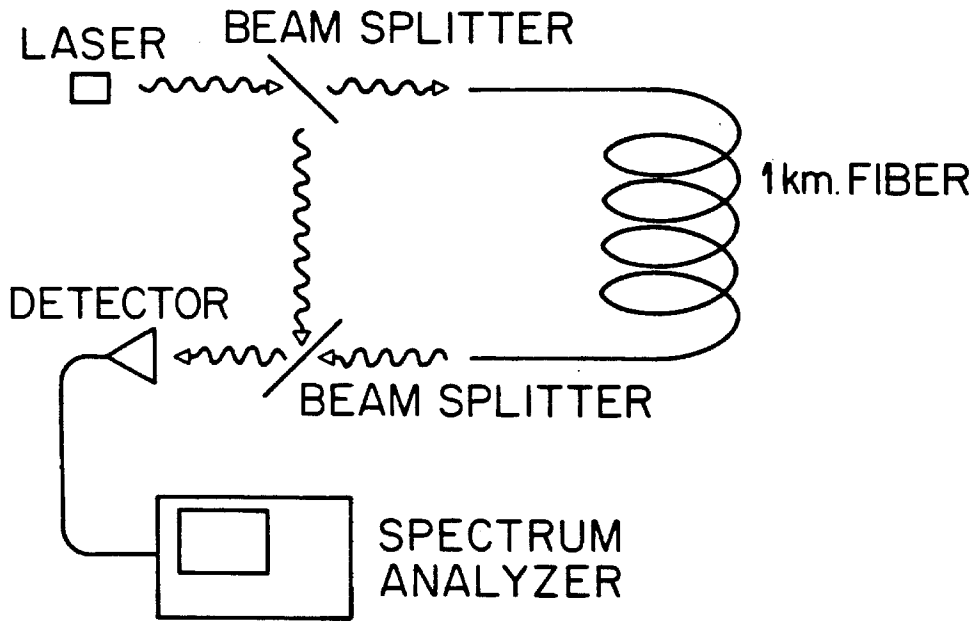

$$\langle e^{\iota\phi(t+\tau)}\, e^{-\iota\phi(t)}\rangle \sim \langle e^{\iota\phi(t)}\rangle \langle e^{-\iota\phi(t)}\rangle$$

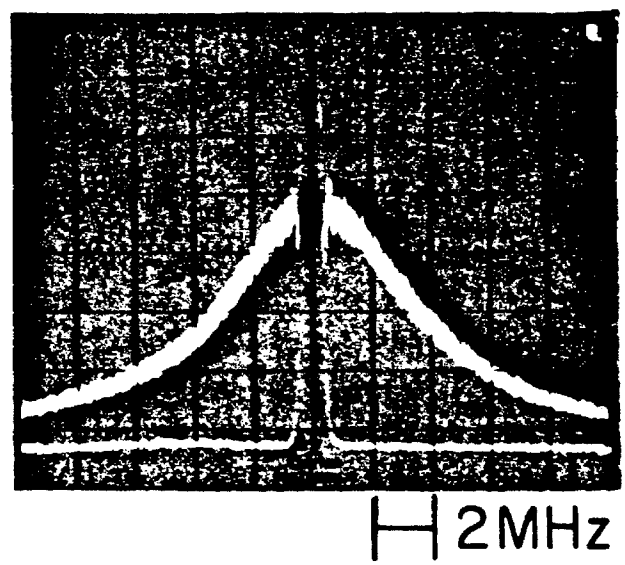

Figure 3.2 Fiber delay-line measurement of the field spectrum of a laser. If the delay τ, introduced by the fiber, is much longer than the coherence time of the laser, then the photomixed signals are independent and the resulting photocurrent contains a component related to the phase noise in the signals. Spectrum analysis of this component produces a lineshape function with twice the linewidth of the original signal provided the original lineshape function is a Lorentzian. A typical photocurrent spectrum is shown in the lower portion of the figure. The baseline was generated by blocking one of the beam arms; the observed lineshape is Lorentzian.

by Mooradian, et. al. [1,44]. Their measurement was the first example of laser phase noise enhancement caused by oscillator detuning, an effect elaborated on this chapter. Besides an enhanced inverse power linewidth component, SL's also exhibit finestructure in their field spectrum [24,45]. This finestructure will be shown to be the composite of $W_p^{mm}(\Omega)$, $W_{\Delta\omega}^{mm}(\Omega)$, and $W_{p\varphi}^{mm}(\Omega)$ as given in (2.17) and are basically a manifestation of the relaxation resonance.

Finally, a power independent contribution to linewidth has been observed in SL's [46,47]. Several fluctuation mechanisms have been proposed to explain this anomaly and indeed it may be the case that several mechanisms cause it. Two potential mechanisms are spatially dependent temperature fluctuations [34] which have already been mentioned in regards to 1/f noise, and electronic state occupation fluctuations (see Ref. [48] and discussion in Section 2.4 of Chapter 2). In this thesis we will not delve into this subject except to show that partition noise can sometimes produce power independent behavior.

3.4 Equations of motion

The semiclassical equations of motion used in this analysis appear below,

$$\dot{b}_l^* = \left[\iota\omega_l - \frac{1}{2\tau_l}\right] b_l^* + \iota \frac{\Gamma_{ll}\omega_l}{2\mu^2}\chi(n,\bar{\omega}_l) b_l^* + s_l^*(t) \tag{4.1}$$

$$\dot{n} = E - R(n) - \sum_l \frac{\omega_l}{\mu^2}\chi_l(n,\bar{\omega}_l)\frac{b_l^* b_l}{V_l} \tag{4.2}$$

where (4.1) gives the time evolution of the field amplitude appearing in (2.1) and (4.2) gives the time evolution of the carrier density n (assumed to be uniform and to adequately characterize the state of the active medium). In (4.1) ω_l and τ_l are the resonant frequency and lifetime of the l^{th} passive mode; Γ_{ll} is a modal

confinement factor to account for incomplete spatial overlap of the l^{th} optical mode and the active medium; μ is the nonresonant contribution to refractive index; $\chi(n,\omega) \equiv \chi_R(n,\omega) + \iota\chi_I(n,\omega)$ is the complex susceptibility; and $s_l^*(t)$ is a Langevin fluctuation force. In (4.2) E is a pumping rate term; R(n) is a carrier recombination rate term; and V sub l is the modal volume [7] of mode l.

These multimode semiclassical equations can be derived by two basic methods. The first has the advantage of simplicity but is somewhat heuristic. In this method one begins with Maxwell's equations and a carrier density rate equation; then introduces phenomenalogical interaction terms (involving the complex susceptibility) to account for the electron radiation interaction, and Langevin fluctuation terms to simulate fluctuations resulting from spontaneous emission as well as other noise mechanisms. This method has been employed by us in Refs. [7,8] to study fluctuations in a single mode SL.

The second method has the advantage of being a "first principles" approach but is for this reason much more complicated. We have presented this fully quantized derivation in Chapter 2. The quantum treatment has the advantage of yielding an analytic expression for the complex susceptibility, and, most important, giving a "first principles" relation between the Langevin sources and the various fluctuation mechanisms in the device. Eqns. (4.1) and (4.2) are consistent with the quantum treatment if we view them as operator equations of motion driven by fluctuation operators and also take the carrier density as uniform over the active volume V_{active}. This matter is discussed in greater detail in Appendix A.

Regardless of how we justify the form of (4.1) and (4.2), they will be treated semiclassically to solve for the spectra discussed in the introduction. We further assume the Langevin force $s_l^*(t)$ accounts only for fluctuations related to

spontaneous emission into mode l. We will, however, take advantage of the correspondence discussed above at certain points in the analysis.

Eqns. (4.1) and (4.2) are the working equations for the remainder of this analysis. As is usual, it is assumed that the fluctuations of the optical modes and the population are only perturbations to the steady-state operating point. This allows a linearization of the equations of motion based on the following small signal representations,

$$b_l^*(t) = B_l^*(t)e^{i\omega_l t} = A_l\Big[1 + \rho_l(t)\Big]e^{-i\left(\bar{\omega}_l t + \varphi_l(t)\right)} \tag{4.3}$$

$$n = n_o + n_l \tag{4.4}$$

$$\chi(n,\bar{\omega}_l) \approx \chi(n_o,\bar{\omega}_l) + \xi(n_o,\bar{\omega}_l)n_l \tag{4.5}$$

$$R(n) \approx R(n_o) + R'(n_o)n_l \tag{4.6}$$

where $\rho_l(t)$ and $n_l(t)$ are small signal quantities, but $\varphi_l(t)$ is not. As the first step in the linearization the operating point equations of state are determined. Using the above forms, the steady-state versions of (4.1) and (4.2) are given by,

$$\left[-i(\omega_l - \bar{\omega}_l) - \frac{1}{2\tau_l} - i\frac{\Gamma_{ll}\omega_l}{2\mu^2}<\chi^*(n,\bar{\omega}_l)>_t\right]<B_l(t)>_t = 0 \tag{4.7}$$

$$\sum_l \frac{\omega_l}{\mu^2}<\chi_l(n,\bar{\omega}_l)>_t \frac{<B_l^*B_l>_t}{V_l} = <E - R(n)>_t \tag{4.8}$$

where $<\ >_t$ signifies temporal averaging. In writing these equations we have assumed that field and susceptibility terms can be averaged separately. It might be expected for these equations to establish the operating point, but there is a problem in discerning the meaning of (4.7). This equation can be

satisfied in several ways. By purely intuitive reasoning, we might conjecture $< B_l >_t = 0$ below threshold and $< B_l >_t \neq 0$ above threshold. This would force the other term in (4.7) to be zero above threshold, leading to the following set of operating point equations,

$$\frac{1}{\tau_l} = \frac{\Gamma_{ll}\omega_l}{\mu^2}\chi_I(n_o,\bar{\omega}_l) \tag{4.9}$$

$$\bar{\omega}_l = \omega_l\left[1 + \frac{\Gamma_{ll}}{2\mu^2}\chi_R(n_o,\bar{\omega}_l)\right] \tag{4.10}$$

which in conjunction with (4.8) would comprise the equations of state for the laser. Although these equations are quite accurate for a laser biased well above threshold, they are in fact only approximate, neglecting the role of spontaneous emission in initiating lasing action. This is easily seen by substituting (4.9) into (4.8). For single mode operation we find,

$$\frac{< B_l^* B_l >_t}{V_l} = \Gamma_{ll}\tau_l < E - R(n) >_t \tag{4.11}$$

The threshold knee predicted by this equation is a sharp corner, showing none of the characteristic signs of spontaneous emission. To include this effect it must be recognized that above threshold the field amplitude is not perfectly coherent so that $< B_l >_t$ is zero always and (4.7) remains indeterminant.

It is clear from (4.8) that the average photon number $P_l \equiv < b_l^* b_l >_t$ of a given mode l must be nonzero above threshold. This suggests that a photon number rate equation will lead to meaningful steady state results. We thus consider an operating point equation which results from the following photon rate equation,

$$\dot{P}_l = -\frac{P_l}{\tau_l} + \frac{\Gamma_{ll}\omega_l}{\mu^2}\chi_I(n,\bar{\omega}_l)P_l + \theta_l + \frac{2n_l}{\tau_l} \tag{4.12}$$

where θ_l is the spontaneous emission rate into mode l and the term involving n_l (number of thermal photons in mode l) can be neglected at optical frequencies. A derivation of this equation based on the quantum counterpart of (4.1) is presented in Appendix B. One can choose to bypass this Appendix by noting that, aside from the term involving n_l, (4.12) is a sensible choice for a photon rate equation, including photon gain and loss terms as well as spontaneous emission into the optical mode. The steady-state form of (4.12) reduces to the following,

$$\frac{1}{\tau_l} = \frac{\Gamma_{ll}\omega_l}{\mu^2}\chi_I(n,\bar{\omega}_l) + \frac{\theta_l}{P_l} \quad . \tag{4.13}$$

This should be compared to Eqn. (4.9). Eqn. (4.13) contains an additional term which involves the spontaneous emission rate. For large modal energies this term is small so that, as mentioned before, the approximation involved in the derivation of (4.9) gets better at higher modal energies. The correction term will be defined as,

$$2\varepsilon_l \equiv \frac{\theta_l}{P_l} \quad . \tag{4.14}$$

As it turns out, ε_l is just the field spectrum linewidth of a tuned laser oscillator (in SL's there is a correction term to this linewidth due to the detuned nature of the gain spectrum). For index guided SL's operated only modestly above threshold $\varepsilon_l^{-1} \approx$ 100nsec., whereas $\tau_l \approx$ 1psec. so that (4.9) is normally quite accurate. Even so, for considerations of the power fluctuation spectrum in a multimode laser serious problems arise (singularities in the noise spectra) unless the discrepancy between (4.9) and (4.13) is taken into account. For this reason only

we will use (4.8), (4.10) and (4.13) as the operating point equations in the analysis to follow.

After separating the steady-state operating point equations from (4.1) and (4.2), the remaining small signal equations are,

$$\dot{\rho}_l = -2\varepsilon_l\rho_l + \frac{\Gamma_{ll}\omega_l}{2\mu^2}\xi_l n_l + \Delta_{rl} \tag{4.15}$$

$$\dot{\varphi}_l = -\frac{\Gamma_{ll}\omega_l}{2\mu^2}\xi_R n_l + \Delta_{il} \tag{4.16}$$

$$\dot{n}_l = -\left(R'(n_o) + \sum_l \frac{\omega_l\xi_l p_l}{\mu^2}\right)n_l - \sum_l \frac{\omega_l\chi_l p_l}{\mu^2}2\rho_l \tag{4.17}$$

where $p_l \equiv P_l/V_l$ is the photon density of mode l and the following definitions apply,

$$\Delta_{rl} \equiv \frac{1}{2\sqrt{P_l}}\left(s_l e^{\imath\varpi_l t} + s_l^* e^{-\imath\varpi_l t}\right) \tag{4.18}$$

$$\Delta_{il} \equiv \frac{1}{2\imath\sqrt{P_l}}\left(s_l e^{\imath\varpi_l t} - s_l^* e^{-\imath\varpi_l t}\right) \tag{4.19}$$

Equations (4.15), (4.16), and (4.17) can be made more compact by assuming that ξ_l, ξ_R, and Γ_{ll} are approximately frequency independent quantities so that an approximately frequency independent small signal gain can be defined,

$$\eta = \frac{\Gamma_{ll}\omega_l\xi_l}{\mu^2}n_l \equiv \Gamma_{ll}G_l n_l \tag{4.20}$$

where a differential gain is defined by,

$$G_l' = \frac{dG_l}{dn} = \frac{\omega_l}{\mu^2}\frac{d\chi_I}{dn} = \frac{\omega_l \xi_I}{\mu^2} \quad . \tag{4.21}$$

Doing so we arrive at the following small signal equations,

$$\dot{\rho}_l = -2\varepsilon_l \rho_l + \frac{1}{2}\eta + \Delta_{rl} \tag{4.22}$$

$$\dot{\varphi}_l = -\frac{\alpha}{2}\eta + \Delta_{il} \tag{4.23}$$

$$\dot{\eta} = -\frac{1}{\tau_R}\eta - \sum_l \omega_{Rl}^2 2\rho_l \tag{4.24}$$

where,

$$\frac{1}{\tau_R} \equiv R'(n_o) + \sum_l G_l' p_l \tag{4.25}$$

$$\omega_{Rl}^2 \equiv \Gamma_{ll} G_l' G_l p_l \tag{4.26}$$

$$\alpha \equiv \frac{\xi_R}{\xi_I} \quad . \tag{4.27}$$

Here, ω_{Rl} is the relaxation oscillation frequency of the l^{th} mode and τ_R is the damping time associated with it. The parameter α, defined in (4.27), has received considerable attention recently. Referred to as the linewidth enhancement factor or amplitude phase coupling factor, it results from the detuned nature of the gain spectrum in SL's and plays a key role in determining the form of various phase noise spectra.

3.5 Calculation of optical spectra

In this section we will solve the fluctuation equations (4.22), (4.23), and (4.24) for the noise spectra associated with $\{\rho_m\}$ and $\{\varphi_m\}$, and then apply the formulae

of Section 3.2 to determine certain important SL optical spectra. The structure of these equations enables solution of the amplitude noise spectra independent of the phase noise spectra (i.e., the inversion reacts to the field intensity $|b|^2$, not the field stength b). For this reason we will consider power fluctuation spectra in single mode and multimode operation before considering the phase noise spectra for these cases. The method of solution will be to transform and solve for ρ_{mT}, φ_{mT}, and η_T, where, for example,

$$\rho_{mT}(\Omega) \equiv \int_{-T}^{+T} e^{-i\Omega t}\rho_m(t)dt \quad . \tag{5.1}$$

The associated spectral density function is then given by,

$$W_\rho^{mn}(\Omega) = \lim_{T\to\infty} \frac{<\rho_{mT}^*(\Omega)\rho_{n,T}(\Omega)>}{2T} \quad . \tag{5.2}$$

All results we obtain will be couched in terms of the spectral density functions of the noise forces. These functions can be found by either a heuristic approach identical to that used by us in Refs. [7,8] or a quantum approach which is given in Appendix C. The results of either calculation are summarized below.

$$F_\tau\left[<\Delta_{rl}(t+\tau)\Delta_{rm}(t)>\right] = \frac{\Theta_l}{2P_l}\delta_{lm} = \varepsilon_l\delta_{lm} \tag{5.3}$$

$$F_\tau\left[<\Delta_{il}(t+\tau)\Delta_{im}(t)>\right] = \frac{\Theta_l}{2P_l}\delta_{lm} = \varepsilon_l\delta_{lm} \tag{5.4}$$

$$F_\tau\left[<\Delta_{rl}(t+\tau)\Delta_{im}(t)>\right] = 0 \tag{5.5}$$

where F_τ signifies Fourier transform with respect to τ, δ_{lm} is the Kronecker delta, and Θ_l is the spontaneous emission rate into mode l.

Power Fluctuation Spectra

SINGLE MODE OPERATION. The criterion used to determine whether a SL is lasing in a single mode depends on one's perspective. In an optical communications system the criterion will be set by factors external to the SL such as receiver performance and properties of the transmission medium. In this analysis, however, we are concerned only with characterizing the physics involved in lasing action, in particular, the dynamic interaction of the active medium with the lasing modes. From (4.24) it is clear that this interaction will involve a single mode if it is possible to make the approximation,

$$\sum_l \omega_{Rl}^2 \rho_l \approx \omega_{Rm}^2 \rho_m \tag{5.6}$$

where mode m is the dominant mode. This leaves a single stimulated rate term in the inversion equation (4.24), but does not imply that the dominant mode m is altering inversion dynamics (i.e., is coupled strongly to the inversion). If, for example, the dominant mode m is so weak that the inversion still exhibits a simple relaxation with time constant τ_R, then it is clear that even the stimulated rate term associated with mode m can be neglected. We thus need to quantify what is meant by strong and weak dynamic coupling of the optical modes with the inversion in order to identify a dominant mode or set of modes as the case may be. Such a condition has already been stated: weak dynamic coupling between a mode m and the inversion implies,

$$2\omega_{Rm}^2 \rho_m << \frac{1}{\tau_R}\eta \quad ; \tag{5.7}$$

that is, the stimulated rate term associated with mode m can be neglected in comparison to the inversion relaxation rate. By solving (4.22) and (4.24) this condition can be reduced to,

$$|c_m(\Omega)| \equiv \left| \frac{\omega_{Rm}^2 \tau_R}{2\varepsilon_m + \imath\Omega} \right| << 1 \tag{5.8}$$

where the dimensionless complex parameter c_m will be referred to as the (dynamic) coupling strength parameter. When the low frequency value of $|c_m(\Omega)|$ is small in comparison to unity, a mode m can be neglected in a calculation of the inversion dynamics (i.e., can be omitted in (4.24)). Otherwise, the mode must be included in the analysis. By using (4.14) and (4.26) we can rewrite $c_m(0)$ as,

$$c_m(0) \equiv \frac{\Gamma_{mm} G_m' \tau_R V_m}{n_{sp}} p_m^2 \tag{5.9}$$

where $n_{sp} \equiv \theta_m / G_m$ is the spontaneous emission factor. In Fig. 3.3 we have plotted this function versus the photon density p_m of mode m along the bottom axis and versus the modal output power per facet along the top axis (assuming a total facet loss rate of $2X10^{11}sec^{-1}$ and a lasing wavelength of $\lambda_m \equiv 0.85\mu M$.). In making this plot we have taken $\Gamma_{mm} = 0.5$, $G_m' = 2.5X10^{-6}$ cm.^{3}/sec, $R(n_o) = 1GHz.$, $V_m = 10^{-10}$cm.^{3}, and $n_{sp} = 2.5$ [7,8] (these values will be assumed in all calculations to follow). It can be seen that $c_m(0) = 1$ when the photon density of mode m reaches $5X10^{12}$ cm.$^{-3}$ which is an equivalent output power of approximately $10\mu W$ per facet. In Fig. 3.4 the field spectrum for an actual device near threshold and well above threshold is presented with the optical modes labeled by their approximate coupling strengths.

Provided $\{|c_l(0)| << 1\}$ holds for all but one mode m, the dominant mode, we can easily solve for $W_p^{mm}(\Omega)$ by applying (5.6) to (4.24). This in turn gives the relative power noise (RPN) spectrum through (1.4),

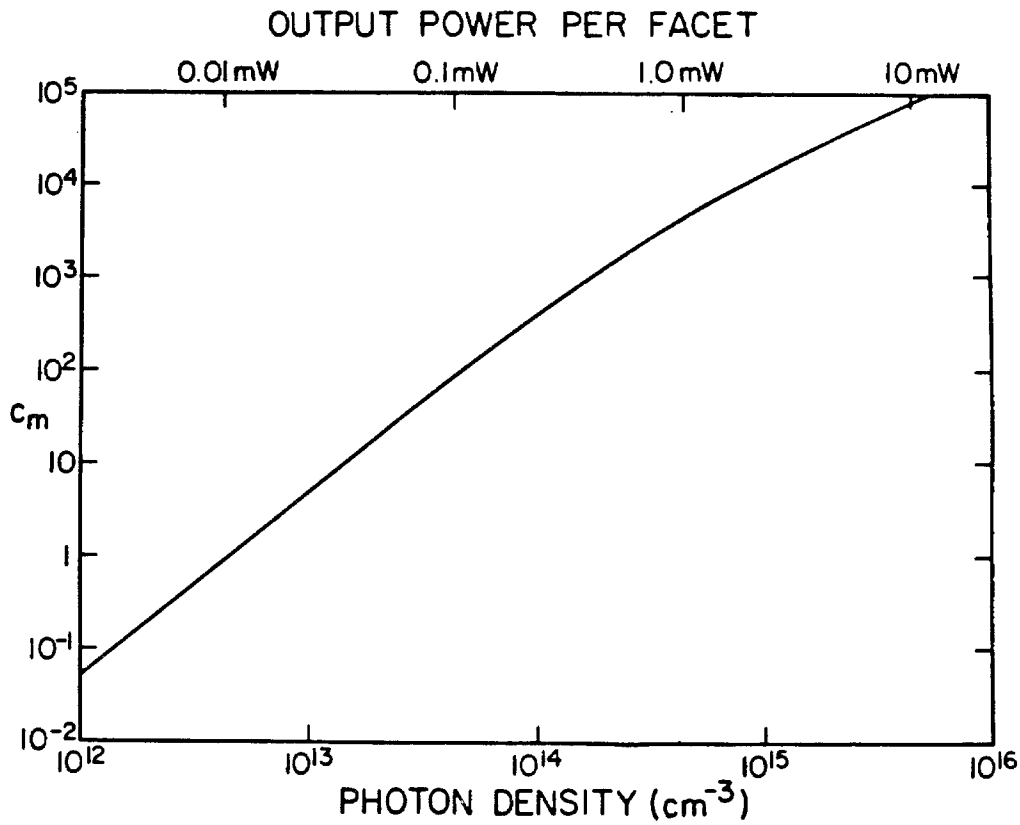

Figure 3.3 Dynamic coupling strength parameter plotted versus photon density in optical mode m and output power per facet due to mode m.

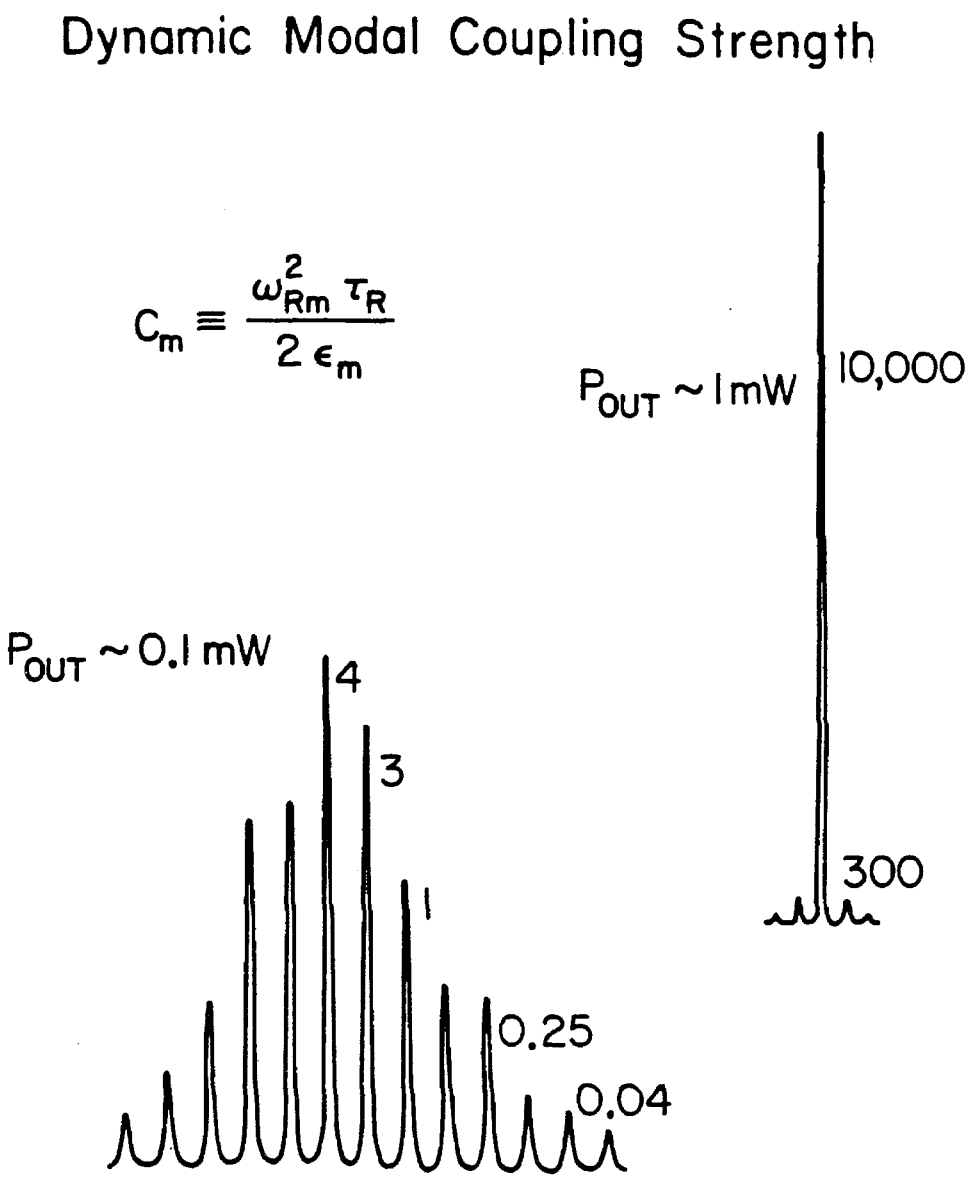

Figure 3.4 Field spectra for a semiconductor laser near threshold and well above threshold with the modes labeled by their approximate dynamic coupling strength parameters.

$$\frac{W_{\Delta I}(\Omega)}{I_T^2} = 4W_p^{mm}(\Omega) = \frac{\Omega^2 + \frac{1}{\tau_R^2}}{\left(\omega_{Rm}^2 + \frac{2\varepsilon_m}{\tau_R} - \Omega^2\right)^2 + \Omega^2\left(\frac{1}{\tau_R} + 2\varepsilon_m\right)^2} \frac{2\theta_m}{P_m} \qquad (5.10)$$

This spectrum is plotted in Fig. 3.5 for several photon densities. At modest output powers the spiking resonance in the Figure is quite accurately given by ω_{Rm}. This resonance behavior was first predicted by McCumber [9] and first observed in SL's by Paoli and Ripper [25]. This relaxation oscillation corner frequency also sets the useful direct modulation bandwidth for these devices [49], and for this reason the portion of the RPN spectrum lying below ω_{Rm} is of considerable importance in optical communication systems employing directly modulated SL's. The RPN strength in the low frequency region ($\Omega < 1/\tau_R$) is given by,

$$\frac{W_{\Delta I}(\Omega \approx 0)}{I_T^2} = \frac{\frac{2\theta_m}{P_m}}{\left(\omega_{Rm}^2\tau_R + 2\varepsilon_m\right)^2} \approx \frac{4\varepsilon_m}{\omega_{Rm}^4\tau_R^2} \qquad (5.11)$$

This function is plotted versus photon density in Fig. 3.6. It exhibits an inverse cubic dependence at moderate power followed by an inverse power dependence at high powers. Relative power fluctuations are thus reduced with increasing excitation of the lasing mode. This phenomenon, characteristic of all regenerative oscillators, is a consequence of the saturation of the inverted medium. At low frequencies where the RPN is flat (i.e., $\Omega < \tau_R^{-1}$) the active medium tracks power fluctuations of the lasing mode and damps them. At higher frequencies the active medium no longer effectively tracks these fluctuations and the RPN rises towards ω_{Rm} (the RPN @ $\Omega = \omega_{Rm}$ is also plotted in Fig. 3.6 for comparison). An interesting feature of (5.11) is its dependence on the corner frequency ω_{Rm}. For all other conditions the same SL's having faster modulation responses also have lower RPN's. This is an added advantage of fast SL's, which often goes

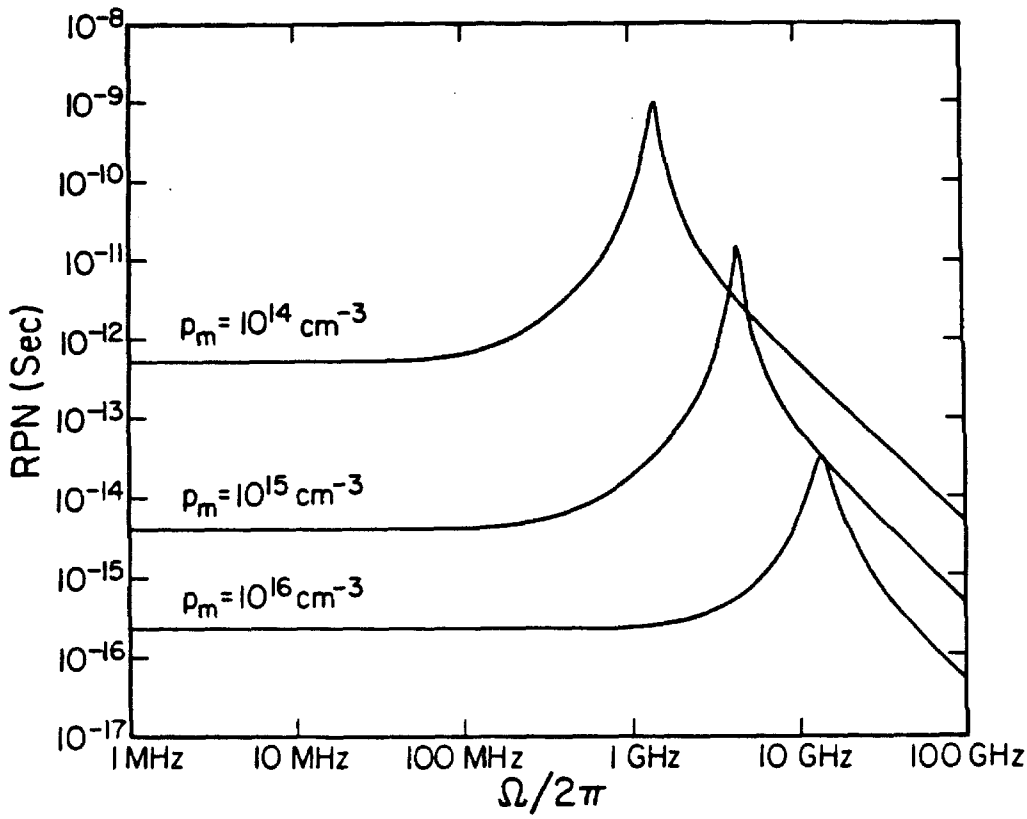

Figure 3.5 Single mode relative power noise spectra.

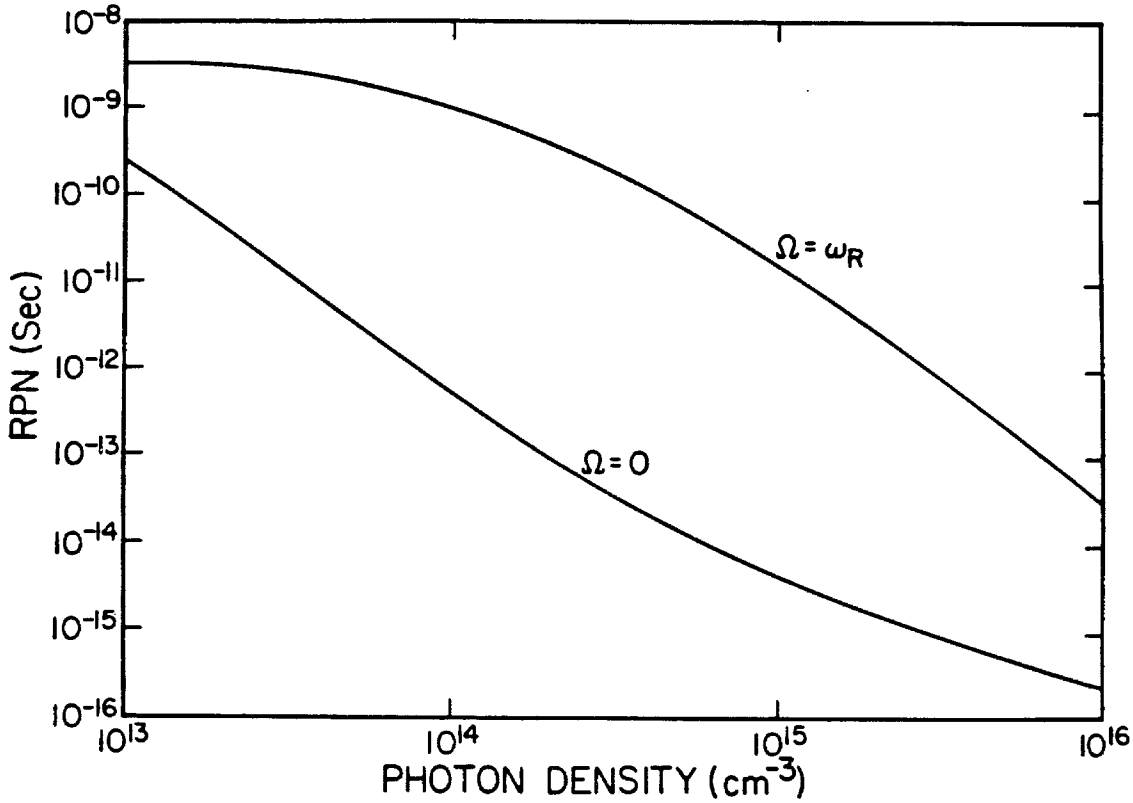

Figure 3.6 Single mode relative power noise spectrum at two frequencies plotted versus modal photon density.

unnoticed.

MULTIMODE OPERATION: If there are several modes which have comparable coupling strength parameters of order one or greater, then the gain medium is dynamically interacting with a group of modes. Under these circumstances the approximation (5.6) amounts to reducing a sum over all modes to a sum over the prescribed set of dominant modes.

$$\sum_{l} \omega_{Rl}^2 \rho_l \approx \sum_{l}^{N} \omega_{Rl}^2 \rho_l \tag{5.12}$$

where there are N dominant modes.

Solving the set of N+1 equations given by (4.22) and (4.24) is easiest when a new dynamic variable is defined as,

$$a \equiv \sum_{l}^{N} \omega_{Rl}^2 2\rho_l \quad . \tag{5.13}$$

The variable "a" is the quantity damped by gain saturation in the multimode situation. That is, the gain reacts to fluctuations in "a" and stabilizes them. Later in this Section it will be demonstrated that under a certain approximation nearly always valid in SL's this variable is proportional to the total power fluctuation resulting from fluctuations in all lasing modes. This is why it is often said that gain saturation tends to stabilize fluctuations of total power in a multimode laser when in fact it is more precise to say that fluctuations of the variable "a" are stabilized. Transforming (4.22) and (4.24) according to (5.1) and then applying definition (5.13), the system of N+1 equations reduces to a pair of equations for a_T and η_T. With knowledge of η_T the fluctuations $\{\rho_{lT}\}$ and their associated spectral density functions are then easily found. For later reference we give the spectral density functions of a and η.

$$W_a(\Omega) = \frac{(1 + \Omega^2\tau_R^2)\sum_1 \frac{4\varepsilon_1}{\tau_R^2}|c_1(\Omega)|^2}{\left|1 + \iota\Omega\tau_R + \sum_1^N c_1(\Omega)\right|^2} \tag{5.14}$$

$$W_\eta(\Omega) = \frac{\sum_1^N 4\varepsilon_1|c_1(\Omega)|^2}{\left|1 + \iota\Omega\tau_R + \sum_1^N c_1(\Omega)\right|^2} \tag{5.15}$$

If a single mode m is isolated, then its RPN will be given by $4W_\rho^{mm}(\Omega)$. Using the prescription for solution outlined above we find for this quantity the following rather complicated expression,

$$W_\rho^{mm}(\Omega) = \frac{\varepsilon_m\left[\frac{1}{\tau_R^2}(1 + D_1)^2 + \Omega^2\left(1 - \frac{1}{\tau_R}D_2\right)^2\right] + \frac{1}{\tau_R^2}D_3}{\left(\omega_{Rm}^2(1 + D_4) + \frac{2\varepsilon_m}{\tau_R} - \Omega^2\right)^2 + \Omega^2\left(\frac{1}{\tau_R} + 2\varepsilon_m + \omega_{Rm}^2 D_5\right)^2} \tag{5.16}$$

$$D_1 \equiv \sum_{l \neq m} \frac{|c_l(\Omega)|^2}{c_l(0)} \tag{5.16a}$$

$$D_2 \equiv \sum_{l \neq m} \frac{|c_l(\Omega)|^2}{c_l(0)2\varepsilon_l} \tag{5.16b}$$

$$D_3 \equiv \sum_{l \neq m} \varepsilon_l|c_l(\Omega)|^2 \tag{5.16c}$$

$$D_4 \equiv \sum_{l \neq m} |c_l(\Omega)|^2 \frac{1 + \frac{\Omega^2}{4\varepsilon_m\varepsilon_l}}{c_l(0)c_m(0)} \tag{5.16d}$$

$$D_5 \equiv \sum_{l \neq m} |c_l(\Omega)|^2 \frac{\frac{1}{2\varepsilon_m} - \frac{1}{2\varepsilon_l}}{c_l(0)c_m(0)} \tag{5.16e}$$

This expression should be compared to (5.10). In the case where $\{c_{l \neq m}(0) < c_m(0)\}$, (5.16) reduces to the single mode expression (5.10). In general, however, additional terms enter the RPN expression for a single mode m which can enhance it by several orders of magnitude. This enhancement is the so-called mode partition noise discussed by McCumber [9]. Gain saturation, which in the single mode case worked to reduce power fluctuations of the lasing mode, acts to reduce the total power fluctuations in the multimode case (a point discussed in some detail below). A single lasing mode amidst the ensemble of lasing modes thus suffers an enhancement of its power fluctuations on account of the partitioning of energy from the gain medium into all lasing modes. To illustrate how large the partition noise can be for a single mode we now use (5.16) to consider a worst possible case in which the number of dominant modes N is very large and all of the dominant modes couple equally well to the inversion (i.e., we assume identical c's and ε's). Under these circumstances the RPN for a single mode m is approximately given by,

$$4W_\rho^{mm}(\Omega) \approx \frac{4\varepsilon}{\tau_R^2} \frac{1 + \Omega^2\tau_R^2 + \frac{(N-1)^2c^2}{1 + \frac{\Omega^2}{4\varepsilon^2}}}{\left(\omega_R^2 N + \frac{2\varepsilon}{\tau_R} - \Omega^2\right)^2 + \Omega^2\left(\frac{1}{\tau_R} + 2\varepsilon\right)^2} \tag{5.17}$$

where we have neglected a term of order $c^2(N-1)$ in the numerator. This expression reduces to the single mode expression (5.10) when N = 1. For N >> 1 the form of the denominator remains essentially the same except for an enhancement of the corner frequency by a factor of N; the numerator, however, contains a new term which is quite large and has a Lorentzian frequency

dependence. (5.17) is plotted in Fig. 3.7 for N = 10. To effectively illustrate the partition noise contribution we have also plotted (5.17) without the numerator term involving $(N-1)^2$. Next consider the low frequency RPN in the multimode worst case versus the single mode case. From (5.17) we have,

$$W_\rho^{mm}(\Omega \approx 0) = \frac{1}{4\varepsilon}\frac{1+(N-1)^2c^2}{(Nc+1)^2} \quad . \tag{5.18}$$

As $N\to\infty$, $W_\rho^{mm}(\Omega \approx 0)$ becomes independent of the dynamic coupling parameter c. In this worst case situation, it is as though gain saturation quieting is completely unable to stabilize the mode. Using (5.18) we find the ratio,

$$\frac{W_\rho^{mm}(\Omega \approx 0)|_{N>>1}}{W_\rho^{mm}(\Omega \approx 0)|_{N=1}} = c_1^2\frac{\varepsilon_1}{\varepsilon_N} \tag{5.19}$$

where the subscripts indicate the number of lasing modes. Partition noise thus enhances the low frequency RPN by a factor c_1^2 over that for an equivalently excited mode in the single mode case. Well-excited modes exhibit c's of order 100 (see Figs. 3.3,3.4) so that partition noise degradation of the single mode RPN can be quite severe.

An important observation made by McCumber is that gain saturation quieting of power fluctuations in a homogeneously broadened laser (a SL has effectively a homogenously broadened gain spectrum owing to rapid intraband thermalization) works to quiet total power fluctuations. The partition noise contribution to single mode RPN is a direct consequence of this principle. A straightforward but tedious method for demonstrating this effect is to construct the total RPN for a group or subgroup of lasing modes as prescribed by (2.4). This calculation requires the off diagonal spectra $W_\rho^{mn}(\Omega)$ in addition to the diagonal spectra given by (5.16). McCumber has actually carried out such a calculation showing

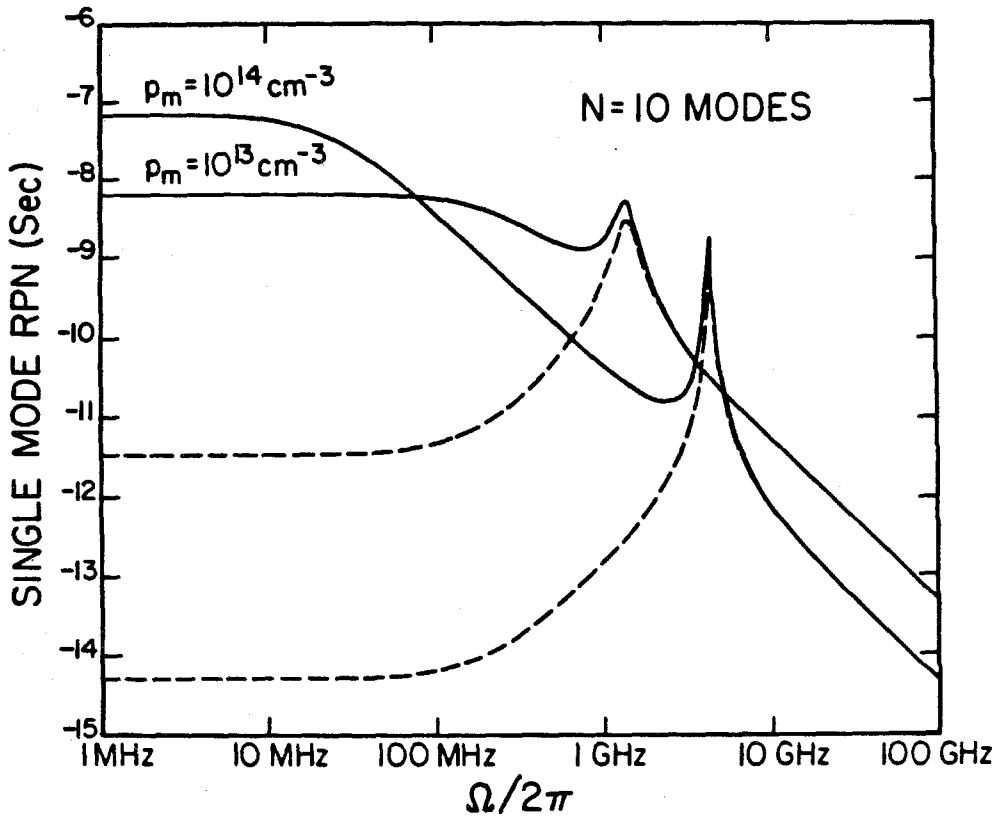

Figure 3.7 Solid curves are relative power noise spectra for a single mode amidst nine other modes of equal strength. Dashed curves are the same spectra with partition noise contributions omitted.

that negative fluctuation correlations exist between the lasing modes. These negative correlations appear as negative terms in the off diagonal spectra and their effect is to offset partition contributions in the diagonal spectra. The sum total contribution from the diagonal and the off diagonal spectra yield a total RPN which exhibits gain saturation damping. The negative cross correlation terms have also been observed experimentally by Armstrong and Smith [17].

To calculate the total RPN in the present analysis we will elaborate on a point made earlier in this section. This is, that the dynamic variable a is approximately proportional to the total power fluctuation. The approximation involved here assumes that Γ_{ll}, G_l and G_l' are nearly frequency independent over the range of frequency space spanned by the lasing modes (part of this approximation, assuming frequency independent Γ_{ll} and G_l', has already been invoked in writing the equations (4.22), (4.23), and (4.24)). It must be remembered that whereas this constitutes an excellent approximation for SL's operating at their gain peak, this is not always the case so that the results we obtain must be applied with some caution. In addition, the approximation is invoked only in the dynamic equations, never in the steady-state operating point equations. There the small variations in G_l which do exist lead to large differences in the distribution of steady-state stimulated power among the lasing modes. With these comments in mind we write,

$$a = \sum_{l}^{N} \omega_{Rl}^2 2\rho_l \approx \bar{\omega}_R^2 \frac{\Delta I(t)}{I_T} \tag{5.20}$$

where (2.3) and (4.26) have been used and we have defined,

$$\bar{\omega}_R^2 \equiv \Gamma G' G \sum_1^N p_m = \sum_1^N \omega_R^2 \tag{5.21}$$

with subscripts on Γ, G', and G suppressed. It is now very easy to write the total RPN. Combining (5.20) and (2.4) we find,

$$\frac{W_{\Delta I}(\Omega)}{I_T^2} = \frac{1}{\bar{\omega}_R^4} W_a(\Omega) \tag{5.22}$$

which upon substitution for $W_a(\Omega)$ using (5.14) followed by expansion of the resulting expression yields,

$$\frac{W_{\Delta I}(\Omega)}{I_T^2} = \frac{1}{\bar{\omega}_R^4} \frac{\left(\Omega^2 + \frac{1}{\tau_R^2}\right) \sum_1^N 4\varepsilon_l \omega_{Rl}^4 \frac{\Omega^2}{\Omega^2 + 4\varepsilon_l^2}}{\left(\Omega^2 - \sum_1^N \omega_{Rl}^2 \frac{\Omega^2}{\Omega^2 + 4\varepsilon^2}\right)^2 + \frac{\Omega^2}{\tau_R^2}\left(1 + \sum_1^N \frac{c_l(0) 4\varepsilon_l^2}{\Omega^2 + 4\varepsilon_l^2}\right)^2} \tag{5.23}$$

In the low frequency limit (5.23) reduces to,

$$\frac{W_{\Delta I}(\Omega \approx 0)}{I_T^2} = \frac{1}{\bar{\omega}_R^4 \tau_R^2} \frac{\sum_1^N 4\varepsilon_l c_l^2}{\left(1 + \sum_1^N c_l\right)^2} \tag{5.24}$$

This expression is very similar in form to the low frequency limit of (5.10) (Eqn. (5.11)) for the RPN in single mode operation. The differences are first, the replacement of ε_l in (5.11) by an effective ε which is an average over all lasing modes weighted by their coupling strength parameters, and second, the appearance of an effective corner frequency $\bar{\omega}_R$ in the present expression. To see that the frequency dependence of (5.23) is also very similar to that of Eqn. (5.10) we will simplify (5.23) by dividing the N lasing modes into Q "strong" modes and N-Q "weak" modes. We conjecture that (5.23) will exhibit a corner frequency ω_R which lies in the band of frequencies $2\varepsilon_{strong} < \Omega < 2\varepsilon_{weak}$ where ε_{strong} is the largest ε_l

in the strong mode set and ε_{weak} is the smallest ε_l in the weak mode set. Confining attention to this band we can approximate (5.23) as,

$$\frac{W_{\Delta I}(\Omega)}{I_T^2} \approx \frac{1}{\bar{\omega}_R^4} \frac{\left(\Omega^2 + \frac{1}{\tau_R^2}\right) \sum_{strong} 4\varepsilon_l \omega_{Rl}^4}{\left(\Omega^2 - \sum_{strong} \omega_{Rl}^2\right)^2 + \frac{\Omega^2}{\tau_R^2}\left(1 + \sum_{weak} c_l(0)\right)^2} \quad . \tag{5.25}$$

Thus within this particular band of frequencies the form of the total RPN is identical to the RPN derived for the single mode case. In the multimode case the strong modes determine the amplitude of the RPN as well as its approximate corner frequency ω_R where,

$$\omega_R^2 \equiv \sum_{strong} \omega_{Rl}^2 \quad . \tag{5.26}$$

Weak modes, on the other hand, contribute to increased damping of the spiking resonance (This dynamic classification of modes we describe here is illustrated in Fig. 3.8). For this reason the spiking resonance in Fig. 3.5, predicted by the single mode expression (5.10), is found in practice to be less pronounced. The same is also true for our worst case multimode plot in Fig. 3.7, since there we assumed that all modes were equally well excited (in practice there will always be weak modes). For further comparison the exact expression (5.23) has been plotted in Fig. 3.9 for the worst possible case conditions described earlier. It is clear from the plot that gain saturation damping is operative.

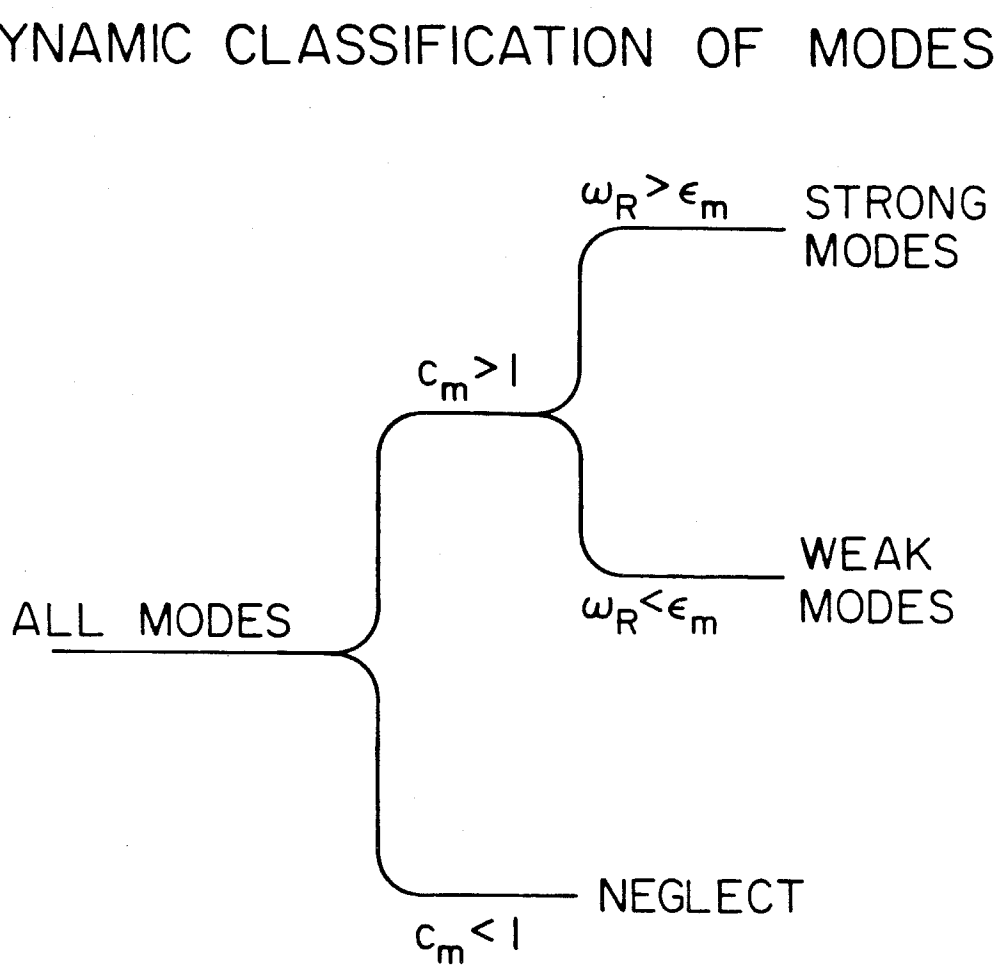

Figure 3.8 A classification of the modes in a SL according to their dynamic interaction with the inversion as given by the coupling strength parameter c.

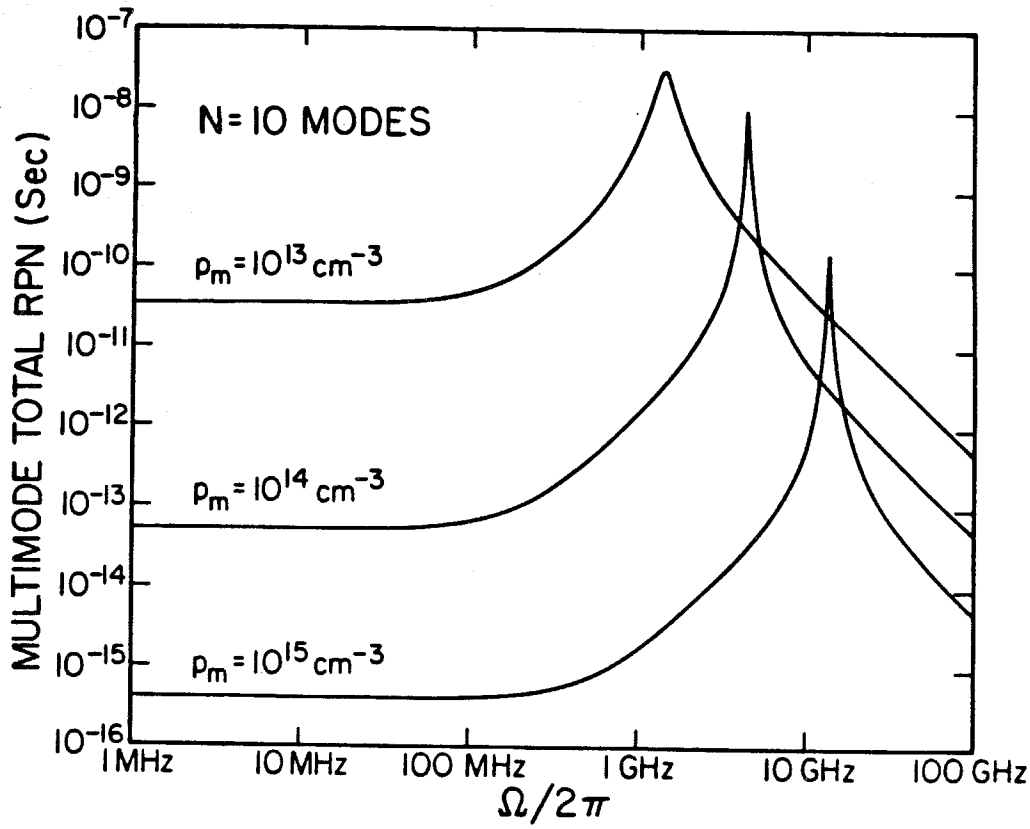

Figure 3.9 Total relative power noise spectra for multimode semiconductor laser consisting of ten equally excited modes. Photon density quoted is per mode.

Frequency Fluctuation Spectra and Linewidth

Using (4.23) and the defining relation (2.6) we find for the frequency fluctuation spectra,

$$W_{\Delta\omega}^{mn}(\Omega) = \frac{\alpha^2}{4} W_\eta(\Omega) + \varepsilon_m \delta_{mn} \tag{5.27}$$

where $W_\eta(\Omega)$ is given by (5.15). $W_{\Delta\omega}^{mn}(\Omega)$ is now expanded for single mode and multimode operation.

$$W_{\Delta\omega}^{mm}(\Omega) = \varepsilon_m \left[1 + \frac{\omega_{Rm}^4 \alpha^2}{\left(\omega_{Rm}^2 + \frac{2\varepsilon_m}{\tau_R} - \Omega^2 \right)^2 + \Omega^2 \left(\frac{1}{\tau_R} + 2\varepsilon_m \right)^2} \right] \tag{5.28}$$

$$W_{\Delta\omega}^{mn}(\Omega) = \varepsilon_m \delta_{mn} + \alpha^2 \frac{\sum_1^N 4\varepsilon_l \omega_{Rl}^4 \frac{\Omega^2}{\Omega^2 + 4\varepsilon_l^2}}{\left(\Omega^2 - \sum_1^N \omega_{Rl}^2 \frac{\Omega^2}{\Omega^2 + 4\varepsilon^2} \right)^2 + \frac{\Omega^2}{\tau_R^2} \left(1 + \sum_1^N \frac{c_l(0) 4\varepsilon_l^2}{\Omega^2 + 4\varepsilon_l^2} \right)^2} \tag{5.29}$$

As a result of amplitude phase coupling (i.e., a nonzero α parameter) these spectra bear a strong similarity to the RPN spectra. A plot of this spectrum at various output powers appears in Fig. 3.10.

For practical considerations by far the most important aspect of these spectra is their flat low frequency region. In accordance with the considerations of Section I the low frequency value of the diagonal frequency fluctuation spectrum gives the field spectrum linewidth $\Delta\omega_m$ of mode m. From (2.12) we write,

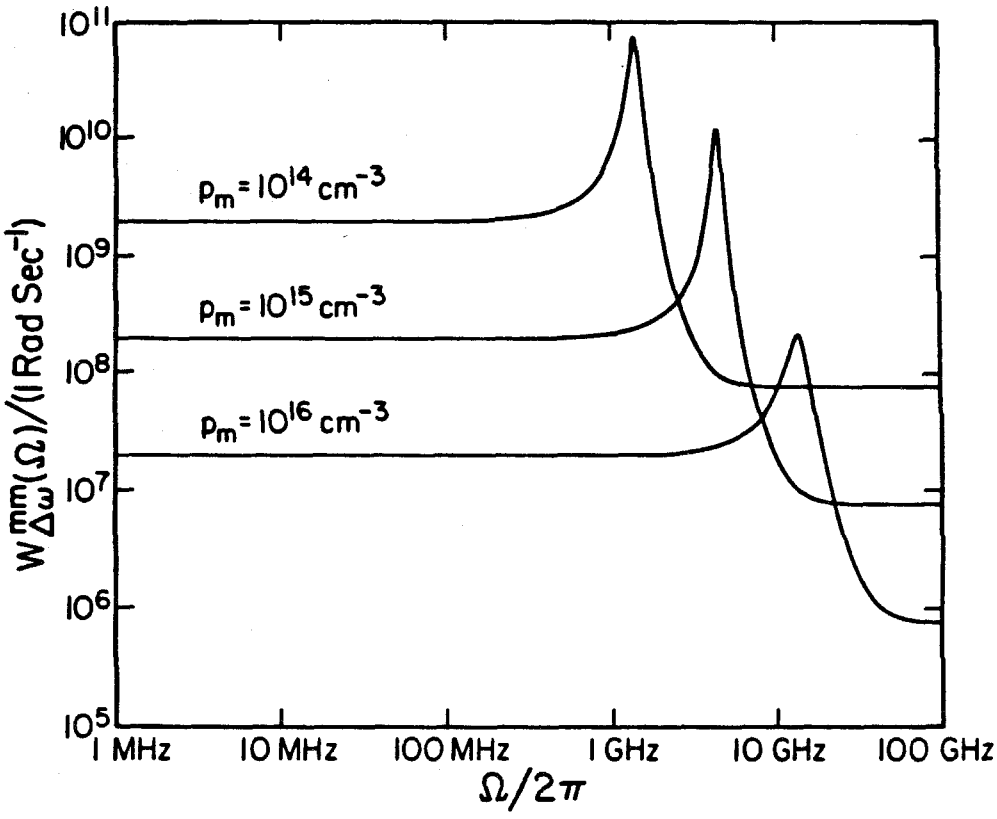

Figure 3.10 Frequency fluctuation spectra at various photon densities.

$$\Delta\omega_m = W_{\Delta\omega}^{mm}(\Omega \approx 0) \quad . \tag{5.30}$$

For single mode operation the substitution of (5.28) into this expression yields,

$$\Delta\omega_m = \varepsilon_m\left[1 + \alpha^2\right] \tag{5.31}$$

where we have assumed $2\varepsilon_m/\tau_R << \omega_{Rm}^2$. The linewidth ε_m, which is given by (4.14), is thus the field spectrum linewidth in the perfectly tuned case ($\alpha = 0$). This linewidth has long been known as the modified Schawlow Townes linewidth. The enhancement factor $1 + \alpha^2$ was first theoretically predicted by Haug and Haken [3], Lax [4], and Arzt et. al. [5]. More recently it has been invoked by several groups to explain the linewidth versus power measurements made by Fleming and Mooradian [1]. Data taken at Caltech showing this enhancement are presented in Figs. 3.11 and 3.12. Experimental estimates of α place it in the range -4 to -6 for bulk GaAs at room temperature [41,43]. These values are also in close agreement with theoretical calculations of the parameter based on Eqn. (4.27) of this chapter and Eqn. (4.9) of Chapter 2 (see Fig. 3.13) [2]. The net effect of the α parameter is thus to degrade spectral purity (enhance linewidth) by nearly 30X.

The α parameter is also responsible for FM generation under direct current modulation of a SL. In fact, it controls the apportioning of modulation energy into FM and AM components. We have conducted an experiment exploiting this fact to measure the α of an undoped active layer in a BOG laser [50]. The results of that measurement are summarized in Appendix D.

For the multimode case the substitution of (5.29) into (5.30) yields the following expression for the linewidth of a single lasing mode among an ensemble of lasing modes,

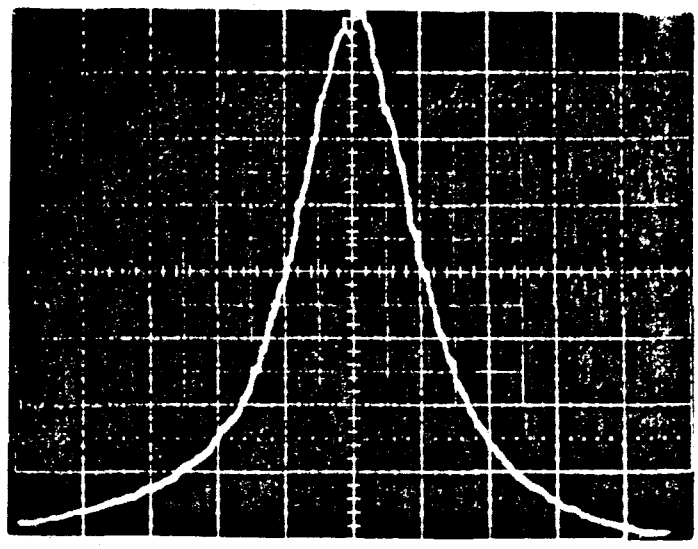

40MHz

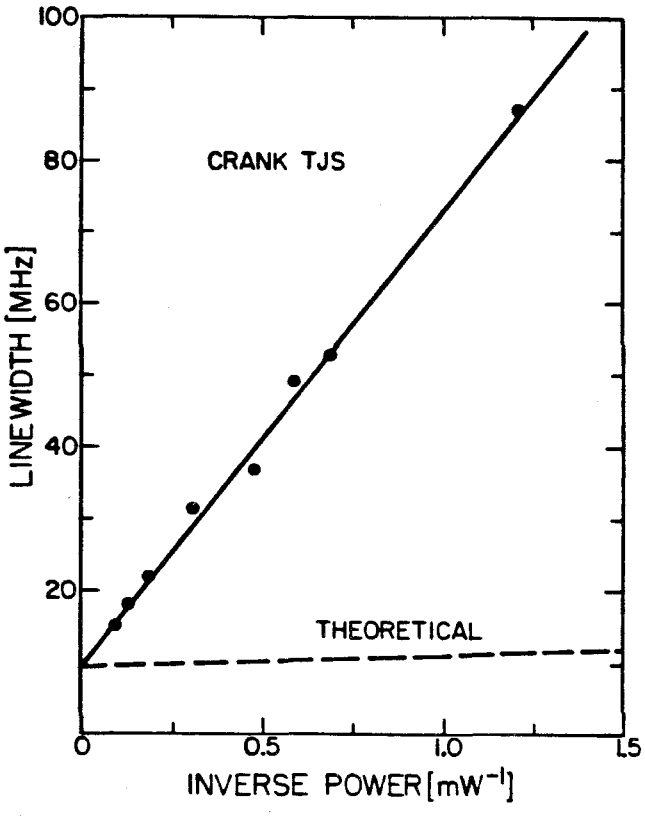

Figure 3.11 Field spectrum data for a single mode Mitsubishi crank transverse junction stripe (TJS) laser measured with a Tropel 240 confocal scanning Fabry Perot etalon having an instrumental bandwidth of 7.5 MHz. The upper portion of the figure shows the Lorentzian field spectrum resolved by the etalon. The lower portion of the figure gives the linewidth versus power data measured for this device. Also shown is the linewidth power relation predicted by the Schalow-Townes linewidth formula.

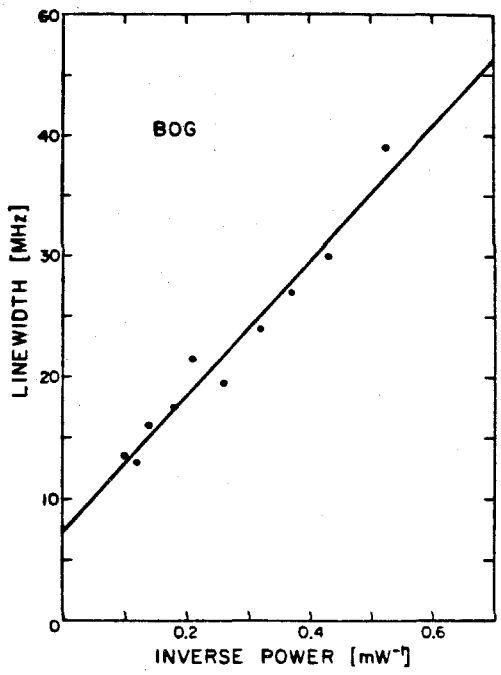

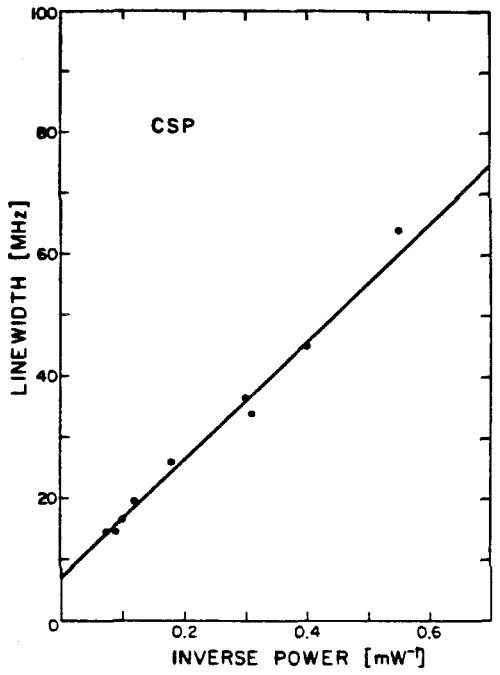

Figure 3.12 Additional linewidth power data taken with Hitachi buried optical guide (BOG HLP 3400) and channeled substrate planar (CSP HLP 1400) lasers.

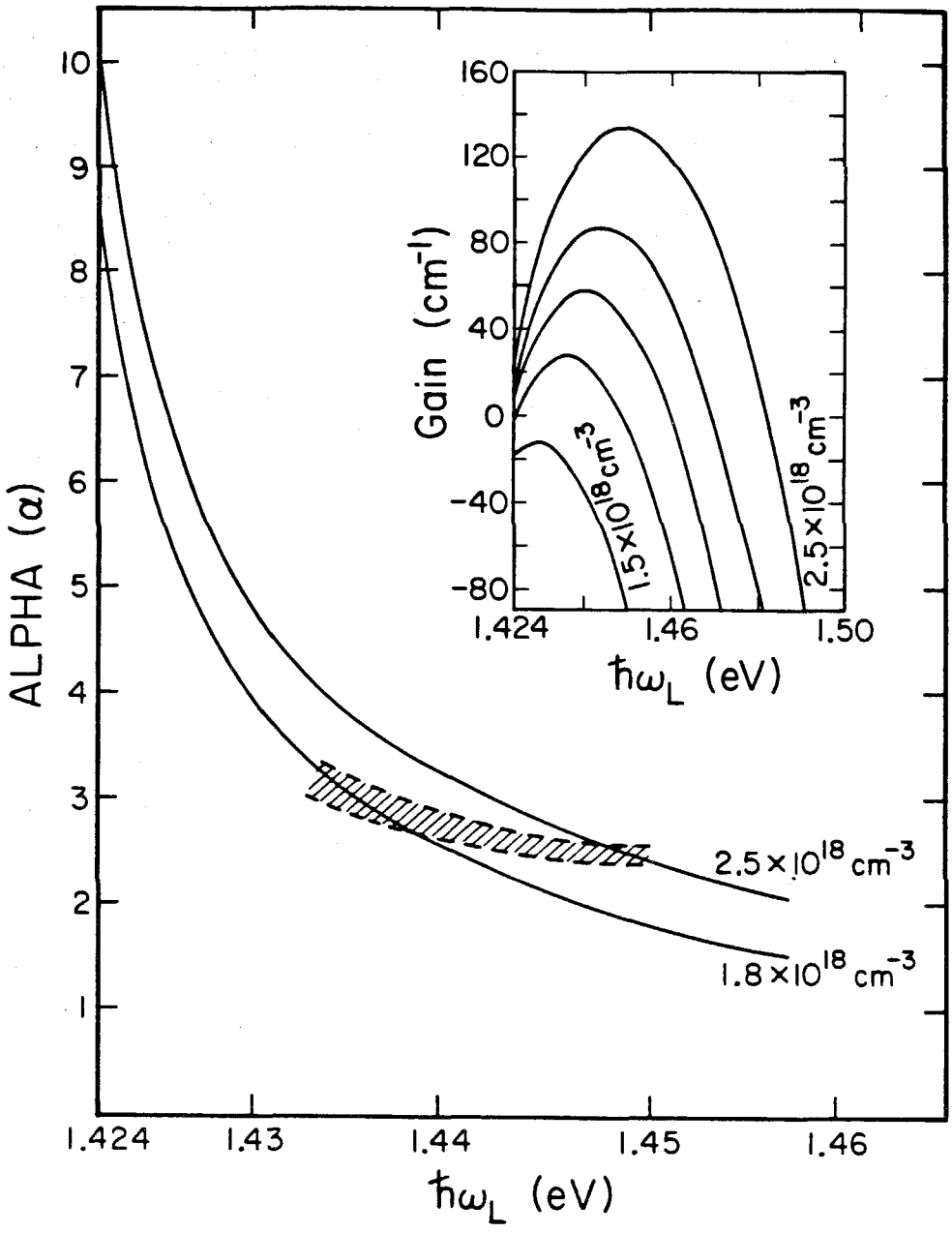

Figure 3.13 The linewidth enhancement factor spectrum at two excitation levels. The shaded area is a region within one laser free spectral range (typically ≈ 120GHz.) of gain peak. This spectrum was calculated for bulk GaAs assuming parabolic bands and includes only the interband contribution to α. The free carrier contribution is approximately unity, giving a total magnitude for α of about 4 at the gain peak. The inset shows the gain spectrum at these excitation levels.

$$\Delta\omega_m = \varepsilon_m + \alpha^2 \frac{\sum_l c_l^2(0)\varepsilon_m}{\left[1 + \sum_l c_l(0)\right]^2} \quad . \tag{5.32}$$

This expression contains the normal "tuned" Schawlow Townes contribution ε_m and in addition a "detuned" contribution consisting of a sum over all lasing modes of the Schawlow Townes linewidths for each mode weighted by the coupling strength parameter. When there is one very strong mode, this expression reduces to (5.31) and the standard inverse power dependence of linewidth results. In general, however, this relationship predicts a rather complicated linewidth power dependence. A specific example of one of the many possibilities is to consider the linewidth of a weak mode, having coupling strength c_W, in the presence of a strong mode having a coupling strength $c_S >> c_W$. Under these circumstances the linewidth of the weak mode is given approximately by,

$$\Delta\omega_W \approx \varepsilon_W + \alpha^2\varepsilon_S \approx \varepsilon_W + \Delta\omega_S \quad . \tag{5.33}$$

A measurement of $\Delta\omega_W$ versus the power in the weak mode would thus show, in addition to an inverse power component due to ε_W, a large component which is approximately the linewidth of the dominant mode. There is mounting experimental evidence which seems to confirm the existence of such a partition noise contribution to linewidth. Elsaber and Gobel have observed large, apparently power independent, contributions to linewidth in multimode lasers and have proposed partition noise as a possible explanation of their findings [47].

This intermodal phase coupling which results from the α parameter has another interesting consequence which was first conjectured by Henry [6] and which we now verify theoretically. We will show that, whereas the linewidths of individual lasing modes show considerable enhancement on account of detuning, their photomixed beatnote linewidth shows little or no such enhancement. A

strong phase noise correlation between modes causes this effect (see (5.29) for $m \neq n$). From (2.15) and (5.27) the beatnote linewidth generated by photomixing modes m and n is given by,

$$\Delta\omega_{mn} = \Delta\omega_m + \Delta\omega_n - \frac{\alpha^2}{2} W_\eta(\Omega \approx 0) = \varepsilon_m + \varepsilon_n \tag{5.34}$$

which is also the result one would obtain in a "tuned" laser, thus confirming theoretically Henry's conjecture. If we use values typical for α this result predicts that the spectral purity of beatnotes generated by photomixing SL lasing modes should be at least an order of magnitude better than the modes themselves, independent of the relative strengths of the modes. Recently, in work not yet published, we have observed this effect [50].

Field Spectrum Finestructure

The preceding calculation of linewidth was based on Eqn. (2.12) which predicts a Lorentzian lineshape function for each lasing mode. As discussed in Section I, however, the derivation of that result remains valid only within the optical frequency band $|\Omega - \omega_m| < 1/\tau_R$ where the assumptions of: (1), a flat $W_{\Delta\omega}^{mm}(\Omega)$ spectrum, and (2), gain saturation damping of amplitude fluctuations are justified. We will now discuss the shape of the field spectrum for a single lasing mode outside this band of frequencies. At these frequencies relaxation resonance effects become important so that conditions (1) and (2) are no longer satisfied, and Eqn. (2.17) must be utilized for the calculation. As can be seen from inspection of (2.17) the shape of this portion of the field spectrum is determined by contributions from two spectra already calculated, the RPN spectrum and the frequency fluctuation spectrum, and in addition the fluctuation coupling spectrum which is now calculated using the dynamic equations and (2.7):

$$W_{\rho\varphi}^{mm}(\Omega) = \frac{-\alpha\varepsilon_m\omega_{Rm}^2\Omega}{\left(\Omega^2+4\varepsilon^2\right)\left[\left(\omega_{Rm}^2-\Omega^2\right)^2+\frac{\Omega^2}{\tau_R^2}\right]}\left[4\varepsilon\left[1-\frac{\frac{2\omega_{Rm}^2}{\tau_R^2}}{\left(\omega_{Rm}^2-\Omega^2\right)^2+\frac{\Omega^2}{\tau_R^2}}\right]\right. \quad (5.35)$$

$$\left. + \frac{2}{\tau_R}\left[1-\frac{2\omega_{Rm}^2(\omega_{Rm}^2-\Omega^2)}{\left(\omega_{Rm}^2-\Omega^2\right)^2+\frac{\Omega^2}{\tau_R^2}}\right]\right] .$$

$W_{\rho\varphi}^{mm}(\Omega)$ is plotted in Fig. 3.14 and exhibits the asymmetry with repect to its argument which was discussed in Section I. In Fig. 3.15 we have plotted the field spectrum using (5.10), (5.28), and (5.35) in (2.17) (the sidebands are normalized by the value of the field spectrum at line center). The effect of the relaxation resonance is thus seen to cause the appearance of sidebands accompanying the central lasing peak. These sidebands are the result of spontaneous emission noise driving the photon-carrier resonance and subsequently causing phase and amplitude "modulation" of the lasing frequency. The asymmetry of the sidebands is due solely to the fluctuation coupling spectrum. As can be seen the finestructure peaks are normally quite small in amplitude. Aging or degradation, however, can have a destabilizing influence on the relaxation resonance and can lead to larger relative amplitudes, as well as higher order finestructure components. These higher-order components do not represent distortion but merely higher order sidebands due to increased phase modulation.

In Fig. 3.16 is finestructure which was observed in the field spectrum of an Hitachi CSP laser at an output power of 1 mW. per facet. These data were taken by first filtering out all weakly excited longitudinal modes with a wideband filter (grating spectrometer) followed by spectrum analysis with a scanning Fabry-Perot having a free spectral range of 7.5 GHz. and an instrumental bandwidth of 75 MHz. Fig. 3.17 gives the calculated finestructure for this device at the quoted

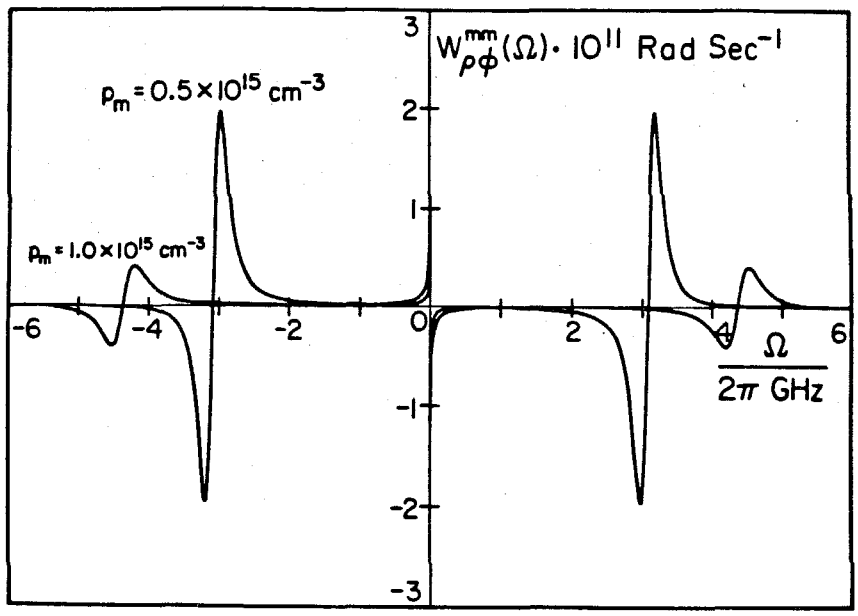

Figure 3.14 Diagonal fluctuation coupling spectra.

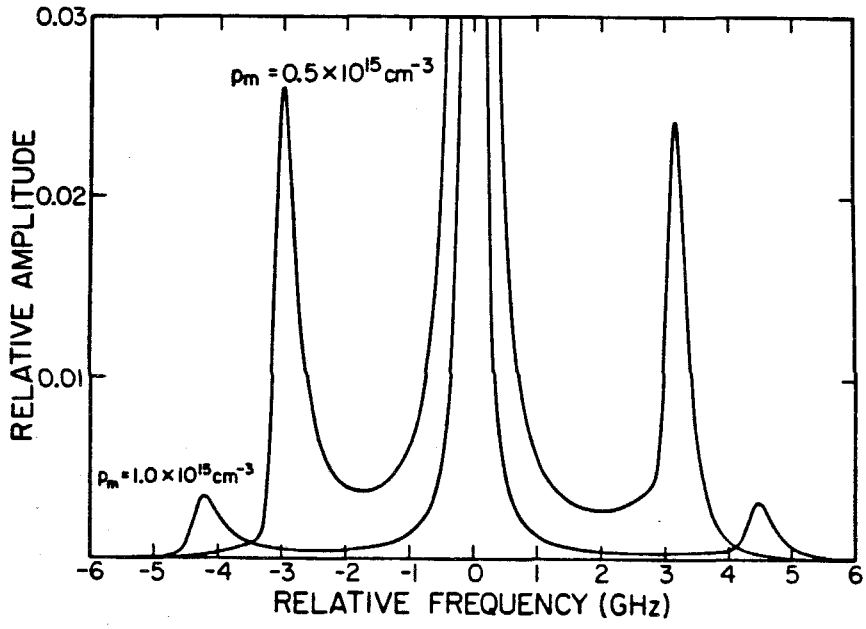

Figure 3.15 Field spectrum finestructure normalized by the field spectrum value at line center.

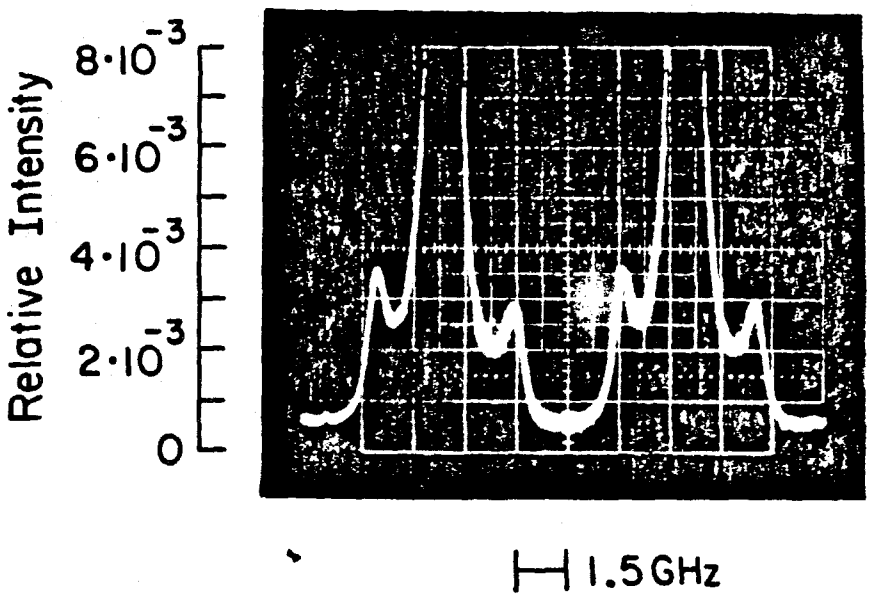

Figure 3.16 Two traces of field spectrum finestructure observed in an Hitachi CSP laser. The vertical scale gives the amplitudes relative to the lasing line center. Note the sideband asymmetry which results from amplitude phase coupling.

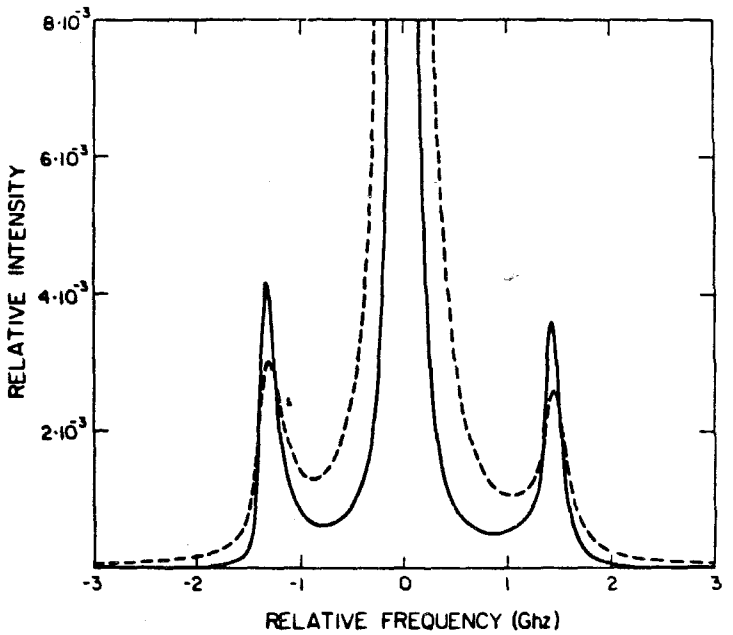

Figure 3.17 Solid curve gives the calculated field spectrum finestructure using parameters characteristic of a CSP laser (see Ref. 24). Dashed curve is the solid curve convolved with a 75 MHz. instrumental bandwidth Lorentzian; the comparison with the observed finestructure in Fig. 3.16 is good.

power level. The dashed curve in that figure was obtained by convolving the calculated curve with an instrumental bandwidth Lorentzian. The agreement is good, including the asymmetry. The drive current dependence of the sideband spacing was also measured and is presented in Fig. 3.18. The variation obeys the square relation indicative of the relaxation resonance frequency. (Note that the threshold for this device was 62 mA.)

3.6 Conclusion

In this chapter we have derived a variety of fluctuation spectra for single and multimode semiconductor lasers, emphasizing the effects of gain spectrum detuning on phase noise spectra. Detuning has long been known to cause intramodal amplitude-phase coupling. We have shown that under single mode operation this coupling leads to a striking similarity between amplitude and phase noise spectra: the frequency fluctuation spectrum, which is flat in the tuned case, exhibits a resonance similar to the well-known spiking resonance in the relative power noise spectrum. A further consequence of the coupling is that low frequency phase noise (and thus linewidth) are enhanced. For multimode operation, detuning produces additional effects. When combined with the intermodal amplitude coupling present in multimode operation, it results effectively in intermodal amplitude-phase and intermodal phase coupling. Thus all fluctuations in a multimode semiconductor laser are coupled (see Fig. 3.19). It is well established that intermodal amplitude coupling is responsible for phenomena associated with partition noise. In this paper we have seen that intermodal phase coupling leads to equally interesting effects. To accommodate the new fluctuation coupling possibilities we have introduced two new spectral density functions: the off diagonal frequency fluctuation spectrum and the fluctuation coupling spectrum.

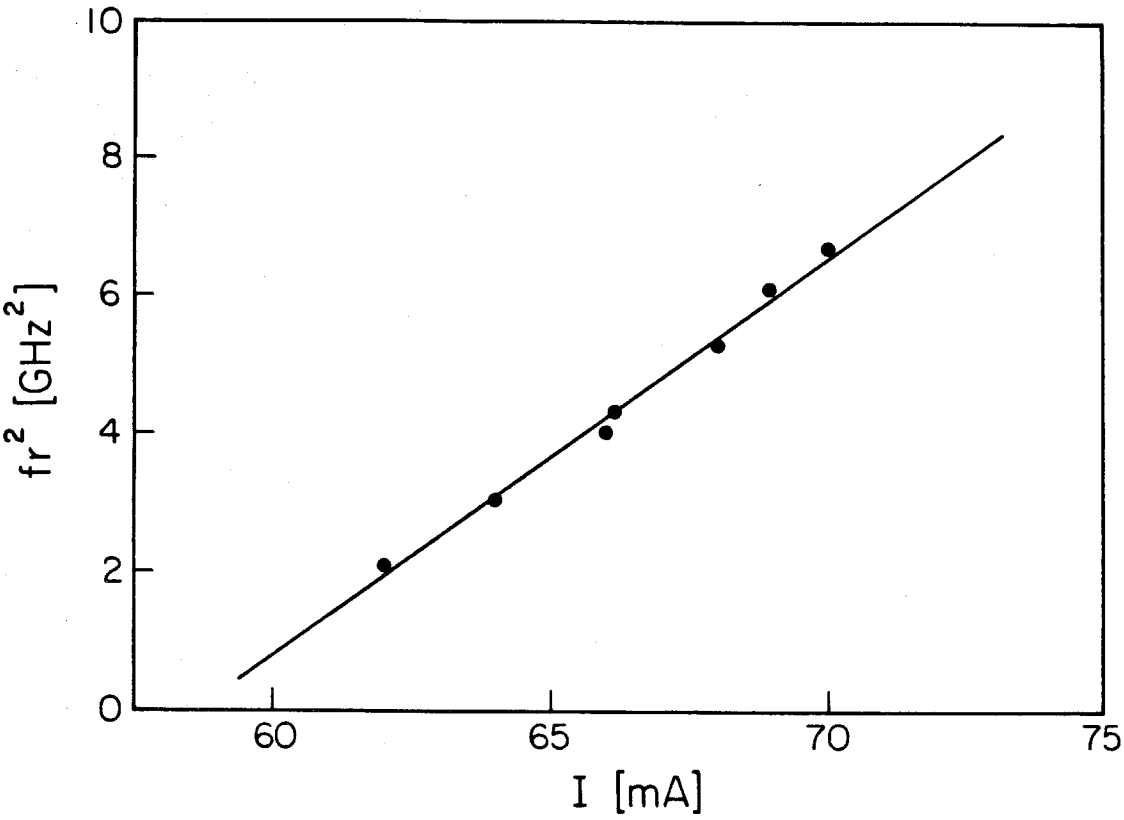

Figure 3.18 Measured frequency separation from line center of field spectrum finestructure as a function of injection current. The dependence is that characteristic of the relaxation oscillation frequency.

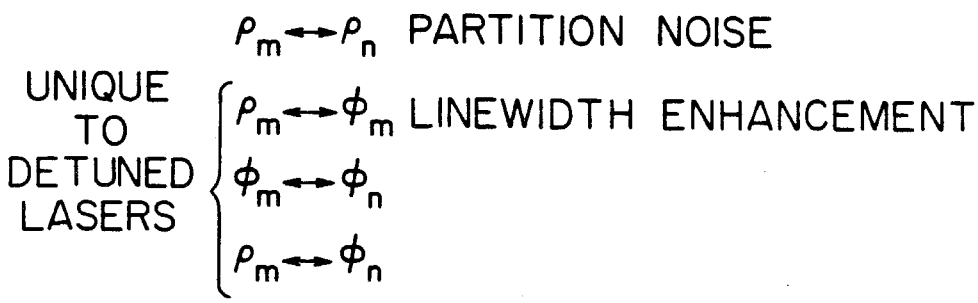

Figure 3.19 Summary of fluctuation coupling in a semiconductor laser.

Certain single mode and multimode amplitude noise spectra were also calculated in the treatment. Discussion of all multimode effects was facilitated by use of a new dimensionless parameter which gauges the dynamic interaction strength between the active medium and a particular mode. Referred to as the dynamic coupling strength parameter, its value relative to unity leads to a dynamic classification of the modes in a SL. We mention again that only sources of noise related to spontaneous emission were considered in the treatment, this being the dominant fluctuation mechanism in semiconductor lasers. In doing this we have neglected noise mechanisms such as population fluctuations, diffusion, and temperature fluctuations which will be discussed separately in Chapter 5.

The two most important quantities in this analysis have been the spontaneous emission rate θ_m into a given mode m and the complex susceptibility χ. We rewrite these quantities below from Appendix B and Chapter 2 for convenience,

$$\theta_m = \frac{1}{(2\pi)^3 \varepsilon \hbar \omega_m} \int d\vec{x} d\vec{k} u_m^2(\vec{x}) |q(\vec{k})|^2 \frac{\gamma f_c'(1 - f_v')}{(\Omega(\vec{k}) - \bar{\omega}_m)^2 + \gamma^2} \tag{6.1}$$

$$\chi(n,\omega) \equiv \frac{-\iota}{(2\pi)^3 \varepsilon_o \hbar \omega^2} \int d\vec{k} \frac{|q(\vec{k})|^2 (f_c' - f_v')}{\iota(\omega - \Omega(\vec{k})) + \gamma} \tag{6.2}$$

Gain G and the resonant contribution to refractive index μ_R are given by (see Ref. [8]),

$$G(n,\omega) = \frac{\omega \chi_I(n,\omega)}{\mu^2} \tag{6.3}$$

$$\mu_R(n,\omega) = \frac{\chi_R(n,\omega)}{2\mu^2} \quad . \tag{6.4}$$

The fact that $\mu_R'(n,\omega_1)$ is nonzero for ω_1 at the gain peak is a statement that semiconductor lasers are detuned oscillators. A variety of other parameters defined in terms of (6.1) and (6.2) determine the spectral and dynamic features of semiconductor lasers. We have summarized these parameters below,

Amplitude-phase coupling factor (linewidth enhancement factor)

$$\alpha(n,\omega) = \frac{\chi_R'}{\chi_I'} = 2\omega\frac{\mu_R'}{G'} \tag{6.5}$$

Tuned laser linewidth

$$\varepsilon_m = \frac{\theta_m}{2P_m} \tag{6.6}$$

SINGLE MODE OPERATION

Relaxation oscillation frequency and damping rate

$$\omega_{Rm}^2 = \Gamma G G' p_m = \frac{G' p_m}{\tau_m} \tag{6.7}$$

$$\frac{1}{\tau_R} = R' + G' p_m \tag{6.8}$$

Linewidth

$$\Delta\omega_m = \varepsilon_m(1 + \alpha^2) \tag{6.9}$$

MULTIMODE OPERATION

Dynamic coupling strength parameter

$$c_m(0) = \frac{\omega_{Rm}^2 \tau_R}{2\varepsilon_m} \tag{6.10}$$

Relaxation oscillation frequency and damping rate

$$\omega_R^2 \approx \sum_{\text{strong modes}} \omega_{Rm}^2 \tag{6.11}$$

$$\frac{1}{\tau} \approx \left[R' + \sum_m G' p_m\right]\left[1 + \sum_{\text{weak modes}} c_m(0)\right] \tag{6.12}$$

Linewidth

$$\Delta\omega_m = \varepsilon_m + \alpha^2 \frac{\sum_l c_l^2(0)\varepsilon_m}{\left[1 + \sum_l c_l(0)\right]^2} \tag{6.13}$$

where prime indicates differentiation with respect to carrier density and where we have suppressed frequency dependences in Γ, G, G', and α.

Appendix A

In this Appendix we show how the semiclassical equations (4.1) and (4.2) are related to a set of fully quantum mechanical equations of motion. This establishes the framework necessary for the supplements given in the remaining appendices. In Chapter 2 a set of local operator equations of motion for the SL were derived. In that treatment the lasing field vector potential is modeled using the standard delocalized annihilation and creation operators which result

from quantizing a passive cavity optical mode as follows,

$$\vec{A}(\vec{r},t) = \sum_l \left(\frac{\hbar}{2\varepsilon\omega_l} \right)^{\frac{1}{2}} \left(b_l(t) + b_l^+(t) \right) \vec{u}_l(\vec{r}) \tag{A.1}$$

where,

$$\int d\vec{r}\, \vec{u}_l(\vec{r}) \cdot \vec{u}_m(\vec{r}) = \delta_{lm} \tag{A.2}$$

$$\left[b_l(t), b_m^+(t) \right] = \delta_{lm} \tag{A.3}$$

$$\left[b_l(t), b_m(t) \right] = 0 \tag{A.4}$$

$$\left[b_l^+(t), b_m^+(t) \right] = 0 \quad . \tag{A.5}$$

In (A.1) ε is the nonresonant dielectric constant of the crystal and ω_l is the resonant frequency of the l^{th} passive mode. In (A.3), (A.4), and (A.5) [ ] signifies commutation. The model for the electronic system employs a nonstandard approach, however. It is based on the operators $\psi^+(m,\vec{x},\vec{k},t)$ and $\psi(m,\vec{x},\vec{k},t)$ which are defined so as to create and destroy electronic wave-packet states $|\psi(m,\vec{x},\vec{k})>$ having well-defined position $\vec{x}$ and crystal momentum $\hbar\vec{k}$ in the m^{th} energy band of the crystal. These operators obey the following set of anticommutation relations,

$$\left\{ \psi(m,\vec{x},\vec{k},t), \psi^+(n,\vec{x}',\vec{k}',t) \right\} = \delta_{mn} < \psi(m,\vec{x},\vec{k}) | \psi(m,\vec{x}',\vec{k}') > \tag{A.6}$$

$$\left\{\psi(m,\vec{x},\vec{k},t),\psi(n,\vec{x}',\vec{k}',t)\right\} = 0 \tag{A.7}$$

$$\left\{\psi^{+}(m,\vec{x},\vec{k},t),\psi^{+}(n,\vec{x}',\vec{k}',t)\right\} = 0 \quad . \tag{A.8}$$

By spatially averaging the local operator equations (Eqns. (4.7) and (4.8) in Chapter 2) we arrive at the quantum counterparts of (4.1) and (4.2),

$$\dot{b}_l^{+} = \left(\iota\omega_l - \frac{1}{2\tau_l}\right)b_l^{+} + \iota\frac{\Gamma_{ll}\omega_l}{2\mu^2}\chi(n,\bar{\omega}_l)b_l^{+} + S_l^{+}(t) + g_l^{+}(t) \tag{A.9}$$

$$\dot{n} = E - R(n) - \sum_l \frac{\omega_l}{\mu^2}\chi_l(n,\bar{\omega}_l)\frac{b_l^{+}b_l}{V_l} \tag{A.10}$$

where we have neglected population fluctuation operators and defined an average carrier density operator as follows,

$$n \equiv \frac{1}{V_{active}}\int d\vec{x}d\vec{k}\psi_c^{+}\psi_c \quad . \tag{A.11}$$

The complex susceptibility function which results from the quantum treatment appears in the conclusion of this chapter.

By comparing (4.1) and (A.9) we get the following correspondence between classical and quantum fluctuation sources,

$$s_l^{\bullet}(t) \rightarrow S_l^{+}(t) + g_l^{+}(t) \quad . \tag{A.12}$$

The fluctuation operator $S_l^{+}(t)$ is actually defined in terms of another fluctuation operator $\Delta(\vec{x},\vec{k},t)$ as follows,

$$S_l^+(t) \equiv \frac{\iota}{\sqrt{2\varepsilon\hbar\omega_l}}\int d\vec{x}d\vec{k}dt' u_l(\vec{x})q(\vec{k})\Delta(\vec{x},\vec{k},t')e^{(\iota\Omega(\vec{k})-\gamma)(t-t')} \tag{A.13}$$

where γ is the collisional dephasing rate between states in the conduction band and states in the valence band; $q(\vec{k})$ is the matrix element for an electrooptic interband transition involving wavepackets having "center of motion" wave vector $\vec{k}$; $\Omega(\vec{k})$ is the frequency associated with an interband transition between states having energy $\varepsilon_c(\vec{k})$ and $\varepsilon_v(\vec{k})$, i.e.,

$$\Omega(\vec{k}) \equiv \frac{\varepsilon_c(\vec{k}) - \varepsilon_v(\vec{k})}{\hbar} \tag{A.14}$$

In Chapter 2 the quantum fluctuation dissipation theorem [52,53] is used to derive the second moments of the fluctuation operators $\Delta(\vec{x},\vec{k},t)$ and $g_l(t)$. These results appear below and will be used in conjunction with (A.12) and (A.13) in the remaining appendices.

$$< g_l(t+\tau)g_m(t) > = 0 \tag{A.15}$$

$$< g_l^+(t+\tau)g_m^+(t) > = 0 \tag{A.16}$$

$$< g_l^+(t+\tau)g_m(t) > = \frac{1}{\tau_l} < b_l^+ b_m > D(\tau) = \frac{n_l}{\tau_l} D(\tau)\delta_{lm} \tag{A.17}$$

$$< g_l(t+\tau)g_m^+(t) > = \frac{1}{\tau_l} < b_l b_m^+ > D(\tau) = \frac{n_l + 1}{\tau_l} D(\tau)\delta_{lm} \tag{A.18}$$

$$< \Delta^+(\vec{x},\vec{k},t+\tau)\Delta^+(\vec{x}',\vec{k}',t) > = 0 \tag{A.19}$$

$$< \Delta(\vec{x},\vec{k},t+\tau)\Delta(\vec{x}',\vec{k}',t)> \; = 0 \tag{A.20}$$

$$< \Delta^{+}(\vec{x},\vec{k},t+\tau)\Delta(\vec{x}',\vec{k}',t)> \; = 2\gamma f_v(1-(2\pi)^3 f_c)D(\vec{x}-\vec{x}',\vec{k}-\vec{k}',\tau) \tag{A.21}$$

$$< \Delta(\vec{x},\vec{k},t+\tau)\Delta^{+}(\vec{x}',\vec{k}',t)> \; = 2\gamma f_c(1-(2\pi)^3 f_v)D(\vec{x}-\vec{x}',\vec{k}-\vec{k}',\tau) \quad . \tag{A.22}$$

In these expressions f_c and f_v are operators giving the thermodynamic occupancy density in the phase spaces associated with the conduction and valence bands. They are given by $f_c = f_c'/(2\pi)^3$ and $f_v = f_v'/(2\pi)^3$ where f_c' and f_v' are quasi-Fermi distribution operators. D(x) is the delta function and n_l is the number of thermal photons in the optical mode l.

Appendix B

In Section 3.4 it was necessary to use a photon rate equation (Eqn. (4.12)) in order to obtain the operating point equations. The derivation of this equation is now given. We do this by applying the following identity,

$$\dot{P}_l = \frac{d< b_l^{+}b_l>}{dt} = < \dot{b}_l^{+}b_l> \; + < b_l^{+}\dot{b}_l> \tag{B.1}$$

where $< >$ signify quantum averaging. Applying this identity to the quantum counterpart of (4.1), given in Appendix A as (A.9), gives the following,

$$\dot{P}_l = -\frac{P_l}{\tau_l} + \frac{\Gamma_{ll}\omega_l}{\mu^2}\chi_l(n,\bar{\omega}_l)P_l + \tag{B.2}$$

$$< S_l^+(t)b_l(t)> \; + < b_l^+(t)S_l(t)> \; + < g_l^+(t)b_l(t)> \; + < b_l^+(t)g_l(t)> \quad .$$

The correlation terms in (B.1) can be expanded by using the integral of (A.9) to replace $B_l(t)$ and $B_l^+(t)$. For example,

$$< b_l^+(t)S_l(t)> \; = < B_l^+(t)e^{i\bar{\omega}_l t}S_l(t)> \; = \tag{B.3}$$

$$\int_{-\infty}^{t} < \left[H_l(n)B_l^+(z) + g_l^+(z)e^{-i\bar{\omega}_l z} + S_l^+(z)e^{-i\bar{\omega}_l z}\right]e^{i\bar{\omega}_l t}S_l(t)> \, dz$$

where

$$H_l(n) \equiv \; i(\omega_l - \bar{\omega}_l) - \frac{1}{2\tau_l} + i\frac{\Gamma_{ll}\omega_l}{2\mu^2}\chi(n,\bar{\omega}_l) \quad . \tag{B.4}$$

In (B.3) $S_l(t)$ is approximately a "white" noise source in comparison to the slowly varying term $H_l(n)B_l^+(z)$ and thus by causality these terms are uncorrelated. The second term involving $g_l^+(z)$ is also uncorrelated with $S_l(t)$ since these noise sources have their origins at independent baths. This reduces (B.3) to the following,

$$< b_l^+(t)S_l(t)> \; = \int_{-\infty}^{t} e^{i\bar{\omega}_l(t\,-\,z)} < S_l^+(z)S_l(t)> \, dz = \int_0^{\infty} e^{i\bar{\omega}_l\tau} < S_l^+(0)S_l(\tau)> \, dz \tag{B.5}$$

with similar expressions holding for the other correlation terms in (B.2). In the second equality in (B.5) we have used the stationary property to shift the time coordinate.

Substituting for $S_l(t)$ and $S_l^+(t)$ in (B.5) using (A.13) and then simplifying the result using (A.22) gives,

$$< S_l^+(0)S_l(\tau)> = \frac{1}{(2\pi)^3 2\varepsilon\hbar\omega_l}\int d\vec{x}d\vec{k}u_l^2(\vec{x})\,|q(\vec{k})|^2 f_c'(1-f_v')e^{\left[-\iota\Omega(\vec{k})\tau-\gamma|\tau|\right]} \quad (B.6)$$

From which we find,

$$< b_l^+(t)S_l(t)> = \frac{1}{(2\pi)^3 2\varepsilon\hbar\omega_l}\int d\vec{x}d\vec{k}u_l^2(\vec{x})\,|q(\vec{k})|^2 \frac{f_c'(1-f_v')}{\iota(\Omega(\vec{k})-\bar{\omega}_l)+\gamma} \quad (B.7)$$

Combining all such results for the correlation terms in (B.2) we find,

$$< S_l^+(t)b_l(t)> + < b_l^+(t)S_l(t)> + < g_l^+(t)b_l(t)> + < b_l^+(t)g_l(t)> = \quad (B.8)$$

$$\frac{1}{(2\pi)^3\varepsilon\hbar\omega_l}\int d\vec{x}d\vec{k}u_l^2(\vec{x})\,|q(\vec{k})|^2 \frac{\gamma f_c'(1-f_v')}{(\Omega(\vec{k})-\bar{\omega}_l)^2+\gamma^2} + \frac{2n_l}{\tau_l} \equiv \theta_l + \frac{2n_l}{\tau_l}$$

which, upon identification of θ_l as the spontaneous emission rate into mode l, gives the desired result.

Appendix C

In this Appendix we calculate the spectral density functions associated with the noise operators $\Delta_{rl}(t)$ and $\Delta_{il}(t)$ which are defined by (4.18) and (4.19) and correspondence relation (A.12). First, it is necessary to calculate time correlation functions for the operators $S_l^+(t)$ and $S_l(t)$ by using (A.13) and (A.19)-(A.22). Doing so yields,

$$< S_l^+(\tau)S_m(0)> = \delta_{lm}\frac{1}{(2\pi)^3 2\varepsilon\hbar\omega_l}\int d\vec{x}d\vec{k}u_l^2(\vec{x})\,|q(\vec{k})|^2 f_c'(1-f_v')e^{\left[\iota\Omega(\vec{k})\tau-\gamma|\tau|\right]} \quad (C.1)$$

$$< S_l(\tau)S_m^{\pm}(0)> = \delta_{lm}\frac{1}{(2\pi)^3 2\varepsilon\hbar\omega_l}\int d\vec{x}d\vec{k}u_l^2(\vec{x})\,|\,q(\vec{k})\,|^2 f_v'(1-f_c')e^{\left(-i\Omega(\vec{k})\tau-\gamma|\tau|\right)} \quad (C.2)$$

$$< S_l^{+}(\tau)S_m^{\pm}(0)> = 0 \quad (C.3)$$

$$< S_l(\tau)S_m(0)> = 0 \quad . \quad (C.4)$$

These results can now be used to form the desired spectral density functions. The case of $\Delta_{rl}(t)$ is worked through as an example. Applying the Wiener-Khintchine Theorem yields,

$$F_\tau\left[\Delta_{rl}(t+\tau)\Delta_{rm}(t)\right]|_{\Omega\approx 0} = \frac{\delta_{lm}}{4P_l}\int d\vec{x}d\vec{k}\frac{\gamma u_l^2(\vec{x})\,|\,q(\vec{k})\,|^2}{(2\pi)^3\varepsilon\hbar\omega_l}\frac{f_c'(1-f_v')+f_v'(1-f_c')}{(\Omega(\vec{k})-\bar{\omega}_l)^2+\gamma^2} \quad (C.5)$$

$$+\frac{\delta_{lm}}{4P_l}\frac{2n_l+1}{\tau_l}$$

where, to simplify matters, the low frequency form of this function is taken. This approximation is allowed since this spectrum is effectively "white" in comparison to all frequencies of interest.

This expression can be simplified by reexpressing $1/\tau_l$ in terms of the susceptibility through the use of (4.13),

$$\frac{1}{\tau_l} \approx \frac{\Gamma_{ll}\omega_l\chi_I(n_o,\omega_l)}{\mu^2} = \int d\vec{x}d\vec{k}\frac{\gamma u_l^2(\vec{x})\,|\,q(\vec{k})\,|^2}{(2\pi)^3\varepsilon\hbar\omega_l}\frac{f_c'-f_v'}{(\Omega(\vec{k})-\bar{\omega}_l)^2+\gamma^2} \quad (C.6)$$

where the expanded form of $\chi_I(n,\omega)$ (see Eqn. (6.2)) and the definition of Γ_{ll} (see [7,8]) have been used here. Using this result, (C.5) reduces to ,

$$F_\tau\left[\Delta_{rl}(t+\tau)\Delta_{rm}(t)\right] = \frac{\delta_{lm}}{2P_l}\left[\frac{n_l}{\tau_l} + \int d\vec{x}d\vec{k}\,\frac{\gamma u_l^2(\vec{x})\,|q(\vec{k})|^2}{(2\pi)^3\varepsilon\hbar\omega_l}\,\frac{f_c'(1-f_v')}{(\Omega(\vec{k})-\bar{\omega}_l)^2+\gamma^2}\right] \quad (C.7)$$

$$= \frac{\delta_{lm}}{2P_l}\left[\frac{n_l}{\tau_l} + \theta_l\right]$$

where θ_l is the spontaneous emission rate into mode l (see B.8) and where the "low frequency reminder" has been omitted. Using the same approach the other possible spectral density functions are found to be,

$$F_\tau\left[<\Delta_{il}(t+\tau)\Delta_{im}(t)>\right] = \frac{\delta_{lm}}{2P_l}\left[\frac{n_l}{\tau_l} + \theta_l\right] \quad (C.8)$$

$$F_\tau\left[<\Delta_{rl}(t+\tau)\Delta_{im}(t)>\right] = 0 \quad . \quad (C.9)$$

In using these results the term involving n_l can be neglected since it is minute at optical frequencies.

Appendix D

The α parameter defined by (4.27) was seen in this chapter to pervade the noise spectra of semiconductor lasers. α gives a measure of gain spectrum detuning and is one of a few parameters which characterize SL noise and dynamics. One way to deduce its value in a given device is to measure linewidth versus power as was done in Figs. 3.11 and 3.12. From the slope of the resulting curve one can deduce α provided θ_l and P_l (i.e., the spontaneous emission rate and photon density for mode l) are known. In practice these quantities must be calculated from other quantities and are not known with good accuracy.

In this Appendix we outline a technique which can be used to directly measure α [50]. It was mentioned in Chapter 3 and will be discussed further in

Chapter 4 that α, in addition to its role in determining phase noise spectra, also controls the apportioning of FM and AM when a semiconductor laser is directly modulated; by measuring this apportioning the value of α can be determined directly.

To see how this can be done consider (4.22) and (4.23) with the spontaneous fluctuation sources omitted,

$$\dot{\rho} = -2\varepsilon\rho_1 + \frac{1}{2}\eta \tag{D.1}$$

$$\dot{\varphi}_1 = -\frac{\alpha}{2}\eta \tag{D.2}$$

where the mode index subscript has been suppressed. These equations can be used to study direct modulation as well as fluctuations. If the SL is modulated at a frequency Ω, then the small signal gain will be given by $\eta(t) = \eta_o(\Omega)\sin(\Omega t)$ where the frequency dependence of $\eta_o(\Omega)$ is unimportant for this analysis. Using this in (D.1) and (D.2) gives,

$$\rho(t) = \frac{\eta_o(\Omega)}{2}\frac{-\Omega\cos(\Omega t) + 2\varepsilon\sin(\Omega t)}{\Omega^2 + 4\varepsilon^2} \tag{D.3}$$

$$\varphi(t) = \frac{\alpha}{2}\eta_o(\Omega)\frac{\cos(\Omega t)}{\Omega} \tag{D.4}$$

If the modulation frequency Ω is much larger than 2ε (recall ε is the conventional Schawlow-Townes linewidth and is therefore typically a few MHz.) then,

$$\hat{\varphi} = -\alpha\hat{\rho} \tag{D.5}$$

$$\varphi(t) \equiv \hat{\varphi}\cos(\Omega t) \tag{D.6}$$

$$\rho(t) \equiv \hat{\rho}\cos(\Omega t) \tag{D.7}$$

where E(t), the real electric field amplitude, is given by,

$$E(t) = A_o\left[1 + \hat{\rho}\cos(\Omega t)\right]\cos\left[\omega t + \hat{\varphi}\cos(\Omega t)\right] \tag{D.8}$$

The experimental arrangement for measureing the intensity and phase modulation index is shown in Fig. 3.20. The semiconductor laser is biased above threshold and a small sinusoidally varying current at frequency Ω is superimposed. The power modulation and spectral density of the radiation field are given by,

$$\delta P = 2A_o^2\hat{\rho}\cos(\Omega t) \tag{D.9}$$

$$\frac{W_{\text{linecenter}}}{A_o^2} = J_o^2(\hat{\varphi}) + \hat{\rho}^2 J_1^2(\hat{\varphi}) \tag{D.10}$$

$$\frac{W_{\pm\text{ sideband}}}{A_o^2} = J_1^2(\hat{\varphi}) + \left[\hat{\rho}\left[J_2(\hat{\varphi}) - J_o(\hat{\varphi})\right]\right]^2 \tag{D.11}$$

where $J_n(\hat{\varphi})$ is the n^{th} order Bessel function. Note that the calculated spectrum is symmetric.

The intensity modulation index was measured with an avalanche photodiode (S171P Telefunken) calibrated in the measurement setup from D.C. to 3.7 GHz. to an accuracy of $\pm$ 1dB. The optical spectrum was measured with a confocal scanning Fabry-Perot (Tropel 240). Care was taken to avoid any feedback into the laser. In a typical measurement, as shown in Fig. 3.21, the modulation

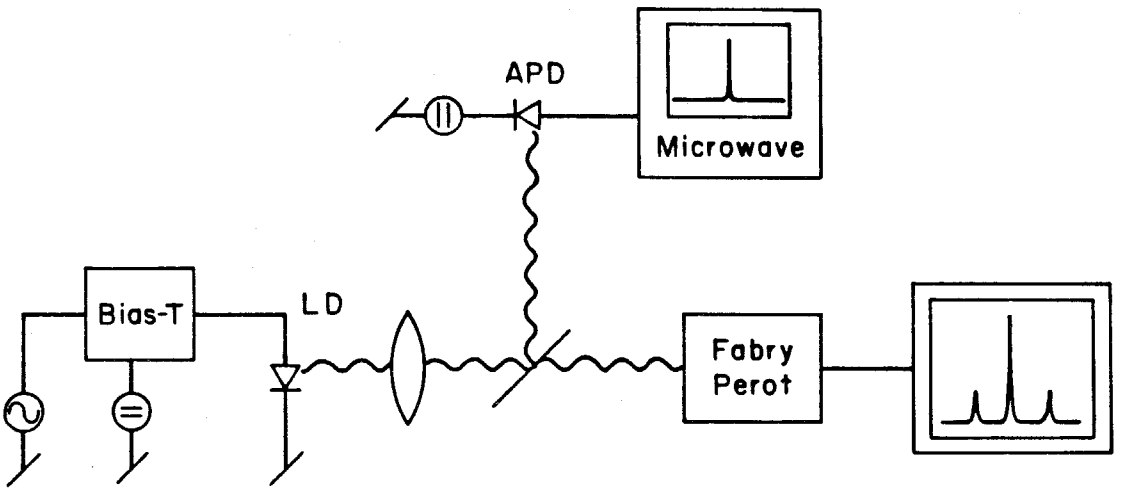

Figure 3.20 AM-FM modulation measurement experimental setup.

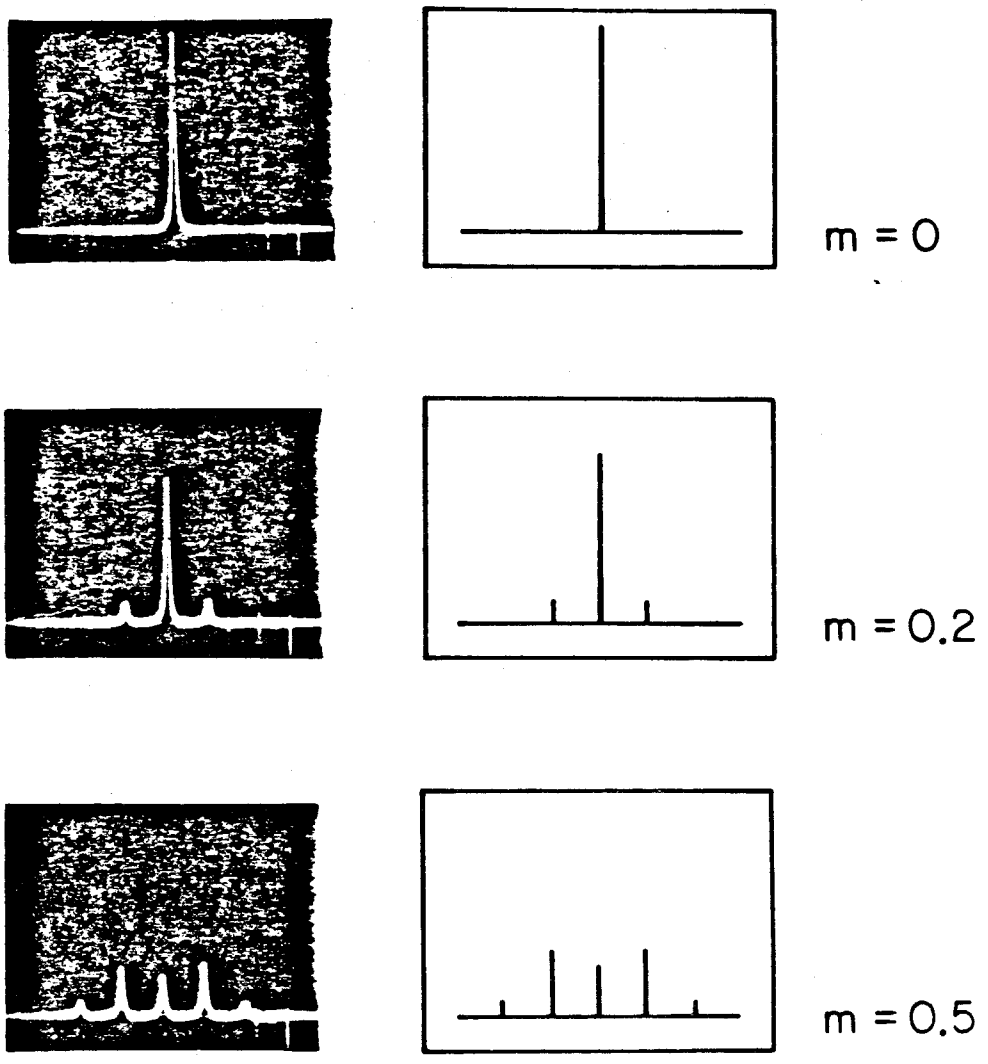

Figure 3.21 Observed and calculated field spectra under different power modulation indices m.

current at frequency Ω was adjusted to produce a desired intensity modulation depth, which was measured with the photodiode. The phase modulation index can be found by measuring the relative sideband amplitude and using (D.10) and (D.11). The factor α is then obtained from (D.5). Since only the absolute value of $\hat{\varphi}$ can be measured, the sign of α must be determined by other means.

A measurement of the α of a buried optical guide laser (BOG Hitachi 3400, λ = 816nm) at Ω = 2GHz., a bias level of 1.3 times threshold, and an intensity modulation depth of 10% gave $|\alpha|$ = 4.5. Repetition of this measurement for about 50 different conditions (Ω varied between 1 and 3.5 GHz., bias level varied between 1.3 and 1.9 times threshold, and modulation depth varied between 10% and 30%) gave $|\alpha|$ = 4.5 + 0.5. This value has an additional uncertainty of ± 10% due to inaccuracy of the photodiode calibration. This value is consistent with the linewidth power data presented in Fig. 3.12 for this device.

References

[1] M. Fleming and A. Mooradian, Appl. Phys. Lett., vol. 38, p. 511 (1981).

[2] K. Vahala, L. C. Chiu, S. Margalit and A. Yariv, Appl. Phy. Lett., vol. 42, p. 631 (1983).

[3] H. Haug and H. Haken, Z. Phys., vol. 204, p. 262 (1967).

[4] M. Lax, Phys. Rev., vol. 160, p. 290 (1967).

[5] V. Arzt, H. Haken, H. Risken, H. Sauermann, Ch. Schmid and W. Weidlich, Z. Phys., vol. 197, p. 207 (1966).

[6] C. H. Henry, IEEE J. Quant. Electron., vol. QE-18, p. 259 (1982).

[7] K. Vahala and A. Yariv, IEEE J. Quantum Electron., vol. QE-19, p. 1096 (1983).

[8] K. Vahala and A. Yariv, IEEE J. Quantum Electron., vol. QE-19, p. 1102 (1983).

[9] D. E. McCumber, Phys. Rev., vol. 141, p. 306 (1966).

[10] K. Vahala and A. Yariv, unpublished.

[11] R. J. Glauber, Phys. Rev., vol. 131, p. 2766 (1963).

[12] M. Lax and M. Louisell, IEEE J. Quantum Electron., vol. QE-3, p. 47 (1967).

[13] H. Risken, C. Schmid and W. Weidlich, Z. Phys., vol. 194, p. 337 (1966).

[14] W. Wiedlich and F. Haake, Z. Phys., vol. 186, p. 203 (1965).

[15] A. Yariv and W. Caton, IEEE J. Quantum Electron., vol. QE-10, p. 509 (1974).

[16] H. Haken, "Laser Theory," Springer-Verlag, New York, 1983.

[17] J. A. Armstrong and A. W. Smith, Phys. Rev., vol. 140, p. 155 (1965).

[18] M. Born and E. Wolfe, "Optics," Pergamon Press, New York, 1975, p. 504.

[19] G. Tenchio, Electron. Lett., vol.12, p. 562 (1976).

[20] G. Tenchio, Electron. Lett., vol. 13, p. 614 (1977).

[21] A. Dandridge and H. F. Taylor, IEEE J. Quantum Electron., vol QE-18, p. 1738 (1982).

[22] T. K. Yee, Paper #TUH3 presented at CLEO 1983, Baltimore.

[23] F. G. Walther and J. E. Kaufmann, Paper #TUJ5 presented at OFC 1983, New

Orleans.

[24] K. Vahala, Ch. Harder and A. Yariv, Appl. Phys. Lett., vol. 42, p. 211 (1982).

[25] T. L. Paoli and J. E. Ripper, Phys. Rev., vol. 2, p. 2551 (1970).

[26] T. L. Paoli, Appl. Phys. Lett., vol. 24, p. 187 (1974).

[27] G. Guekos, H. Jackel and K. F. Schmid, Electron. Lett., vol. 12, p. 64 (1976).

[28] H. Jackel, Electron. Lett., vol. 12, p. 289 (1976).

[29] H. Jackel and G. Guekos, Opt. Quantum Electron., vol. 9, p. 233 (1977).

[30] T. Ito, S. Machida, K. Nawata and T. Ikegami, IEEE J. Quantum Electron., vol. QE-13, p. 574 (1977).

[31] H. Melchior, Paper MA2 at Topical meeting on integrated and guided wave optics, Jan. 1980.

[32] H. Haug, Phys. Rev., vol. 184, p. 338 (1969).

[33] D. J. Morgan and M. J. Adams, Phys. Stat. Sol., vol. 11, p. 243 (1972).

[34] R. Lang, K. Vahala and A. Yariv, IEEE J. Quant. Electron., vol. QE-21, no. 5 (1985).

[35] A. Dandridge, A. B. Tveten, R. O. Miles, D. A. Jackson and T. G. Giallorenzi, Appl Phys. Lett., vol. 38, p. 77 (1981).

[36] A. Dandridge and A. B. Tveten, Appl. Phys, Lett., vol. 39. p. 530 (1981).

[37] S. Piazzolla, P. Spano and M. Tamburrini, Appl. Phys. Lett., vol. 41, p. 695 (1982).

[38] A. Dandridge, L. Goldberg and R. O. Miles, Paper #TUJ9 presented at OFC 1983, New Orleans.

[39] J. A. Armstrong and A. W. Smith, Appl. Phys. Lett., vol. 4, p. 196 (1964).

[40] E. D. Hinkley and C. Freed, Phys. Rev. Lett., vol. 23, p. 277 (1969).

[41] T. Okoshi, K. Kikuchi and A. Nakayama, Electron. Lett., vol. 16, p. 630 (1980).

[42] W. Elsasser, E. Gobel and J. Kuhl, IEEE J. Quant. Electron., vol. QE-19, p. 981 (1983).

[43] C. Freed, J. W. Bielinski and W. Lo, Appl. Phys. Lett., vol. 43, p. 629 (1983).

[44] D. Welford and A. Mooradian, Appl. Phys. Letts., vol. 40, p. 865 (1982).

[45] J. M. Osterwalder and B. J. Rickett, Proc. IEEE, vol. 67, p. 1671 (1979).

[46] D. Welford and A. Mooradian, Appl. Phys. Lett., vol. 40, p. 560 (1982).

[47] W. Elsaber and E. Gobel, presented at the 1983 European conference on optical communications, Geneva.

[48] K. Vahala and A. Yariv, Appl. Phys. Lett., vol. 43, p. 140 (1983).

[49] K. Y. Lau, N. Bar-Chaim, I. Ury, Ch. Harder and A. Yariv, Appl. Phys. Letts., vol. 43, p. 1 (1983).

[50] Ch. Harder, K. Vahala and A. Yariv, Appl. Phys. Lett., vol. 42, p. 328 (1983).

[51] K. Lau, K. Vahala and A. Yariv, unpublished.

[52] M. Lax, Phys. Rev., vol. 145, p. 110 (1966).

[53] H. Haken and W. Weidlich, Z. Physik, vol. 189, p. 1 (1966).

Chapter 4

Detuned loading in semiconductor lasers

4.1 Introduction

In Chapter 3 the fluctuation properties of semiconductor lasers were considered in detail. In this chapter we expand the scope to include modulation properties. Unlike Chapter 3, however, which characterized the state of the art device, this chapter will address the problem of improving the state of the art. Only a cursory overview of modulation properties will be provided, enough to establish what is important. More detailed discussions of these properties can be found in Refs. [1,2].

Ideally, one would like to find techniques which improve modulation speed, control the generation of FM (dynamic linewidth broadening or chirp), and reduce power noise and phase noise. Such techniques exist, but often a penalty is exacted on one property for improvements made in another. Reduction of noise, for instance, by increasing facet reflectivity (i.e., improving the passive cavity Q) also degrades modulation performance [3,4]. In fact, to date only two techniques are available which simultaneously improve modulation speed and reduce noise: operation at high modal photon densities or operation at reduced temperatures [4,5,6].

This chapter considers the control of these properties by a technique we call "detuned loading" [7,8]. It involves the introduction of a frequency dependent loss mechanism in the spectral proximity of the lasing frequency and relies upon the strong carrier density dependent refractive index component of the

active medium (resulting from the detuned gain spectrum). Such a frequency dependent loss mechanism can be implemented in several ways which include coupled-cavity devices and lasers with distributed feedback. In this chapter a generic description of the detuned loading mechanism is presented and its effect on modulation and noise performance is calculated from this general point of view. This formalism is then applied to study a specific implementation consisting of an active cavity loaded by a passive cavity. Measurement of modulation speed, linewidth, and chirp in this system will be compared with calculations based on the formalism.

To begin we will first review results for the solitary single mode SL: modulation reponse, frequency modulation, power noise, and phase noise. We then consider the control of these properties using the detuned loading mechanism. Specifically, we show that by using this technique it is possible to simultaneously increase device speed, suppress or altogether eliminate dynamic linewidth broadening (chirp), and reduce spontaneous power noise and phase noise as compared to the conventional device. Finally, data and calculations are presented for the coupled-cavity implementation.

4.2 The conventional device

In this section modulation dynamics and noise in the conventional SL are reviewed. This will establish the framework necessary for the discussion of the detuned loading mechanism in the next section.

The essential features of modulation and noise in a conventional SL can be described in terms of a field equation and a carrier density rate equation as follows (see Chapter 3 Section 2 and Appendix D or see Ref. [3,7]),

$$\dot{a} = \left[-\iota\Delta\omega - \gamma\right]a + \frac{\Gamma}{2}\left[g(n) - \iota\frac{2\omega_L}{\mu_o}u(n)\right]a + \Delta \tag{2.1}$$

$$\dot{n} = -g(n)P|a|^2 - R(n) + B \quad . \tag{2.2}$$

In Eqn. (2.1) a(t) is the slowly varying normalized complex field amplitude (i.e., the lasing field amplitude is given by $E(t) = \sqrt{P}a(t)\exp(\iota\omega_L t)$ where ω_L is the lasing frequency and field normalization is defined so that P is the photon density of the lasing mode); $\Delta\omega \equiv \omega_L - \omega_m$ gives the pulling of the lasing frequency ω_L from the unpumped cavity resonance at ω_m; γ is the cavity loss rate (note: $(2\gamma)^{-1}$ is the unpumped cavity photon lifetime); Δ is a Langevin noise source to account for fluctuations resulting from spontaneous emission into the lasing mode; μ_o is the nonresonant component of refractive index; and Γ is a filling factor to account for incomplete spatial overlap of the lasing mode and the active medium (assumed to be spatially uniform with gain g(n) and resonant refractive index $\mu(n)$ which depend on carrier density n). In the carrier density rate equation, Eqn. (2.2), R(n) is a combined spontaneous and nonradiative recombination rate term and B is a pumping term.

In practice one solves this set of equations by linearization based on the following representations.

$$n = n_o + n_1 \tag{2.3a}$$

$$g(n) = g(n_o) + g'n_1 \tag{2.3b}$$

$$\mu(n) = \mu(n_o) + \mu' n_1 \tag{2.3c}$$

$$R(n) = R(n_o) + R' n_1 \tag{2.3d}$$

$$B = B_o + B_1 \tag{2.3e}$$

where n_o is the operating point carrier density and n_1 is a small signal variation of carrier density; B_o is the DC pumping and B_1 is the pump variation. For the purposes here it is only necessary to consider the effect of this linearization on Eqn. (2.1) (we have defined the carrier density rate equation and associated terms in it to merely clarify certain results to be quoted momentarily). Using the representations given by (2.3b) and (2.3c) in Eqn (2.1) we find (upon time averaging) the following equations of state,

$$\Gamma g(n_o) = 2\gamma \tag{2.4a}$$

$$-\Gamma \frac{\omega_L}{\mu_o} \mu(n_o) = \Delta\omega \tag{2.4b}$$

which in part establish the operating point (P, ω_L, n_o) for a given device being pumped at rate B_o (the complete operating point equations would also include the time averaged carrier rate equation). Upon separation of (2.4a) and (2.4b) from Eqn. (2.1) the following dynamic equation results.

$$\dot{a} = \frac{\Gamma}{2}\left\{g' - \iota \frac{2\omega}{\mu_o}\mu'\right\} n_1 a + \Delta \quad . \tag{2.5a}$$

For later discussion we define a normalized complex differential gain as,

$$\Xi_{\text{unloaded}} \equiv 1 - \iota\alpha \tag{2.5b}$$

$$\alpha \equiv \frac{2\omega_L}{\mu_o}\frac{\mu'}{g'} \tag{2.5c}$$

where α is the linewidth enhancement factor. Although (2.5a) is still nonlinear it can be simplified by dividing through by a(t) and absorbing a(t) into Δ (see Refs. [3,9]). The result is,

$$\frac{d}{dt}\left(\ln a\right) = \frac{\Gamma}{2}\left(g' - \iota\frac{2\omega}{\mu_o}\mu'\right)n_1 + \Delta \quad . \tag{2.5d}$$

Yet another way to express this result is to separate a(t) into time dependent amplitude and phase terms, $a(t) = (1 + \rho(t))\exp(\iota\varphi(t))$, which reduces (2.5d) to the following set of equations,

$$\frac{\dot{\rho}}{1+\rho} = \frac{\Gamma}{2}g'n_1 + \Delta_R \tag{2.5e}$$

$$\dot{\varphi} = -\Gamma\frac{\omega}{\mu_o}\mu' n_1 + \Delta_I \tag{2.5f}$$

where $\Delta \equiv \Delta_R + \iota\Delta_I$ and in Chapter 3 it has been shown that,

$$< \Delta_R(t+\tau)\Delta_R(t) > \; = \varepsilon\delta(\tau) \tag{2.6a}$$

$$< \Delta_I(t+\tau)\Delta_I(t) > \; = \varepsilon\delta(\tau) \tag{2.6b}$$

$$< \Delta_R(t+\tau)\Delta_I(t) > \; = 0 \tag{2.6c}$$

In these expressions ε is the Schawlow-Townes linewidth; $< >$ denotes ensemble averaging; and $\delta(\tau)$ is the delta function. It should be noted for later reference that the various representations given by (2.5adef) result from

linearization of only the optical gain and the resonant refractive index.

In calculations of small signal modulation or noise spectra the additional approximation of neglecting terms higher order than first in ρ is made. Small signal results can be summarized as follows. The strength of amplitude and frequency variations (dynamic linewidth broadening) under direct modulation are proportional to the differential quantities g' and μ', respectively (this is obvious from (2.5ef)). The direct modulation bandwidth is set by the relaxation oscillation corner frequency ω_R where (see Fig. 4.1 and ref. [4]),

$$\omega_R^2 = 2g'P\gamma \ ; \tag{2.7}$$

the spontaneous relative power noise (RPN) spectral density for frequencies well below ω_R is taken from Chapter 3 Eqn. (5.6),

$$\text{RPN} = \frac{4\varepsilon}{\omega_R^4 \tau_R^2} \tag{2.8a}$$

where,

$$\frac{1}{\tau_R} \equiv g'P + R'(n_o) \ ; \tag{2.8b}$$

and the field spectrum linewidth, which is a direct measure of phase noise in the single mode device, is taken from Chapter 3 Eqn. (5.20),

$$\Delta\omega_L = \varepsilon(1 + \alpha^2) \ . \tag{2.9}$$

In the next section we show how these same properties are affected by detuned loading. It will be seen that the only change will be to replace g', μ', and ε by new effective quantities which are controlled by varying the detuned loading mechanism.

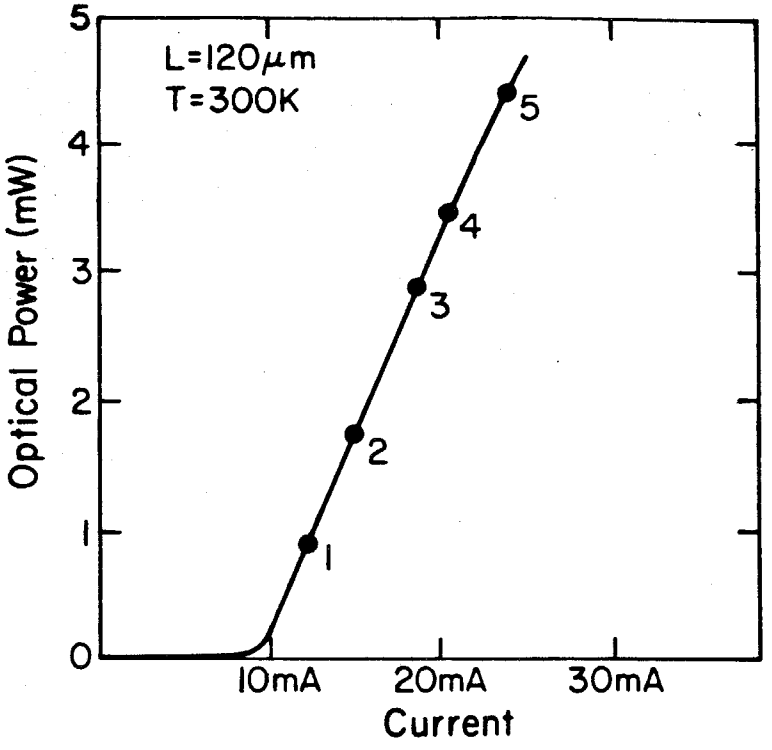

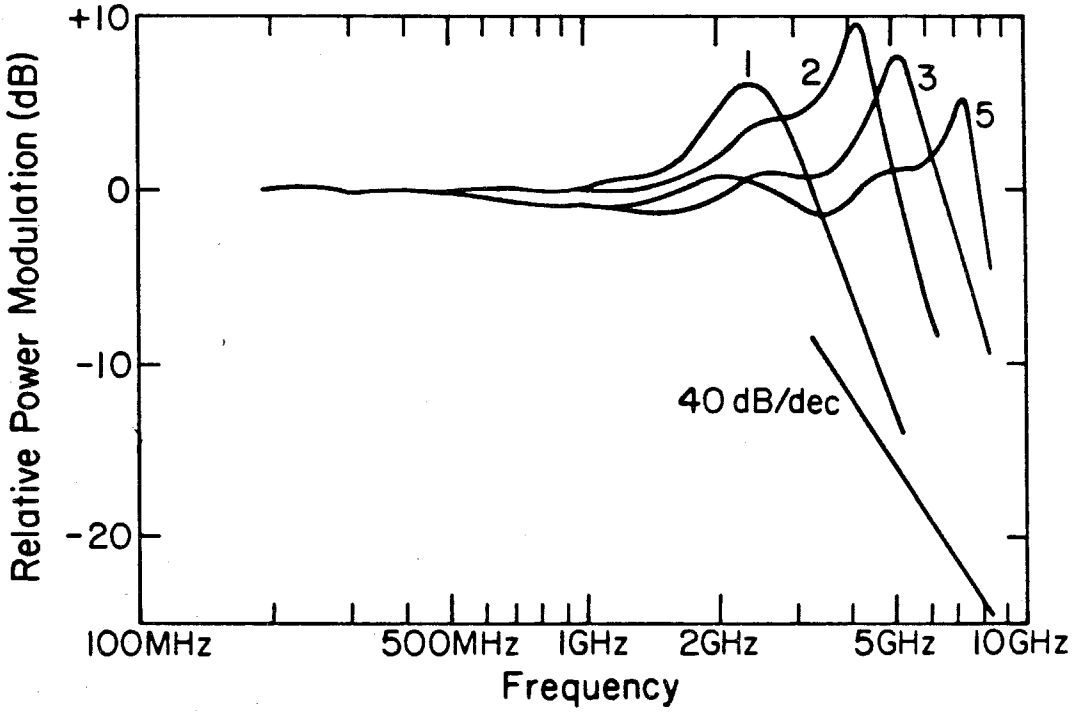

Figure 4.1 Modulation response at various operating points for a conventional semiconductor laser. The device in this case was an Ortel buried heterostructure laser operated at room temperature. The modulation corner frequency increases as the square root of the output power.

4.3 Detuned loading

As discussed in the introduction, "detuned loading" is simply the introduction of a frequency dependent loss mechanism in the spectral proximity of the lasing frequency. Such a mechanism so configured is in fact a detuned load on the laser oscillator, hence the name detuned loading. That one might expect improvements in device performance from the introduction of a detuned load can be argued intuitively as follows. Consider, for instance, the field spectrum linewidth. A heuristic, but quite useful, interpretation of linewidth is to picture it as many perturbations $\delta\omega_L$ to the lasing frequency. These perturbations would result from spontaneous photons emitted into the mode. Averaged out over time these disturbances would smear the lasing line producing the observed lineshape function. Now introduce a detuned load as illustrated in Fig. 4.2 and consider its effect on the perturbations to the lasing frequency. The sequence of events is also illustrated in Fig. 4.2. Owing to the detuned load, perturbations to frequency now cause a change $\delta\gamma$ in the cavity loss rate. This in turn changes the operating point carrier density by δn and thus also the refractive index by $\delta\mu$. This finally produces a correction to the lasing frequency. Thus, a feedback loop results which can either damp the spontaneous frequency fluctuations (i.e., reduce linewidth) or enhance them, depending on which side of the load spectrum the lasing line resides. Similar arguments can be constructed for power noise, modulation speed, and other properties.

To quantify this mechanism we again begin with the field equation (Eqn. (2.1)). The presence of the load mechanism alters not only the cavity loss rate, but also introduces its own form of frequency pulling on the lasing mode. Therefore, the load can be absorbed into $\Delta\omega$ and γ as a strong frequency dependence previously absent. The linearization proceeds as before, except that now

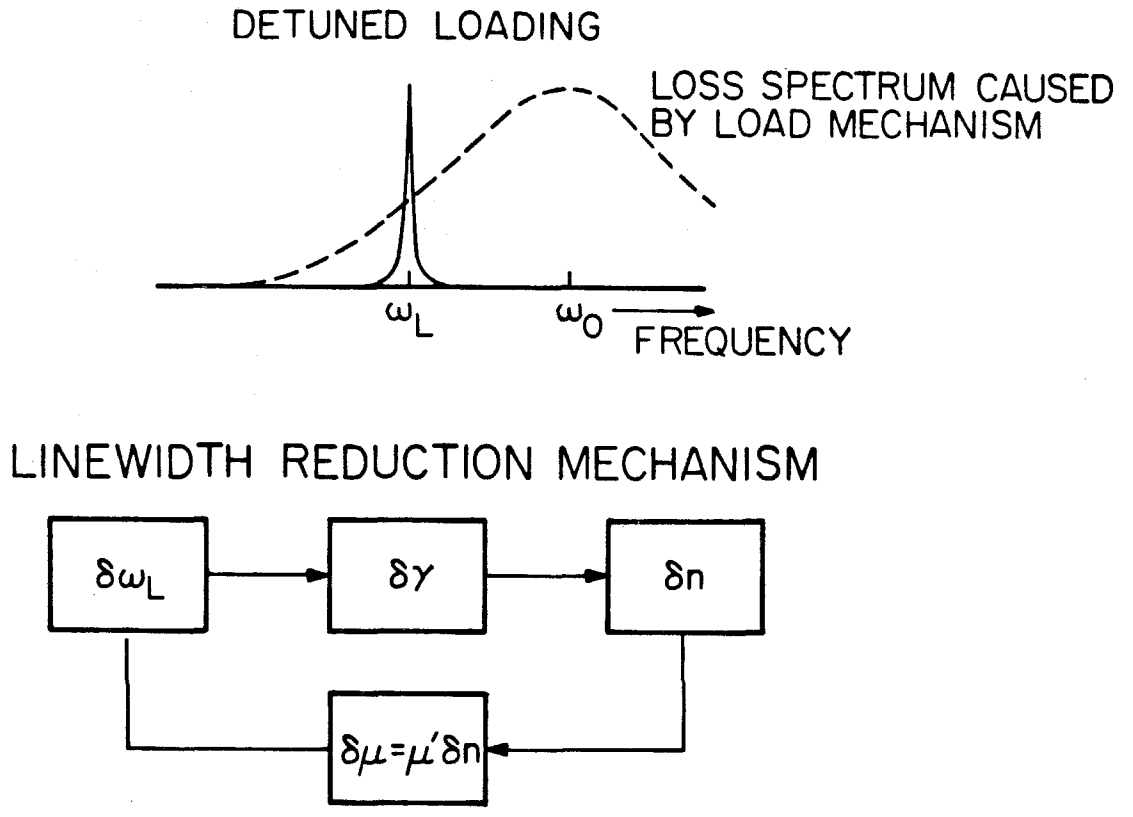

Figure 4.2 Detuned loading is the introduction of a frequency dependent loss in the spectral proximity of the lasing frequency. One effect of this loading, a change in the field spectrum linewidth, is described intuitively in the lower half of the figure.

linearization of γ and $\Delta\omega$ also occurs.

$$\gamma(\omega_L + \delta\omega_L,\vec{L}) \approx \gamma(\omega_L,\vec{L}) + \beta_1\delta\omega_L \tag{3.1a}$$

$$\Delta\omega(\omega_L + \delta\omega_L,\vec{L}) \approx \Delta\omega(\omega_L,\vec{L}) + \beta_2\delta\omega_L \tag{3.1b}$$

where ,

$$\beta_1 \equiv \frac{\partial\gamma(\omega_L,\vec{L})}{\partial\omega_L} \tag{3.1c}$$

$$\beta_2 \equiv \frac{\partial\Delta\omega(\omega_L,\vec{L})}{\partial\omega_L} \tag{3.1d}$$

The additional argument $\vec{L}$ accounts for the possibility that the loading mechanism may depend on other parameters. The expansions (3.1a,b) are valid only for load functions γ and $\Delta\omega$ which are approximately linear over the frequency range $\delta\omega_L$ where,

$$\delta\omega_L = \frac{d}{dt}\Big(\varphi(t) - \iota\ln(1 + \rho(t))\Big) = -\iota\frac{\dot{a}}{a} \tag{3.2}$$

is the instantaneous complex frequency deviation function.

If we rederive Eqn. (2.5a), including the new linearizations for the load functions γ and $\Delta\omega$, then the form of the operating point equations remains unchanged aside from a new dependence on the load argument $\vec{L}$. Eqn. (2.5a), however, is modified as follows,

$$\dot{a} = \frac{\Gamma}{2}\frac{g' - \iota\frac{2\omega}{\mu_o}\mu'}{1 + \beta_2 - \iota\beta_1}n_1 a + \frac{\Delta}{1 + \beta_2 - \iota\beta_1} \tag{3.3a}$$

with a complex differential gain under loading given by,

$$\Xi_{\text{loaded}} = \frac{\Xi_{\text{unloaded}}}{1 + \beta_2 - \iota\beta_1} \tag{3.3b}$$

Eqn. (3.3a) is identical in form to Eqn. (2.5a). The complex differential gain and the Langevin fluctuation force are modified, however. Expanding (3.3a) further as was done for (2.5a) gives,

$$\frac{\dot{\rho}}{1 + \rho} = \frac{\Gamma}{2}g'_{\text{eff}}n_1 + f_R \tag{3.3c}$$

$$\dot{\varphi} = -\Gamma\frac{\omega}{\mu_o}\mu'_{\text{eff}}n_1 + f_I \tag{3.3d}$$

where,

$$g'_{\text{eff}} \equiv g'\frac{1 + \beta_2 + \alpha\beta_1}{(1 + \beta_2)^2 + \beta_1^2} \tag{3.4a}$$

$$\mu'_{\text{eff}} \equiv \mu'\frac{1 + \beta_2 - \frac{\beta_1}{\alpha}}{(1 + \beta_2)^2 + \beta_1^2} \tag{3.4b}$$

$$f_R \equiv \frac{(1 + \beta_2)\Delta_R - \beta_1\Delta_I}{(1 + \beta_2)^2 + \beta_1^2} \tag{3.4c}$$

$$f_I \equiv \frac{(1 + \beta_2)\Delta_I + \beta_1\Delta_R}{(1 + \beta_2)^2 + \beta_1^2} \tag{3.4d}$$

It is easily verified that f_I and f_R obey the same correlation relations as Δ_R and Δ_I (see Eqns. (2.6a,b,c)) except with ε replaced by ε_{eff} where,

$$\varepsilon_{eff} \equiv \frac{\varepsilon}{(1+\beta_2)^2 + \beta_1^2} \quad . \tag{3.4e}$$

We thus reach an important conclusion: the effect of the detuned load on modulation dynamics and noise is solely to replace g', μ', and ε by new effective quantities. It is important to realize that this conclusion holds under large signal modulation of the field, since we have not invoked the small signal approximation in (2.5a) or (3.3a) (we do, however, assume a linear complex gain dependence on carrier density). This simple result has some important consequences which are discussed below.

4.4 Discussion

To apply this formalism the operating point equations must be derived; then, β_1 and β_2 are calculated from the operating point equations using (3.1c,d); and finally, g'_{eff}, μ'_{eff}, and ε_{eff} can be found and used in existing expressions for modulation corner frequency, power noise spectra, linewidth, etc. In general, simultaneous modulation speed enhancement, chirp suppression, and reduction of noise are possible. All of these improvements can be accomplished from an increase in g'_{eff} and reduction of μ'_{eff} (see discussion in Section 4.2). From (3.4a,b) it is apparent that such a complementary variation is possible with detuned loading because of the term involving α (α is typically in the range -4 to -6). A negative β_1 thus tends to increase g'_{eff} and decrease μ'_{eff}. A very important case is where $\mu'_{eff} = 0$ which occurs for,

$$\beta_1 = \alpha(1 + \beta_2) \quad . \tag{4.1}$$

This is the criterion for elimination of chirp by detuned loading.

Perhaps of less importance, but equally interesting, is the case of positive β_1. In this case g'_{eff} decreases and μ'_{eff} increases. For $|\beta_1|$ large enough, g'_{eff} passes through zero and becomes negative. In this case the lasing mode is unstable to small changes in amplitude and we would expect pulsations to occur. These results can be reformulated in terms of the phasor representation of the complex differential gain Ξ as illustrated in Fig. 4.3. There we have drawn the unloaded phasor assuming an α of -5. The projection of this phasor on the vertical axis is proportional to the differential refractive index and thus indicates the amount of phase noise or chirp under modulation; the horizontal projection is proportional to the differential gain and thus determines modulation speed and intensity noise (negative horizontal projections indicate the system is unstable to variations in intensity). The effect of detuned loading is to both rescale and rotate this phasor thus varying the magnitude of the effective differential gain and refractive index. To reduce chirp, phase noise, and intensity noise while enhancing modulation speed the phasor could be rotated as shown. The zero chirp condition occurs when the phasor lies along the positive horizontal axis.

The various possibilities we have discussed here are summarized in Fig. 4.4. It should be stressed that β_1 and β_2 (and hence g'_{eff}, μ'_{eff}, and ε_{eff}) are functions of the lasing frequency ω_L which is normally not a parameter under direct control. Therefore whether specific tuning regions illustrated in Fig. 4.4 are in practice obtainable is a question which must be answered on a case by case basis through consideration of the operating point equations.

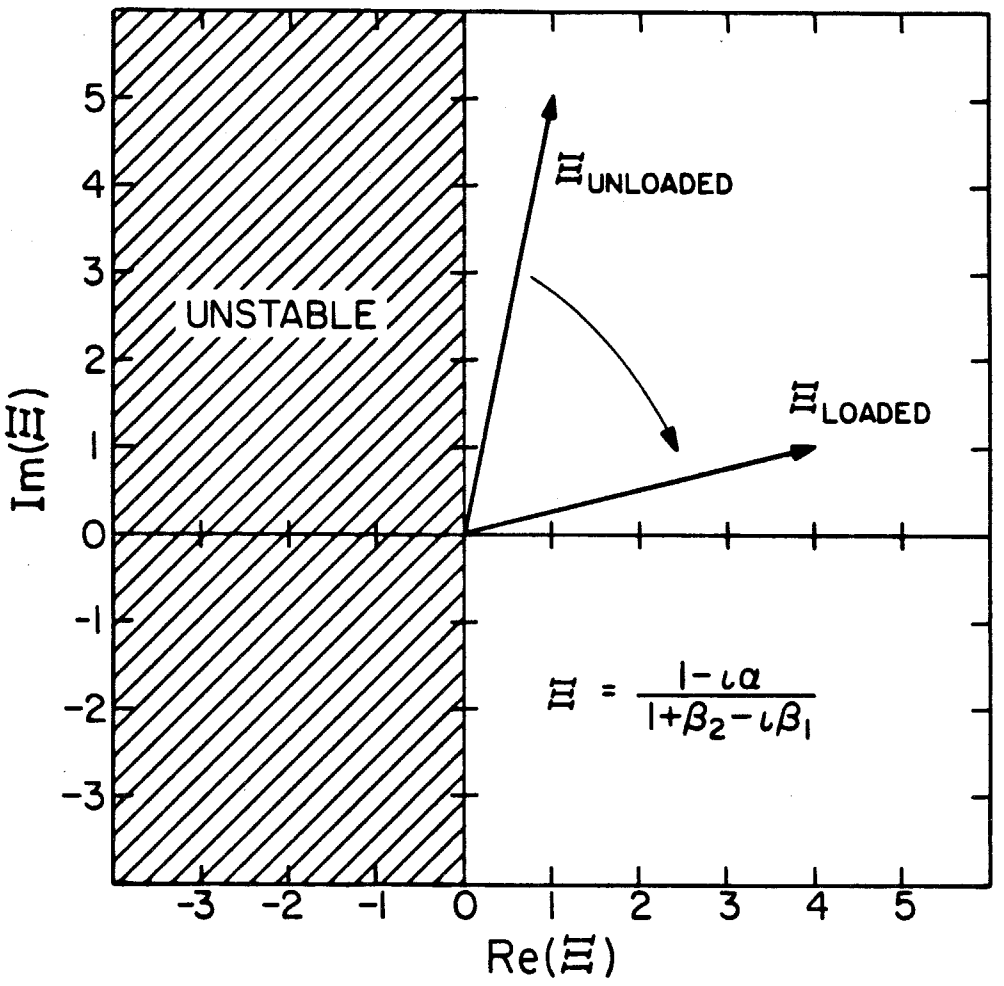

Figure 4.3 The complex differential gain determines how the modulation of carrier density transfers into changes in the field amplitude and phase. To improve dynamics and reduce noise as compared to the solitary (unloaded) device the complex differential gain should be rotated as illustrated. Detuned loading can perform such a rotation. It is also possible to select a load which rotates the phasor into the unstable region of this space.

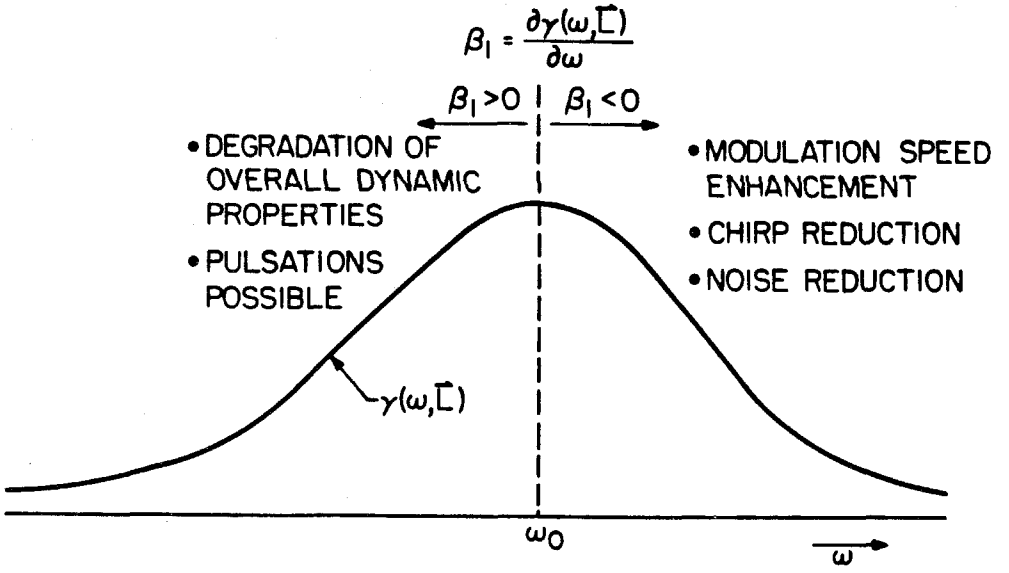

Figure 4.4 Summary of the effects of detuned loading.

So far we have discussed only the consequences of control of g'_{eff} and μ'_{eff} with detuned loading. ε_{eff} also is under control and affects the strength of the spontaneous power noise and phase noise through expressions (2.8a) and (2.9a). To conclude this section we give the loaded forms for the low frequency RPN spectrum and the field spectrum linewidth $\Delta\omega_L$ normalized by their conventional forms.

$$\frac{RPN^{loaded}}{RPN} = \frac{(1+\beta_2)^2+\beta_1^2}{(1+\beta_2+\alpha\beta_1)^2} \tag{4.2a}$$

$$\frac{\Delta\omega_L^{loaded}}{\Delta\omega_L} = \frac{1}{(1+\beta_2+\alpha\beta_1)^2} \tag{4.3b}$$

A term involving α again makes possible improvements in device performance and negative β_1's, as mentioned earlier, lead to reductions in noise as compared to the conventional case.

4.5 An application of the formalism

One method for introducing a strongly frequency dependent loss into the SL system to achieve detuned loading is to couple it to a passive resonator. In this section we apply the formalism of Section 4.3 to consider this possibility and then present measurements of modulation speed, linewidth, and frequency modulation in an active-passive coupled-cavity device.

A schematic of the system we consider here is shown in Fig. 4.5. Henry and Kazarinov [10] have shown that the eigenvalue equation for such a system is given by,

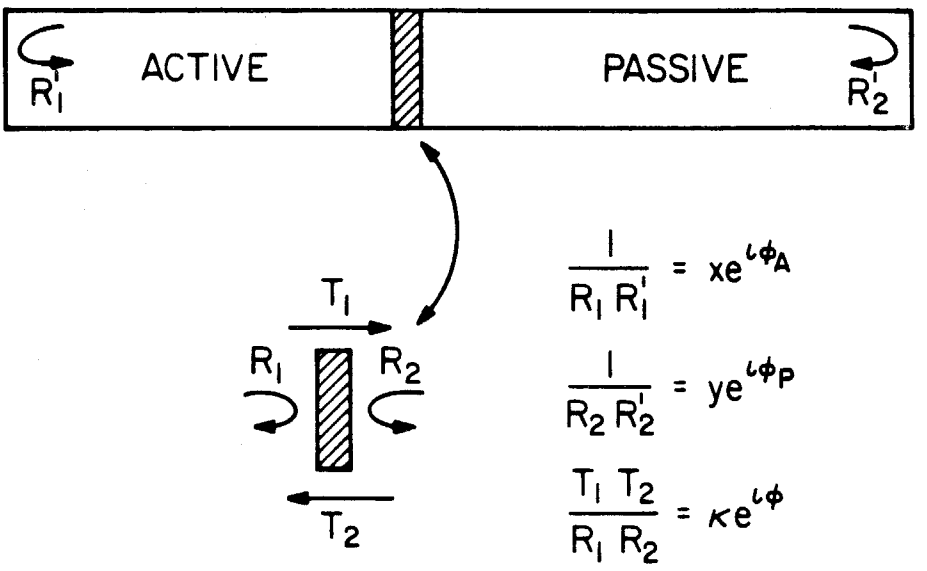

Figure 4.5 Schematic of the active-passive coupled-cavity system studied as an implementation of the detuned loading mechanism.

$$\left[xe^{(2ik_Al_A - \bar{g}l_A + \varphi_A)} - 1\right]\left[ye^{(2ik_Pl_P + \varphi_P)} - 1\right] = \kappa e^{i\varphi} \tag{5.1a}$$

with,

$$xe^{i\varphi_A} \equiv 1/(R_1R_1') \tag{5.1b}$$

$$ye^{i\varphi_P} \equiv 1/(R_2R_2') \tag{5.1c}$$

$$\kappa e^{i\varphi} \equiv \frac{T_1T_2}{R_1R_2} \tag{5.1d}$$

and where R_1, R_2, T_1, and T_2 describe the interface between the two cavities (this could be a simple air-semiconductor interface or could be more complex such as the air gap in a cleave coupled cavity device [11]). k_A and k_P are propagation constants in the active and passive cavities, and $\bar{g}$ is the optical gain in units of [cm.$^{-1}$].

When $\kappa = 0$ (i.e., no coupling) Eqn. (5.1a) has the following solutions,

$$x\exp\left(-\bar{g}_o(n,\omega_m^A)l_A\right) \equiv x\exp\left(-\frac{g_c(n,\omega_m^A)}{2\Gamma_A}\right) = 1 \tag{5.2a}$$

$$2k_Al_A + \varphi_A \equiv \frac{\omega_m^A}{\Gamma_A} + \varphi_A = 2\pi m \tag{5.2b}$$

$$2k_Pl_P + \varphi_A \equiv \frac{\omega_n^P}{\Gamma_P} + \varphi_P = 2\pi n \tag{5.2c}$$

where Γ_A and Γ_P are the free spectral ranges of the active and the passive resonators; m and n are integers; g_o is the optical gain in units of [sec.$^{-1}$]; $\{\omega_n^P\}$ are the resonant frequencies of the uncoupled passive cavity. $\{\omega_m^A\}$ are potential lasing frequencies with threshold gains given by (18a). In writing g_o we have explicitly shown its dependence on excitation and frequency. Also, note that Γ_A is

weakly dependent on excitation (n) through the resonant contribution to refractive index.

When coupling is present (5.1a) again yields a multiplicity of potential lasing frequencies with associated threshold gains. We assume one such frequency ω has a threshold gain g lower than all others and is preferred to lase. It is convenient to define these solutions relative to the uncoupled solutions by defining the following parameters,

$$\Delta\gamma \equiv \frac{1}{2}(g - g_o) \tag{5.3a}$$

$$\Delta\omega \equiv \omega - \omega_m^A \tag{5.3b}$$

$$\Delta\omega^P \equiv \omega - \omega_n^P \tag{5.3c}$$

where we have suppressed the m and n dependences in $\Delta\omega$ and $\Delta\omega^P$. Notice that $\Delta\gamma$ is up to the additive constant $-g_o$ just the loss function γ and $\Delta\omega$ is the frequency pulling function which appear in (2.1). By rewriting (5.1a) in terms of these quantities we get the simplified eigenvalue expression,

$$\left[xe^{\left(\frac{-\Delta\gamma + \iota\Delta\omega}{\Gamma_A}\right)} - 1\right]\left[ye^{\left(\frac{\Delta\omega^P}{\Gamma_P}\right)} - 1\right] = \kappa e^{\iota\varphi} \tag{5.4a}$$

which can be solved to yield,

$$-\Delta\gamma + \iota\Delta\omega = \Gamma_A \ln\left[1 + \frac{\kappa e^{\iota\varphi}}{ye^{\iota\frac{\Delta\omega^P}{\Gamma_P}} - 1}\right] . \tag{5.4b}$$

This equation can be used to find β_1 and β_2 as given by (3.1cd). The noise and dynamics then follow directly from (3.4abe).

We now apply this equation and our formalism to an actual device. A schematic of this device is given in the inset of Fig. 4.6. The active resonator was formed by an Ortel large optical cavity buried heterostructure GaAs/GaAlAs injection laser (cavity length ≈ 300 μM.) which lased in predominantly one mode and had a threshold current of 25.6 mA. The passive cavity was formed by one facet of the laser and a small gold- coated concave mirror, having an 800μm. radius of curvature. Piezoelectric micropositioners controlled the mirror's position relative to the laser for tuning purposes.

In order to calculate the dynamics for this system it is necessary to know Γ_A, Γ_P, κ, φ, and y in (5.4b). We take Γ_A = 119GHz. and Γ_P = 188GHz. based on knowledge of the cavity lengths and the refractive index of GaAs. Direct measurement gives R_2 = 0.58 and R_2' = 0.88 so that from (5.1c) y = 1.96. The other quantities can be deduced by a number of methods which involve measurement of the steady-state properties of the system. These methods are discussed in the Appendix. The dynamic measurements presented here were taken when the system was configured so that κ = 0.5 and $\varphi = -0.67\pi$ and these values will be assumed in the calculations to follow. We note that this configuration corresponds to a condition of slight misalignment of the cavities. The reason for choosing such a configuration is also discussed in the Appendix.

Calculations of g_{eff}' and μ_{eff}' spectra for this system configuration are presented in Fig. 4.7. These plots result from applying the prescription outlined in Section 4.3 to Eqn. (5.4b). The complex differential gain is also plotted in Fig. 4.8. $\alpha = -3$ was assumed in these calculations and those which follow. Large variations can be seen in these plots as a result of detuned loading. In practice, however, the strength of the effect (i.e., steepness of the loss spectrum at the lasing frequency) is limited by mode hopping. To see this consider Fig. 4.6.

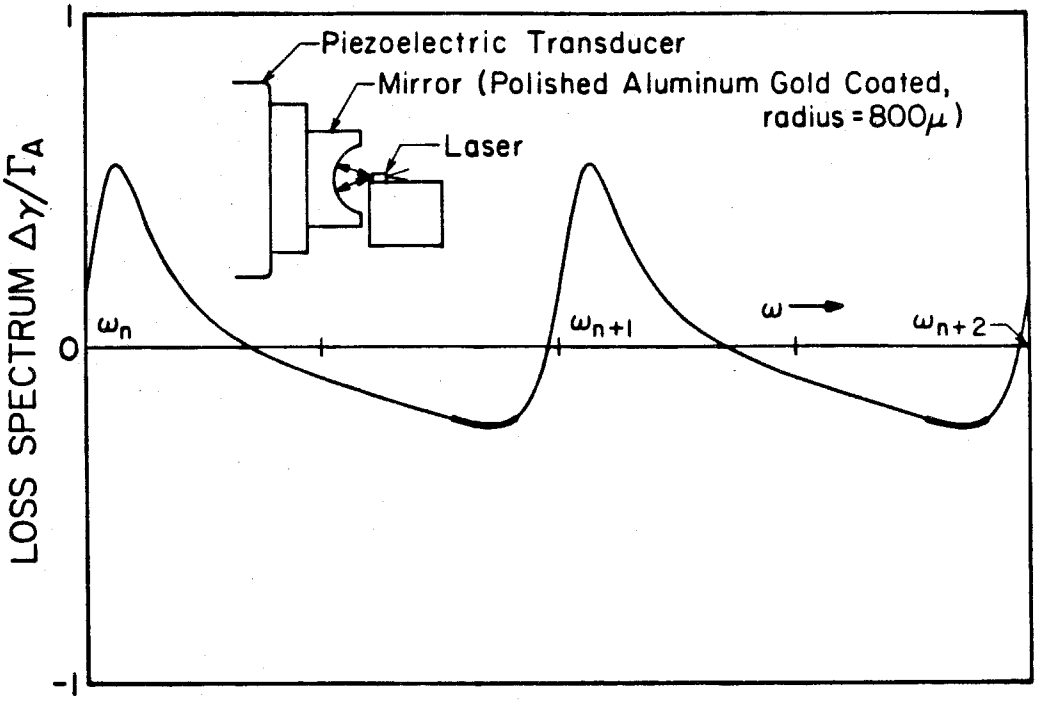

Figure 4.6 Loss spectrum normalized by the free spectral range of the active resonator; coupling parameters are $\kappa = 0.5$ and $\varphi = -0.67\pi$. The emboldened sections are the low loss regions where lasing can be sustained during tuning of the external cavity. Inset: coupled cavity device used in the measurement of the detuned loading effect.

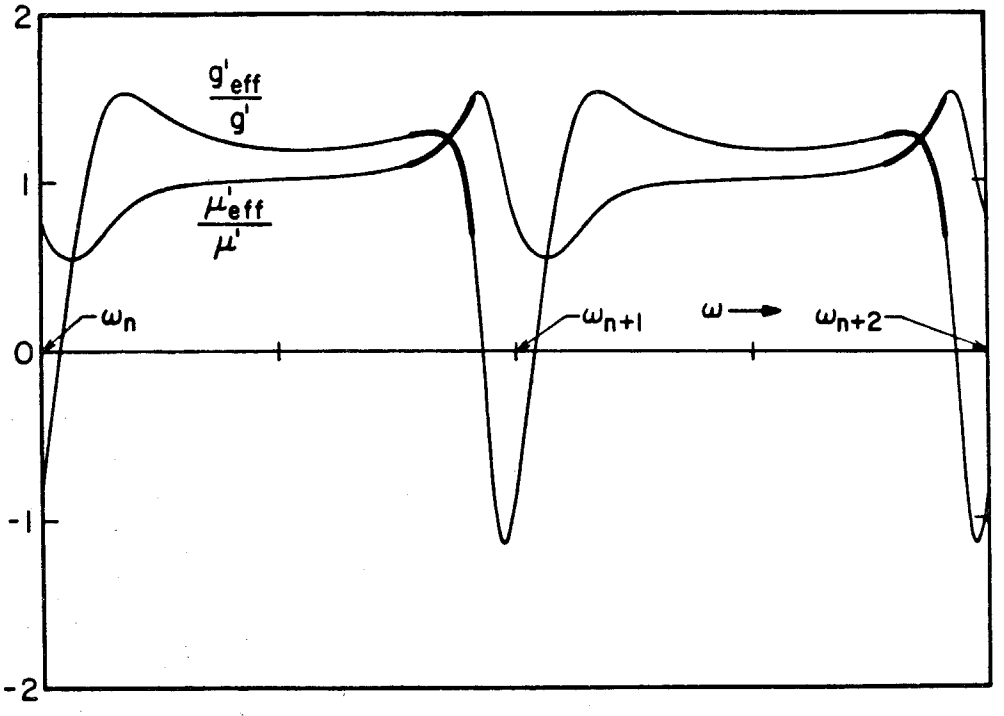

Figure 4.7 Spectral variation of differential gain and differential refractive index resulting from detuned loading. The emboldened sections correspond to the low loss tuning regions where lasing action occurs.

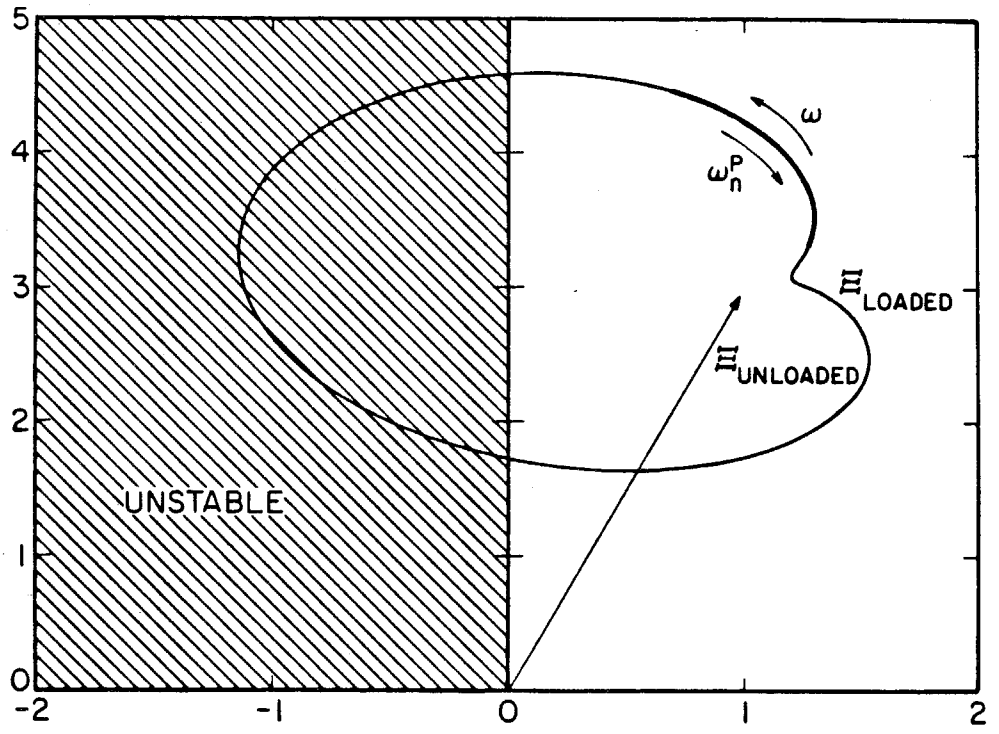

Figure 4.8 Complex differential gain for the coupled cavity system with the region of operation emboldened. The unloaded complex differential gain assumed in all calculations is also given.

which shows the loss spectrum for this device configuration. This function can be seen to vary with a period given by the free spectral range of the passive cavity and it is this variation with frequency which gives rise to the detuned loading effect. Lasing action is preferred in the low loss regions of this spectrum (these emboldened tuning regions are determined in the Appendix).

When tuning the passive cavity piezoelectrically a lasing mode will sweep through a particular emboldened region and will continue to lase until its threshold gain exceeds that of another mode. At this point a mode hop will occur. The tuning characteristics of the coupled-cavity system were such that the passive cavity resonances could be shifted by 30 Ghz. (via piezoelectric control of the concave mirror) or nearly 15% of a passive free spectral range before a longitudinal mode jump would occur in the system. (Over this tuning range the oscillation was single mode to better than 20 dB and power in the lasing mode varied by no more than 20 %, peaking near the middle of the tuning range.) The emboldened tuning ranges are also illustrated in Figs. 4.7 and 4.8, showing clearly the limitations imposed by mode hopping on the detuned loading effect in this system.

The measurement setup used here included a high speed silicon avalanche photodetector for measurement of the modulation response, both high and low resolution (7.5 Ghz. and 75 Ghz. instrumental bandwidth) scanning Fabry-Perot etalons for measurement of linewidth and modulation, and a grating spectrum analyzer equipped with a multichannel analyzer to monitor mode suppression and modal power. Feedback effects in the system were controlled by insertion of neutral density filters.

The measured modulation response for this device taken at extremes of the tuning region for a single mode is presented in Fig. 4.9. The output powers (and

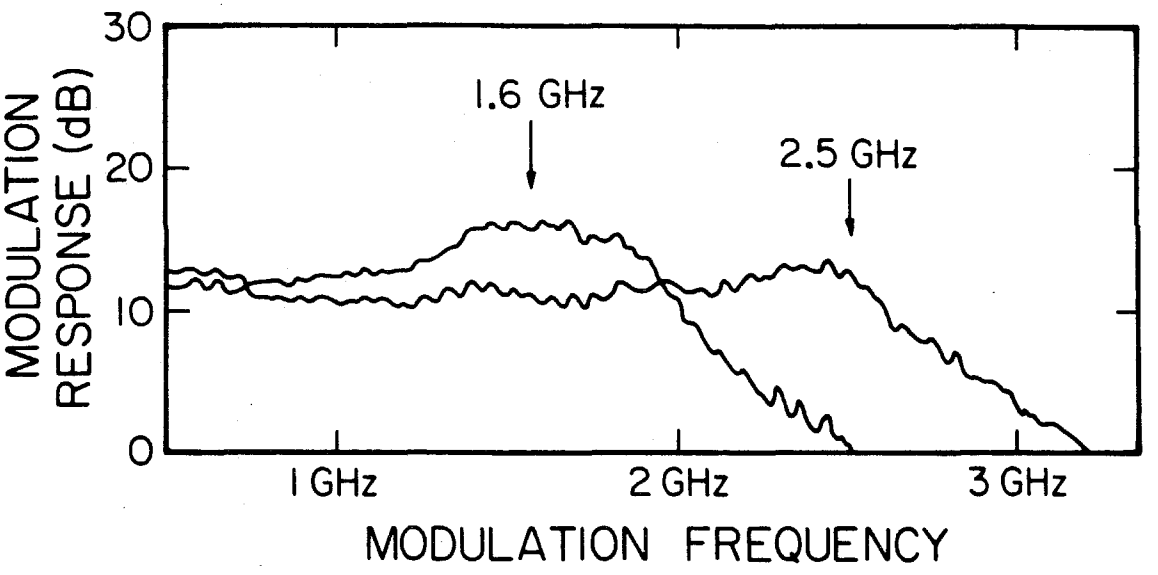

Figure 4.9 Measured modulation response at extremes of the tuning range. The observed variation of the corner frequency is caused entirely by the detuned loading mechanism.

hence the photon densities) at these points were the same (Output Power ≈ 1 mW.). The effective photon lifetimes are also equal in the two cases as these are endpoints of the tuning range. Therefore, from Eqn. (2.7) the observed corner frequency variation from 1.6 GHz. to 2.5 GHz. results solely from variation of the effective differential gain with tuning, that is from the detuned loading effect. In this case the net variation in g'_{eff} was roughly 2X. Qualitative measurements of frequency modulation were also performed at these tuning extremes by using the low resolution Fabry-Perot to measure suppression of the optical carrier under direct modulation. These measurements showed that the FM component of modulation was smaller (i.e., the optical carrier was larger) at the tuning extreme where modulation bandwidth was enhanced.

Linewidth as a function of tuning was also measured. These data are presented with additional modulation corner frequency data in Fig. 4.10. Again the data were taken over a single tuning range at roughly 1 mW. output power. It can be seen that linewidth varied from around 180 Mhz. at one extreme of the tuning range to below 60 MHz. at the other extreme. Resolution in this measurement was limited by microphonics coupling into the system through the concave mirror mount.

It is important to note that these measured variations result from changing the passive cavity resonances and not the lasing frequency directly. For this reason the spectra of Fig. 4.7, being functions of the lasing frequency, are not entirely helpful in making a quantitative comparison of theory and experiment. In Fig. 4.11 a calculation of the differential gain and linewidth as functions of a passive cavity resonance near the lasing frequency is given; i.e., these plots correspond to the measured results of Fig. 4.10. If measurements are compared with the predicted variations given by the emboldened tuning regions, the

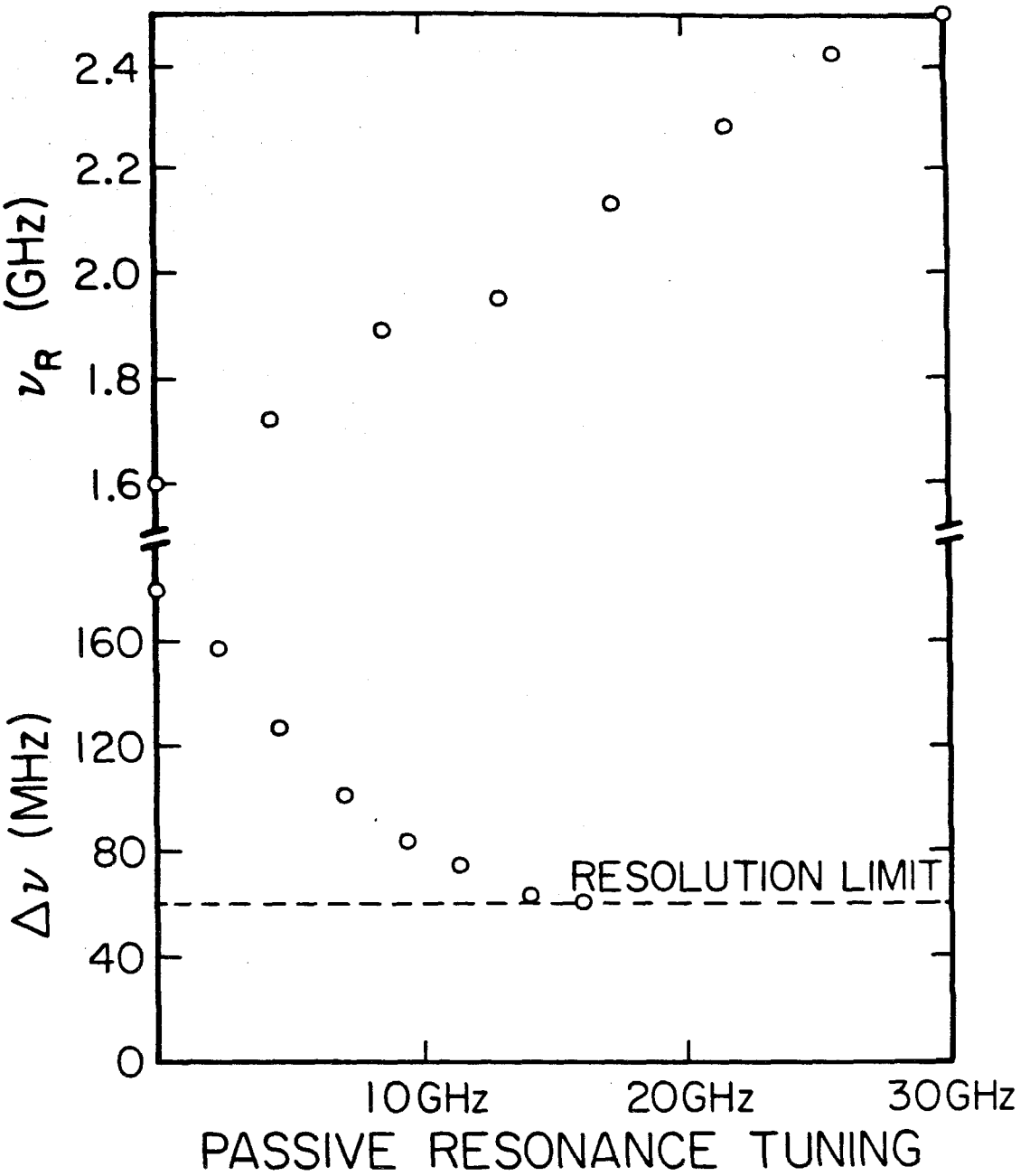

Figure 4.10 Linewidth and modulation corner frequency measured versus tuning of the passive cavity resonances near the lasing frequency. The observed variations result primarily from the detuned loading mechanism.

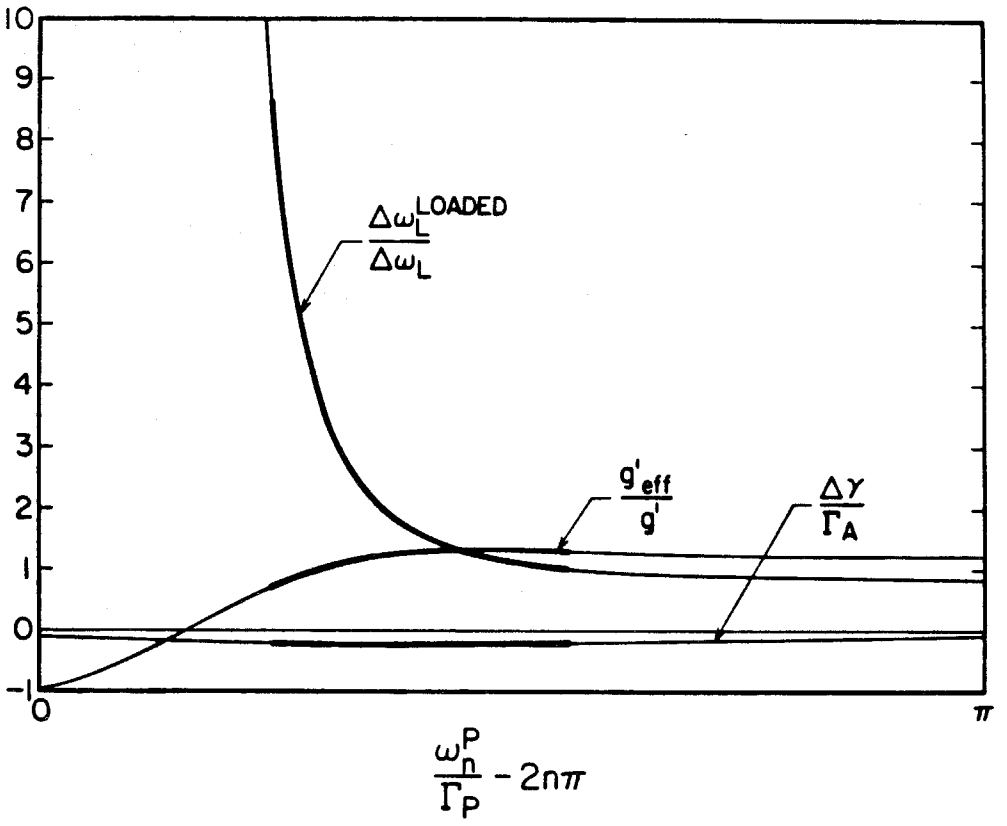

Figure 4.11 Calculated variation of linewidth and differential gain as functions of the n^{th} passive cavity resonance (Note: the normalization Γ_P is fixed). Also shown is the loss function. Tuning regions are emboldened.

the agreement is good. The predicted total variation of g'_{eff} is roughly 2X and the predicted total variation of linewidth is roughly 4X, both consistent with the measured variations. It is also interesting to note that over the same tuning range for which linewidth is decreasng, modulation response is increasing. RPN was not measured in this system.

4.5 Conclusion

In this chapter we have described detuned loading as a generalized method which can be used to improve the modulation dynamics and noise properties of semiconductor lasers. We have also presented a generic formalism for the treatment of detuned loading and have used it to show that the effect of detuned loading on dynamics and noise can be reduced to consideration of detune induced changes in the effective quantities g'_{eff}, μ'_{eff} and ε_{eff}. General expressions were derived which can be used to calculate these effective quantities with only knowledge of the operating point equations for a particular implementation. Possible implementations of this effect include coupled cavity devices and semiconductor lasers employing distributed feedback or Bragg reflectors.

We have also discussed some of the potential benefits of detuned loading. These included elimination of dynamic linewidth broadening (chirp), modulation speed enhancement, and reduction of power noise and phase noise. To demonstrate some of these effects we presented measurements of modulation response, chirp, and linewidth in a coupled-cavity implementation of detuned loading. These results were found to be in good agreement with calculations based on the generalized formalism.

The effective quantity variations produced by detuned loading in this system were only modest ones intended mainly to demonstrate the principle. It should

be possible to design systems with much larger variations and we are currently investigating this possibility.

Appendix

In Section 4.5 the values of κ and φ for the coupled-cavity system were required for the calcultations presented there. In this Appendix we show how these values were deduced from steady-state measurements on the coupled-cavity system. In doing this it will also be seen why a slightly misaligned configuration of the system was chosen for the measurement.

κ and φ will be determined through measurement of coupling induced frequency pulling. One could also perform measurements of mode suppression, change in threshold current and change in quantum efficiency caused by coupling, but we did not find this necessary. The complete steady-state characterization of this system is presented in greater detail in Ref. [12]. The discussion here will center on two configurations of the coupled-cavity system, one highly aligned, one slightly misaligned. The parameter values and loss curves (calculated from (5.4b)) which will be deduced for these two cases are given in Fig. 4.12. The low loss regions where lasing is preferred are emboldened. It is clear from these plots why the misaligned configuration of the system is desirable for demonstration of the detuned loading effect. In that case the emboldened regions vary more rapidly with frequency and thus cause a more pronounced detuned loading effect. To demonstrate this fact we have plotted g'_{eff} for these two cases in Fig. 4.13. In the emboldened tuning regions the variation of g'_{eff} is much smaller in the well-aligned case. This was also born out in the measurement.

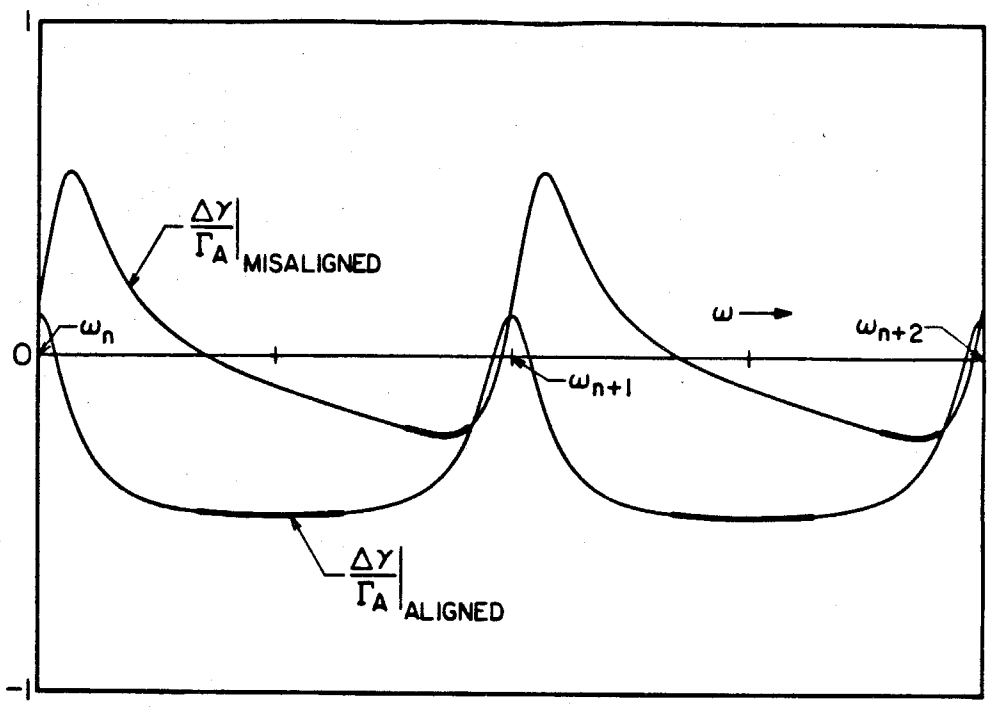

Figure 4.12 Loss spectra for the highly aligned and slightly misaligned configurations of the coupled cavity system. The misaligned case is preferable for the detuned loading measurement since the loss slope varies more strongly in the emboldened tuning region. Parameter values are $\kappa = 1.8$ and $\varphi = -\pi$ for the aligned case and $\kappa = 0.5$ and $\varphi = -0.67\pi$ for the misaligned case.

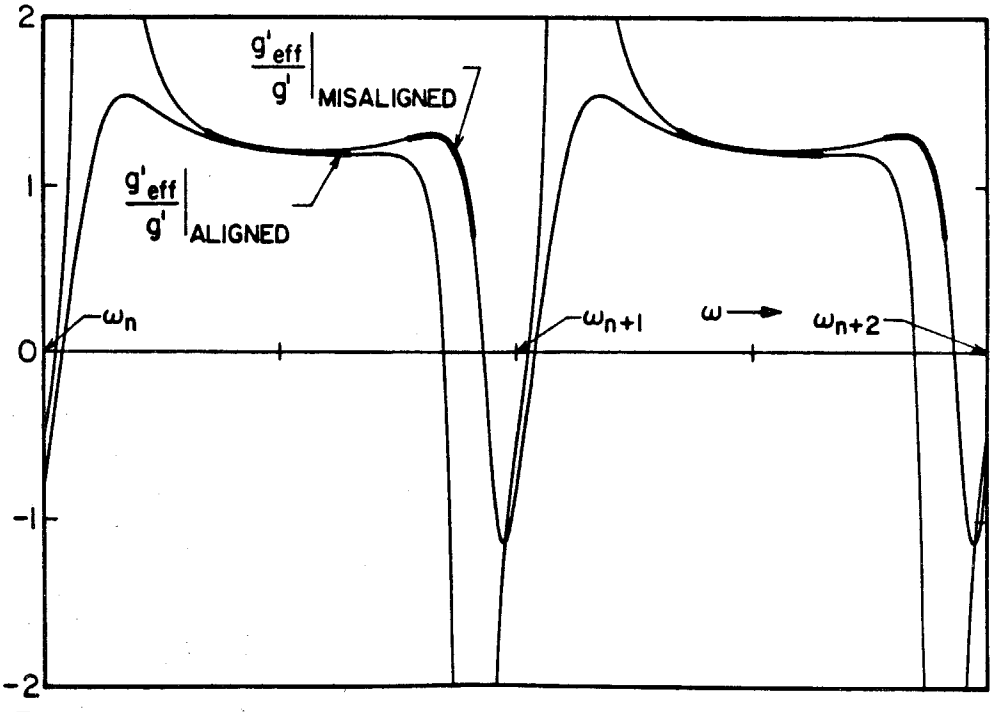

Figure 4.13 Normalized effective differential gain spectra in the aligned and misaligned cases. The observable detune induced variation of this quantity is larger in the misaligned case (see emboldened tuning region).

We will consider a measurement of coupling induced frequency pulling. This measurement, by itself, uniquely determines κ and φ. It is performed by monitoring the lasing frequency with a scanning Fabry-Perot (having a free spectral range of 7.5 GHz. and an instrumental bandwidth of 7.5 MHz.) while sweeping the external cavity length, thereby tuning the passive cavity resonances. Data for the highly aligned and slightly misaligned cases are presented in Figs. 4.14,15. As will be seen this measurement gives a good indication of system alignment, being very sensitive to the coupling phase φ.

To solve for the frequency pulling curves the imaginary part of the eigenvalue equation (5.4b) is separated,

$$\omega - \omega_m^A = \Gamma_A U\left(\frac{\omega - \omega_n^P}{\Gamma_P}, \kappa, \varphi, y_i\right) \tag{A.1}$$

where,

$$U\left(\frac{\omega - \omega_n^P}{\Gamma_P}, \kappa, \varphi, y_i\right) \equiv \mathrm{Im}\left[\ln\left[1 + \frac{\kappa e^{i\varphi}}{y e^{i\frac{\Delta\omega^P}{\Gamma_P}} - 1}\right]\right] \tag{A.2}$$

$$V\left(\frac{\omega - \omega_n^P}{\Gamma_P}, \kappa, \varphi, y_i\right) \equiv \mathrm{Re}\left[\ln\left[1 + \frac{\kappa e^{i\varphi}}{y e^{i\frac{\Delta\omega^P}{\Gamma_P}} - 1}\right]\right] . \tag{A.3}$$

Frequency pulling results from two effects: one is the direct effect of the load on the round trip phase and is represented by the function U; the other is indirect and results from a shift in ω_m^A as the active resonator carrier density (and thus refractive index) changes with tuning induced changes in loss. It is straightforward to show that,

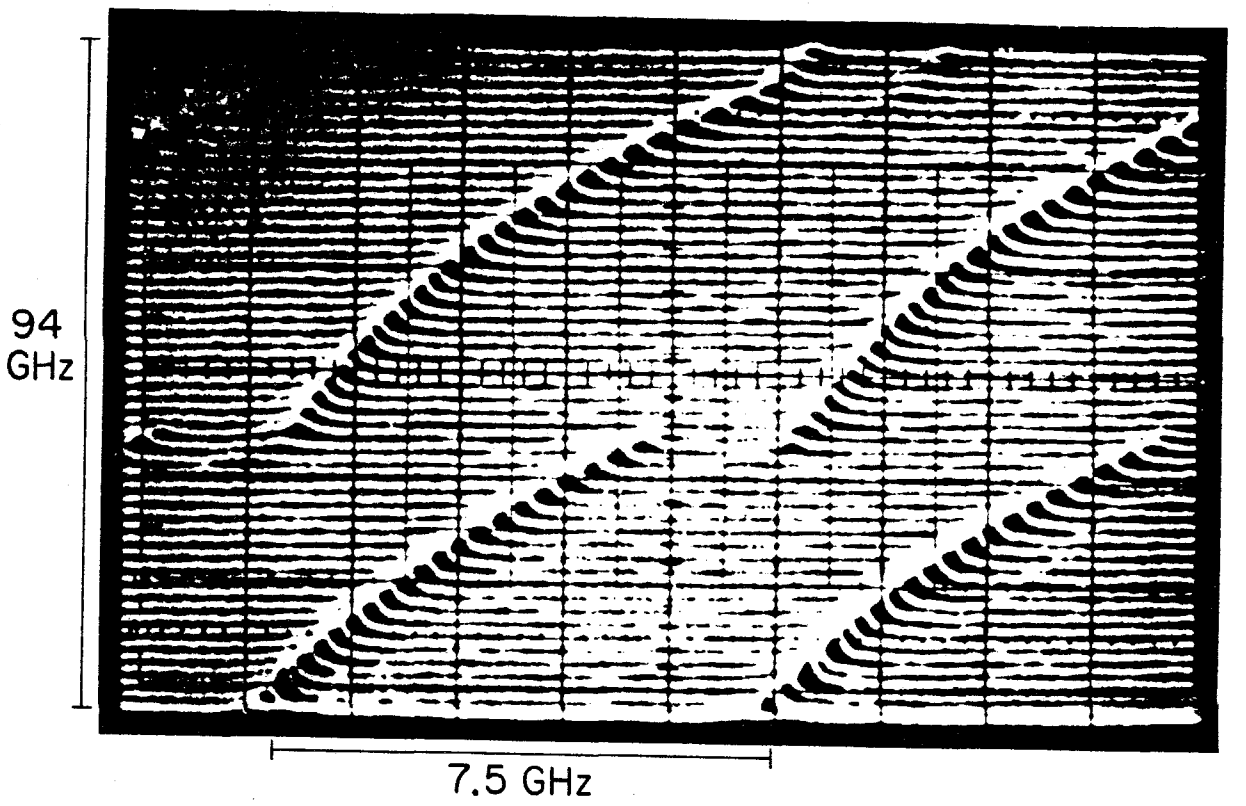

Figure 4.14 Frequency pulling data for the highly aligned configration of the coupled cavity system. The vertical axis gives the frequency shift of a passive cavity resonance near the lasing frequency. The horizontal axis gives the shift in the lasing frequency.

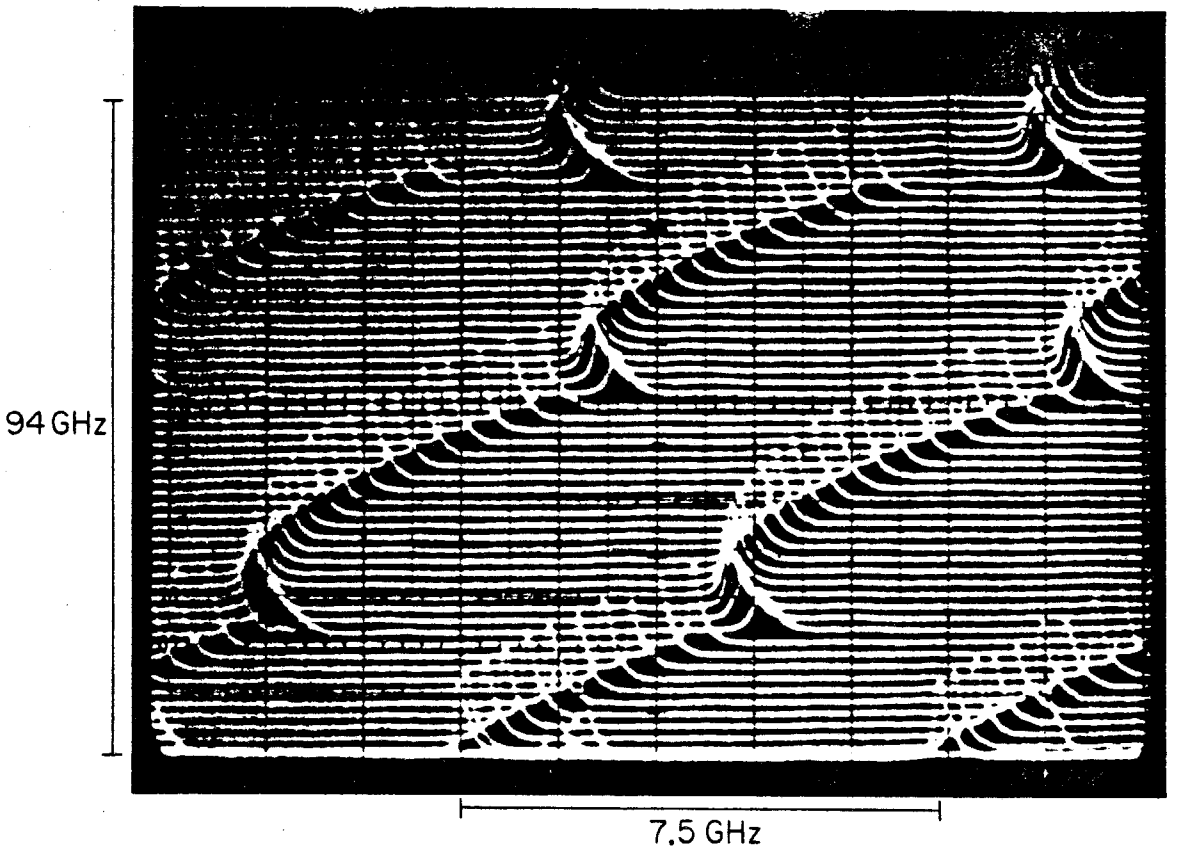

Figure 4.15 Frequency pulling data for the misaligned configration of the coupled cavity system.

$$\omega_m^A = \omega_m^A|_{\text{uncoupled}} - \alpha\Delta\gamma = \omega_m^A|_{\text{uncoupled}} - \alpha\Gamma_A V \quad . \tag{A.4}$$

Thus the pulling equation becomes,

$$\omega - \omega_m^A|_{\text{uncoupled}} = \Gamma_A(U - \alpha V) \quad . \tag{A.5}$$

Frequency pulling is plotted in Figs. 4.16,17 for two sets of parameters. The loss spectra are also plotted to indicate the low loss tuning regions where lasing is preferred (note: these spectra differ from that plotted in Fig. 4.6 because they are plotted versus ω_n^P instead of ω) Slightly "bowed" pulling curves like the curves in Fig. 4.14 always result from taking $\varphi = \pi$. It can be shown that $\varphi = \pi$ corresponds to the case of lossless coupling (i.e., excellent alignment) between the cavities. Therefore, the frequency pulling data in Fig. 4.14 are interpreted to indicate a situation of excellent alignment between the cavities. When $\varphi \neq \pi$ more complicated frequency pulling curves are possible. The "hooked" features calculated in Fig. 4.17 resulted from taking $\varphi = -0.67\pi$. These same features could be produced experimentally (see Fig. 4.15) by slight lateral misalignment of the cavities (which presumably introduces a coupling loss between the cavities).

Quantitative results in these cases were obtained by first identifying structure such as the "bowed" or "hooked" features thereby, establishing a first guess for φ. Then a calculation of the pulling rate $d\omega/d\omega_n^P$ combined with measured values of this quantity in the linear regions of Figs. 4.14,4.15 could be used to determine a κ. By iterating this procedure one arrives at a κ and φ which yield a calculated pulling curve nearly identical to that measured. from the frequency pulling data.

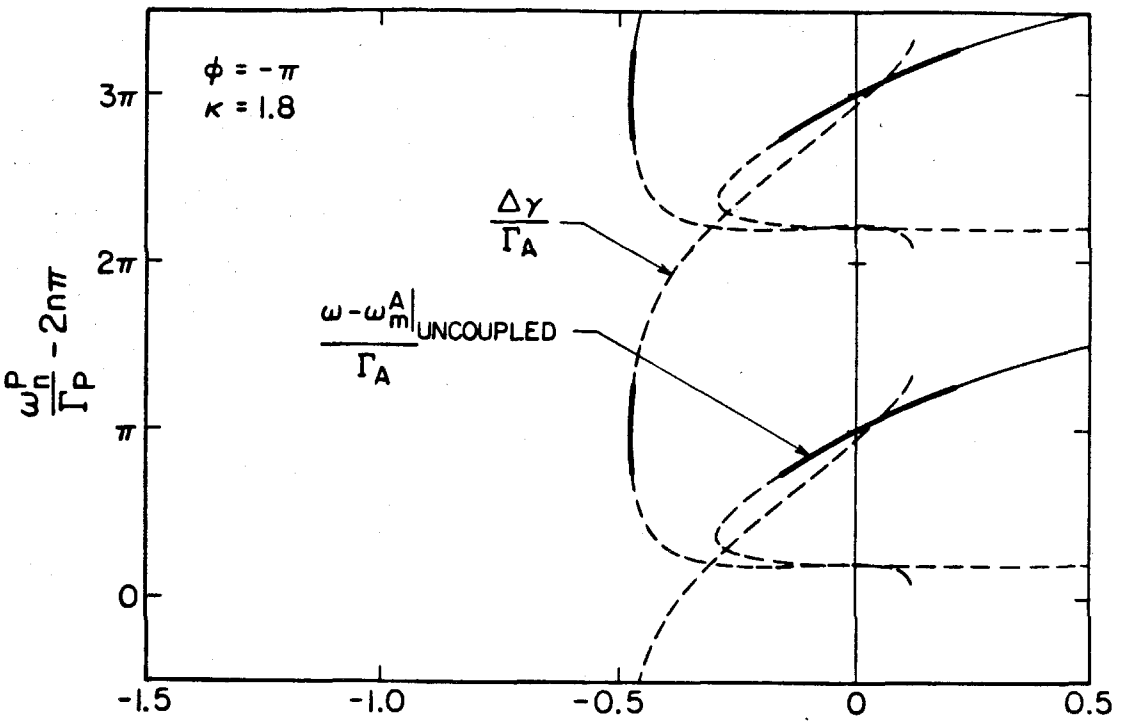

Figure 4.16 Calculated frequency pulling curves using coupling parameters characteristic of a well-aligned system (note: the normalization Γ_P is fixed). The loss function is also plotted so that the tuning region can be determined. Note the "bowed" pulling behavior.

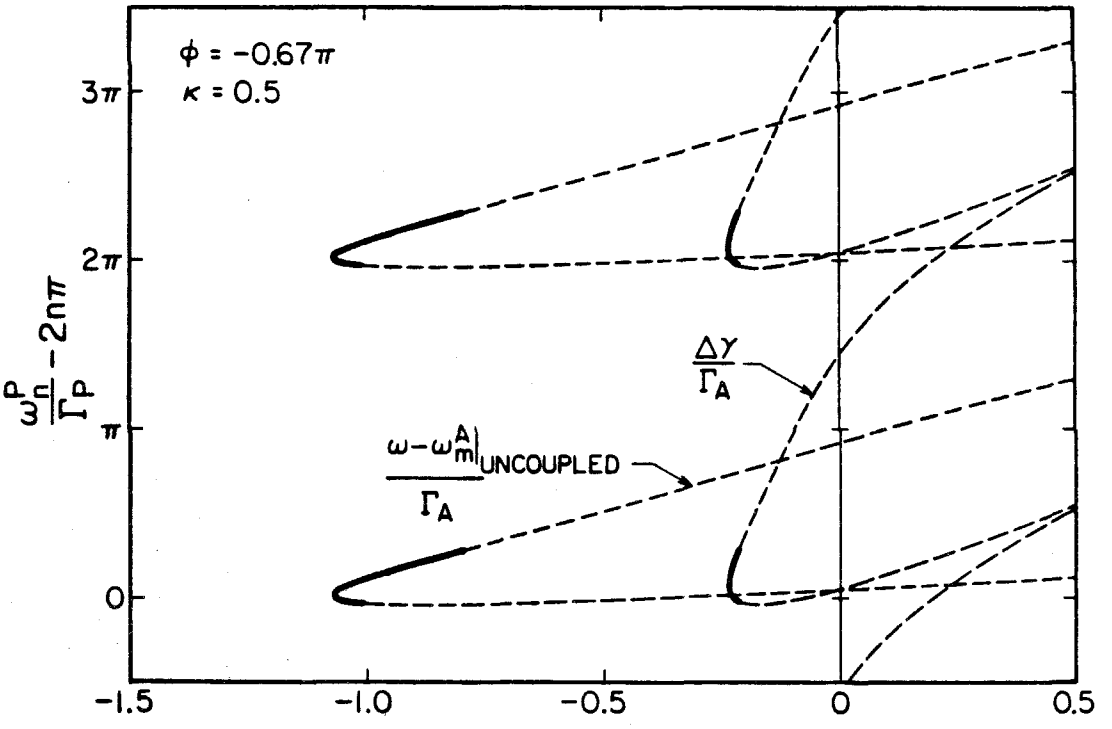

Figure 4.17 Calculated frequency pulling curves using coupling parameters characteristic of a misaligned system. Note the "hooked" pulling behavior.

References

[1] Ph.D. dissertation by Christoph Harder, California Institute of Technology, Pasadena, CA (1983).

[2] Ph.D. dissertation by Kam-Yin Lau, California Institute of Technology, Pasadena, CA (1981).

[3] K. Vahala and A. Yariv, IEEE J. Quant. Electron., vol. QE-19, p. 1096 (1983); p. 1102 (1983).

[4] K. Y. Lau, N. Bar Chaim, I. Ury, Ch. Harder and A. Yariv, Appl. Phys. Lett., vol. 43, p. 1 (1983).

[5] M. Fleming and A. Mooradian, Appl. Phys. Lett., vol. 38, p. 511 (1981).

[6] Private communication with Hank Blauvelt, Ortel Corporation, Alhambra, CA.

[7] K. Vahala and A. Yariv, Appl. Phys. Lett., vol. 45, p. 501 (1984).

[8] K. Vahala and A. Yariv, Paper #WE23 presented at IOEC Conference, Anaheim, CA (1984).

[9] M. Lax, Phys. Rev., vol. 160, p. 290 (1967).

[10] C. H. Henry and R. F. Kazarinov, IEEE J. Quant. Electron., vol. QE-20, p. 733 (1984).

[11] W. T. Tsang, N. A. Olsson and R. A. Logan, Appl. Phys. Lett., vol. 42, p. 650 (1983).

[12] J. Paslaski, K. Vahala and A. Yariv, unpublished.